Understanding the structure and deformation of titanium-containing silicate glasses from their elastic responses to external stimuli

Garth Scannell

2016

THÈSE / UNIVERSITÉ DE RENNES 1
sous le sceau de l'Université Européenne de Bretagne

En Cotutelle Internationale avec
Rensselaer Polytechnic Institute, USA

pour le grade de

DOCTEUR DE L'UNIVERSITÉ DE RENNES 1

Mention : Science des Matériaux

Ecole doctorale : SDLM

présentée par

Garth Scannell

préparée à l'unité de recherche UMR 6251

Understanding the structure and deformation of titanium-containing silicate glasses from their elastic responses to external stimuli

Thèse soutenue à Madison, WI, USA

le 23/05/2016

devant le jury composé de :

Minoru TOMOZAWA
Examinateur
Timothy GROSS
Rapporteur/ Examinateur
Lothar WONDRACZEK
Rapporteur/ Examinateur
E. Bruce WATSON
Examinateur
Mark DAVIS
Examinateur
Scott Glaesemann
Examinateur
Liping HUANG
Directeur de thèse
Tanguy ROUXEL
Co-directeur de thèse

2016

Understanding the structure and deformation of titanium-containing silicate glasses from their elastic responses to external stimuli

by
Garth Scannell

A Thesis Submitted to the Graduate
Faculty of Rensselaer Polytechnic Institute
in Partial Fulfillment of the
Requirements for the degree of
DOCTOR OF PHILOSOPHY
Major Subject: MATERIALS SCIENCE AND ENGINEERING

Approved by the Examining Committee:

_____
Minoru TOMOZAWA
Member

_____
Timothy GROSS
Reviewer, Member

_____
Lothar WONDRACZEK
Reviewer, Member

_____
E. Bruce WATSON
Member

_____
Mark DAVIS
Member

_____
Scott Glaesemann
Member

_____
Liping HUANG
Thesis Adviser (RPI)

_____
Tanguy ROUXEL
Thesis Adviser (UR1)

Rensselaer Polytechnic Institute
Troy, New York
May, 2016
(For Graduation August 2016)

Table of Contents

Table of Tables

Table of Figures

Acknowledgements

This work was supported by the US National Science Foundation under Grant No. DMR-1105238 and DMR-1255378, by the European Research Council through the Advanced Grant 320506 (DAMREG) of the 7th framework programme "Ideas". I am indebted to the Chateaubriand Fellowship program for funding one year study in Rennes (France), hence promoting collaboration between RPI and IPR. Thanks to Dr. Koike for providing TiO_2-SiO_2 samples prepared through flame hydrolysis deposition and for measuring the thermal expansion of the TiO_2-SiO_2 sol-gel glasses. Thanks to Corning Inc. for the help in measuring the thermal expansion coefficient of Na_2O-TiO_2-SiO_2 glasses. Thanks to Dr. Erik Robin for the software used to monitor indentation crack growth.

I would like to thank the undergraduates who have helped me throughout my doctoral research: Nicole Valderrabano, Nathaniel Mowell, Shannon Barra, and HoMei Leung at RPI. Thanks to Dr. Fabrice Celarie, Theany To, and Arnaud Bazin at IPR for help with fracture toughness measurements. Thanks to Dr. Denis Laille in INSA at the University of Rennes 1 for help with AFM measurements. And thanks to Dr. Michael Guerette for help with light scattering experiments.

I would particularly like to thank Brian Ozsdolay for his insightful discussions and always being available when I needed someone to work through ideas with. Thanks to both my advisers, Drs. Liping Huang and Tanguy Rouxel, who provided an excellent balance of guidance when I needed it and independence to do my own research when I didn't. Thanks to my friends for dragging me out into the sun occasionally and helping me keep a proper work-life balance. And thanks to my family for their continual support throughout my doctorate.

Abstract

The responses of structure and properties to composition and temperature have been investigated for glasses in TiO_2-SiO_2 and Na_2O-TiO_2-SiO_2 systems. Additionally, the response of Na_2O-TiO_2-SiO_2 glasses to plastic deformation has been studied. (x)TiO_2-(1-x)SiO_2 glasses were prepared through the sol-gel process with compositions $0 \leq x \leq 10$ mol% and compared to commercial glasses prepared through flame hydrolysis deposition with x = 0, 5.4, and 8.3 mol%. (x) Na_2O - (y) TiO_2 - (1-x-y) SiO_2 glasses were prepared with x = 10, 15, 20, and 25 mol% and y = 4, 7, and 10 mol% through a melt-quench process. Density and index of refraction of glasses was measured through the Archimedes's method and using a prism coupler, respectively. The glass transition temperature of Na_2O-TiO_2-SiO_2 glasses was measured through differential thermal analysis.

The structure and elastic moduli have been studied through Raman spectroscopy and Brillouin light scattering, respectively, at room temperature and *in-situ* up to 1200 °C for TiO_2-SiO_2 glasses and up to 800 °C for Na_2O-TiO_2-SiO_2 glasses. Young's modulus was observed to decrease from 72 GPa to 66 GPa with the addition of 8.3 mol% TiO_2 in TiO_2-SiO_2 glasses and to increase from 65 GPa to 73 GPa with the addition of 10 mol% TiO_2 in 10 Na_2O - (0-10) TiO_2-SiO_2 glasses. The addition of TiO_2 was observed to shift the 460, 490, and 600 cm^{-1} Raman peaks to lower frequencies in TiO_2-SiO_2 glasses, suggesting a more open and flexible network, and the 720, 800, and 840 cm^{-1} Raman peaks to higher frequencies in Na_2O-TiO_2-SiO_2 glasses, suggesting a lower free volume and stiffer network. The addition of TiO_2 has little effect on the temperature response of the elastic moduli in either system, but decreases the thermal expansion and increases the frequency shifts in the 950 and 1100 cm^{-1} Raman peaks in the TiO_2-SiO_2 system while the thermal expansion increases with initial additions of TiO_2 and then remains constant in the Na_2O-TiO_2-SiO_2 system.

Changes in structure and property with composition have been discussed, and structural models were proposed. The reduction of thermal expansion and elastic moduli in TiO_2-SiO_2 glasses occurs through the promotion of cooperative, inter-tetrahedral rotations facilitated by the longer and weaker Ti-O bonds. The increase in elastic moduli in the Na_2O-TiO_2-SiO_2 glasses occurs through the formation of small clusters with local, relatively high Ti and Na concentrations, promoted by Ti adopting a five-fold coordination in a square-pyramidal

geometry. These clusters work to shield the silica network from non-bridging oxygens from the presence of Na while simultaneously increasing the volume bond density of the glass.

For Na_2O-TiO_2-SiO_2 glasses, the response to mechanical damage and plastic deformation has been examined through Vickers indentation experiments at loads from 10 mN to 49 N. Fracture toughness was measured through the single-edge precracked beam method. The permanent deformation volumes around Vickers indents were investigated through atomic force microscopy. Critical loads for crack initiation and cracking patterns were systematically investigated and correlated with the elastic properties of glass. Vickers indents were observed to change from a mixture of radial/median and cone cracks to radial/median and lateral cracks as Poisson's ratio increases. As Poisson's ratio increases hardness decreases from 5.5 GPa to 4.5 GPa, the average radial/median crack length roughly doubles, and fracture toughness remains constant. A minimum in the critical crack initiation load was observed at ν = 0.21-0.22. The volume of glass deformed through shear flow increases gradually with increasing Poisson's ratio, becomes larger than the densified volume at ν =0.237. The volume of densified glass increases between ν = 0.18 and ν = 0.21 and decreases rapidly from 16.5 μm^3 to 8.7 μm^3 at ν = 0.235 - 0.237. A correlation between the minimum in crack initiation load and the change in deformation mechanisms over the same Poisson's ratio range was observed.

Résumé

Dans cette recherche, on a étudié les effets provoqués par des changements de composition et de température sur la structure et les propriétés des verres des systèmes TiO_2-SiO_2 et Na_2O-TiO_2-SiO_2. On a également examiné la réponse des verres du système Na_2O-TiO_2-SiO_2 à la déformation plastique. On a fabriqué des verres (x)TiO_2-(1-x)SiO_2 par le procédé sol-gel avec des compositions de $0 \leq x \leq 10$ mol%, puis on les a comparés avec des verres commerciaux fabriqués par la déposition provoquée par l'hydrolyse à la flamme x = 0 ; 5,4 ; et 8,3 mol%. On a fabriqué des verres (x) Na_2O - (y) TiO_2 - (1-x-y) SiO_2 avec x = 10, 15, 20, et 25 mol% et y = 4, 7, and 10 mol% par trempage depuis l'état fondu. On a mesuré la densité des verres en utilisant le principe d'Archimède et on a mesuré l'indice de réfraction des verres par prisme coupleur. On a évalué la température de transition vitreuse des verres Na_2O-TiO_2-SiO_2 par analyse thermique différentielle.

On a étudié la structure et les modules d'élasticité par spectroscopie Raman et par diffusion Brillouin, respectivement, à température ambiante et *in situ* jusqu'à 1 200 °C pour les verres TiO_2-SiO_2 et jusqu'à 800 °C pour les verres Na_2O-TiO_2-SiO_2. On a constaté que le module de Young des verres TiO_2-SiO_2 a diminué de 72 GPa à 66 GPa avec l'addition de 8,3 mol% TiO_2, et que le module de Young des verres 10 Na_2O - (0-10) TiO_2-SiO_2 a augmenté de 65 GPa à 73 GPa avec l'addition de 10 mol% TiO_2. On a vu que l'addition de TiO_2 aux verres TiO_2-SiO_2 a décalé les sommets du spectre Raman de 460, 490, et 600 cm^{-1} aux fréquences plus basses, ce qui suggère un réseau structural plus ouverte et flexible ; et que l'addition de TiO_2 aux verres Na_2O-TiO_2-SiO_2 a décalé les sommets du spectre Raman 720, 800, and 840 cm^{-1} aux fréquences plus élevées, ce qui suggère une réduction de volume libre et un réseau structural plus rigide. L'addition de TiO_2 n'a que peu d'effet sur la réponse thermique des modules élastiques des deux systèmes, mais elle diminue l'expansion thermique et augmente les décalages de fréquences des sommets Raman de 950 and 1100 cm^{-1} du système TiO_2-SiO_2, alors que l'expansion thermique du système Na_2O-TiO_2-SiO_2 augmente avec les premières additions de TiO_2 et puis reste constante.

Les changements de structure et de propriétés liés à la composition sont examinés, et des modèles structuraux sont proposés. La réduction d'expansion thermique et des modules d'élasticité des verres TiO_2-SiO_2 se produit par la promotion des rotations coopératives inter-

tétraèdres facilitées par les liaisons Ti-O plus longues et plus faibles. L'augmentation des modules d'élasticité des verres Na_2O-TiO_2-SiO_2 est due à la formation de petits groupes avec des concentrations élevées de Na et Ti, produit par l'adoption de Ti d'une coordination quintuple d'une géométrie de pyramide à base carrée. Ces petites « globules » protègent le réseau silice des oxygènes non-pontants tout en augmentant la densité des liaisons du verre.

On a étudié la réponse des verres Na_2O-TiO_2-SiO_2 au dommage mécanique et la déformation plastique par des essais d'indentation Vickers de charges de 10 mN to 49 N. La dureté de fracture a été mesurée sur éprouvette préfissurée sur une seule face (méthode SEPB). On a examiné les volumes de déformation permanente auprès des indentations Vickers par microscopie à force atomique. On a étudié de façon systématique les charges critiques pour le début de la propagation de fissure et les motifs de fissure et fait les corrélations avec les propriétés élastiques de verre. Les indentations Vickers ont changé d'un mélange de radial/médian et des fissures coniques à un mélange de radial/médian et des fissures latérales, suivant l'augmentation du coefficient de Poisson. Avec la croissance du coefficient de Poisson, la dureté de verre diminue de 5,5 GPa à 4,5 GPa ; la longueur moyenne de fissure radial/médian double, à peu près ; et la dureté de fracture reste constante. On a vu un minimum de charge critique de début de propagation de fissure à $\nu = 0{,}21 - 0{,}22$. Le volume de verre déformé par l'écoulement de cisaillement augmente petit à petit avec l'augmentation du coefficient de Poisson et devient plus grand que le volume densifié à $\nu = 0{,}237$. Le volume de verre densifié diminue entre $\nu = 0{,}18$ et $\nu = 0{,}21$ et augmente subitement de 7 μm^3 jusqu'à 16 μm^3 à $\nu = 0{,}23$. Entre ces mêmes limites de coefficient de Poisson, on a constaté une corrélation entre la charge critique minimum d'initiation de propagation de fissure et le changement de mécanismes de déformation.

Chapter 1 : Motivation and Background

1.1: Motivation

1.1.1: Need for Understanding of Intrinsic Behavior of Glasses

Glasses have been used throughout history in a range of applications. These applications largely take advantage of the hard and transparent properties of glass while being restricted by its brittleness. As new types of glasses have been developed, the range of applications has expanded. Commonly used glasses include traditional soda-lime window glasses, vitreous silica, borate glasses, fluoride glasses, aluminosilicate glasses, oxynitride glasses, and metallic glasses. Glasses cover a range of chemical systems and primary bonding types (Van der Waals, metallic, ionic, and covalent), and their structure and properties vary accordingly [1].

As technology has increased, the demand for high performance materials has grown. The development of stronger, tougher, and less brittle glasses would reduce the consumption of glass in current applications and enable new ones [2]. Several methods have been developed to create stronger and tougher glasses. Thermal tempering creates a compressive stress on the surface of the glass through rapid quenching. Ion-exchange toughening creates compressive stresses in the surface of a glass through the exchange of small ions in the glass for larger ions. These methods are commonly employed in the fabrication of commercial glasses and can increase the strength considerably. For instance, the strength of simply annealed window glass is ~45 MPa, and reaches ~120 MPa for coated float glass. Values of 150-250 MPa are reported for thermally tempered safety glass and 450-750 MPa for chemically tempered glass (e.g., Corning's Gorilla® glass).

However, the strength values used by engineers to design glass structure are well below the intrinsic strength of glass. Glass has been shown to have a tensile strength of up to 14 GPa for silica glass drawn to fibers in vacuum at 77 K [3]. In working environments, glass is prevented from reaching its intrinsic strength because it suffers from mechanical aggressions (e.g., cracks and scratches) [4]. The search for damage resistant glasses is of paramount importance with the increasing demand for light-weight and durable glasses for applications in architecture, the automobile industry, telecommunications and touch screen displays. The fundamental need is to understand the properties of glass from its atomic structure and bonding viewpoint.

1.1.2: Early Attempts at Predicting Properties

To meet this need, scientists have tried to understand the structure and behavior of glasses in the atomic and inter-molecular scales so as to predict the properties of a wide range of glass systems. Two models that have been extensively used to predict the properties and behavior of glasses are briefly described below.

In the 1970s, Makishima and Mackenzie developed a theoretical model for predicting the Young's moduli of glasses based on their packing density and the dissociation energy of the oxide constituents [5]. Their model was quite accurate for four-coordinated cations, but had to be corrected for three coordinated borate glasses and was significantly less accurate for other glasses. In addition, their model did not predict whether or not the composition in question could be formed into a glass. They later expanded their model to be able to predict the bulk and shear moduli and the Poisson's ratio of glasses [6]. Many other theoretical models developed later have either been slight improvements or expansions of the Makishima and Mackenzie model [7-14].

Around the same period, Phillips developed the topological constraint theory, which accurately predicted glass forming compositions [15]. He found that optimum glass forming ability occurred when the number of constraints in inter-atomic force field space equaled the number of degrees of freedom. For network glass formers, the constraints were expressed as two-body bond stretching and three-body bond bending, which could be calculated from the average coordination numbers. The topological constraint model has been expanded to include mechanical properties and has been used to explain trends observed in many glass systems [2]. These models have been partially successful, in that they can predict the properties of a limited number of glass systems with a reasonable degree of accuracy. However, for most of them the degree of accuracy was achieved by empirical refinement using experimental data. It remains a grand challenge of how to design glasses with the desired properties using a systematic theoretical approach (non-Edisonian), but this is required for the development of the next generation of glasses to be used in modern applications [2]. This challenge can only be addressed after significant improvements in our fundamental knowledge of how to understand and control the glass structure and its response to contact damage.

1.1.3: Current Studies of Structure and Properties of Glass

Recent attempts to study and understand the behavior and properties of glasses have been a mixture of elastic and visco-elastic/plastic deformation experiments. The structure and properties of glasses can be studied through a wide variety of techniques, including Raman light scattering, Brillouin light scattering (BLS), neutron scattering, x-ray diffraction, infrared spectroscopy, dilatometry, etc. Raman light scattering has been used to determine the structure and bonding information of a large number of glasses. It can also provide information on local structures, such as the D_1 and D_2 defect bands in the Raman spectrum of silica glass that describe the breathing mode of three- and four-member rings. McMillan et al. analyzed the structural changes of vitreous silica with Raman spectroscopy, explaining its anomalous volume behavior with temperature [16].

Information on the structure and elastic properties of glasses can also be obtained through BLS. On the macroscopic level, glass is structurally homogenous and isotropic; only two independent elastic constants are needed to characterize its elasticity. Elastic constants are simple to define and easy to measure, and are directly related to the inter-atomic forces and potentials, embodying the local structure and bonding information [17]. Therefore, perturbing the glass with thermal or mechanical agitation and measuring the changes in elastic moduli can be used as a probe to gain insights into the atomic-level structure of glass [18]. Zhao et al. used a combination of Raman and BLS over a range of temperatures to reveal the structural causes of temperature independent elastic moduli in sodium-silicate glasses [19]. Smedskjaer et al. used a variety of experimental techniques including BLS to examine the glass transition temperatures in alumino-silicate glasses and used those results to test the applicability of the shoving model in their glasses [20].

Elastic moduli and their dependence on temperature and pressure are critical inputs for developing and validating computer models of glasses with accurate short- and long-range interactions. Inversely, reliable computer models can complement experiments to obtain detailed structure-property relationships, and to study large-scale deformation of glasses.

Silica is a good example of a system where experimental [21-23] and computational techniques [24-27] have been used separately and complementarily to provide a detailed picture of the structure and behavior of silica under a wide range of conditions. Rau et al. measured the sound velocities in vitreous silica under pressures up to 6 GPa with BLS, which he used to

support or disprove various models of its structure [28]. Huang et al. used molecular dynamics simulations [24-26] to predict the behavior of silica glass under extreme pressures (up to 20 GPa) and temperatures (up to 2000 K). Raman light scattering experimental results up to 2 GPa [29] agreed with the reversible structural rearrangements under applied pressure predicted by Huang et al. The combination of computer models and experiments allows for a better understanding of the structure and more reliable predictions of structures and properties under conditions not reachable in a laboratory setting.

While the elastic properties of glasses strongly depend on the composition of the glasses and the large-scale structure, the viscosity is more dependent on the short-range structural details of glass [1]. Thus, information on the structure of glasses and glass melts can be obtained by examining their flow behavior under applied stresses over a range of temperatures. The viscosity and activation energy for shear flow can be obtained through indentation creep tests at elevated temperatures [30]. Bruckner studied the changes in the structure of glasses caused by temperature and stress when the glasses were drawn into fibers through flow birefringence [31]. The change from elastic behavior below the glass transition temperature to viscoelastic at and above the glass transition temperature corresponds to changes in toughness, elastic moduli, and strength.

Rouxel studied these changes in soda-lime-silicate glasses, characterizing the temperature dependence of the Young's modulus, shear viscosity, and relaxation kinetics to develop a model that predicted at what temperature the glass changed from elastic, brittle behavior to a viscoelastic, ductile behavior [32]. At the ductile-to-brittle transition, soda-lime-silicate glasses show a change in deformation behavior, switching from primarily densification under indentation loading to a mixture of densification and shear flow [33].

Glasses do not all show the same changes in behavior, however, and based on their structural response to temperature they have been divided into strong glasses and fragile glasses. Strong liquids retain a highly connected structure and exhibit slow softening with temperature above their glass transition temperatures. Fragile liquids instead soften extremely quickly above their glass transition temperatures and undergo extensive changes in their structures [1]. The extent of the de-structuration of the glass network shows up in the Poisson's ratio; fragile glasses show a sudden increase in Poisson's ratio above their glass transition temperatures, while for strong glasses the Poisson's ratio remains relatively constant (Fig. 1-1) [18].

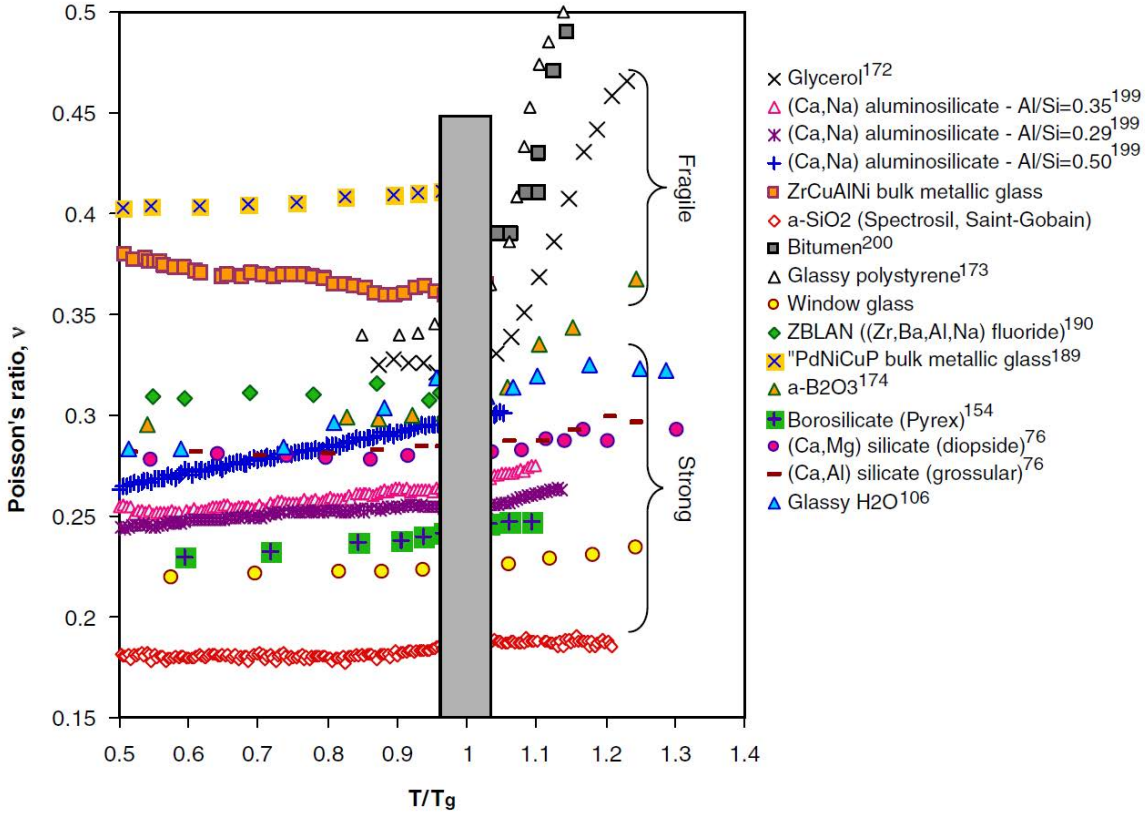

Fig. 2-1. Temperature dependence of Poisson's ratio for different glass systems [18].

It has also been shown that Poisson's ratio (ν) of glasses changes roughly linearly with increasing pressure, but has markedly different slopes depending on the structure or bonding of the systems (Fig. 1-2) [34]. For silica-rich glasses, their Poisson's ratio decreases with increasing pressure, contrary to normal glasses such as soda-lime silicate glass. For various bulk metallic glasses (BMGs) with different values of ν, their ν increases with increasing pressure and their $d\nu/dP$ has a positive value. The different pressure responses of BMGs and oxide glasses reflect their different structures and chemical bondings. For a $Ce_{70}Al_{10}Ni_{10}Cu_{10}$ BMG, so-called metallic plastic, it has markedly different structural and electronic characteristics compared to other BMGs. It shows a

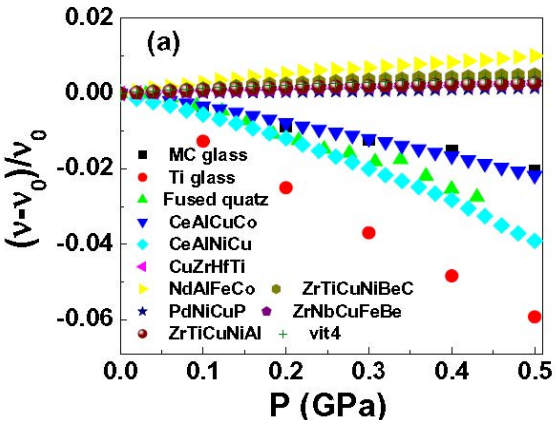

Fig. 2-2. Variation of Poisson's ratio of silicate glasses and BMGs with pressure. [34]

similar response of v under pressure like silica-rich glasses and a negative dv/dP. These results indicate that elastic moduli, and their temperature and pressure dependence, can be used to distinguish the chemical bonding or structure in different glasses.

Hojamberdiev and Stevens recently showed that for soda-lime-silicate glasses, replacement of silicon with larger tetravalent cations (Ti, Zr, or Hf) decreased the indentation recovery at low temperatures (25°C and 100°C) [35]. This decrease corresponded with an increase in Poisson's ratio, which agrees with the findings of Rouxel. It was shown that densification (which is the recovered portion of the deformation caused during indentation) is dominant over shear flow for glasses with low atomic packing densities [36]. Once densification is achieved, further deformation occurs primarily through shear flow. Poisson's ratio was found to be strongly correlated with the magnitude of the densification process. This is an interesting finding, since Poisson's ratio is strictly defined for linear elastic deformations. In a recent review article, Greeves et al. highlighted the importance of the Poisson's ratio for a wide range of materials [37].

Rouxel showed that densified silica, when v increases from 0.15 to 0.25, is capable of shear flow under indentation resulting in pile-ups [38] and found that v is directly correlated with the atomic packing density (C_g) and the glass network dimensionality [18]. An intriguing relation was recently observed in oxide glasses and in metallic glasses [39]: the fracture energy (G) increases with the Poisson's ratio (v), with a sharp brittle-to-ductile (BTD) transition at a critical v_{BTD}=0.31-0.32 (Fig. 1-3). Such a far-from-equilibrium fracture property versus near-equilibrium elastic property relation is unexpected, yet highly beneficial by setting ν as an optimization target to design damage resistant glasses through chemistry and process control.

1.1.4: Glasses with Temperature/Pressure Independent Elastic Moduli

Most glasses have what is called normal behavior. Normal behavior, as the name suggests, is how we expect materials to behave. The stiffness and hardness decrease with increasing temperature and increase with increasing pressure. Anomalous glasses behave in the opposite manner. The most well-known anomalous glass, silica, has anomalous

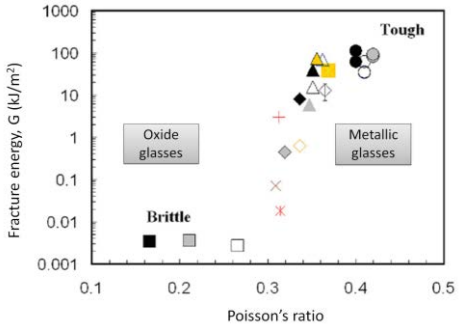

Fig. 2-3. Fracture energy versus Poisson's ratio for oxide glasses and metallic glasses [39].

mechanical behavior. With increased temperature and pressure, they stiffen and soften respectively (Fig. 1-4). Its elastic moduli increase with temperature and tensile strain and decrease with pressure. Silica glass exhibits anomalous behavior with pressure up to 7 GPa before switching to a normal behavior [24].

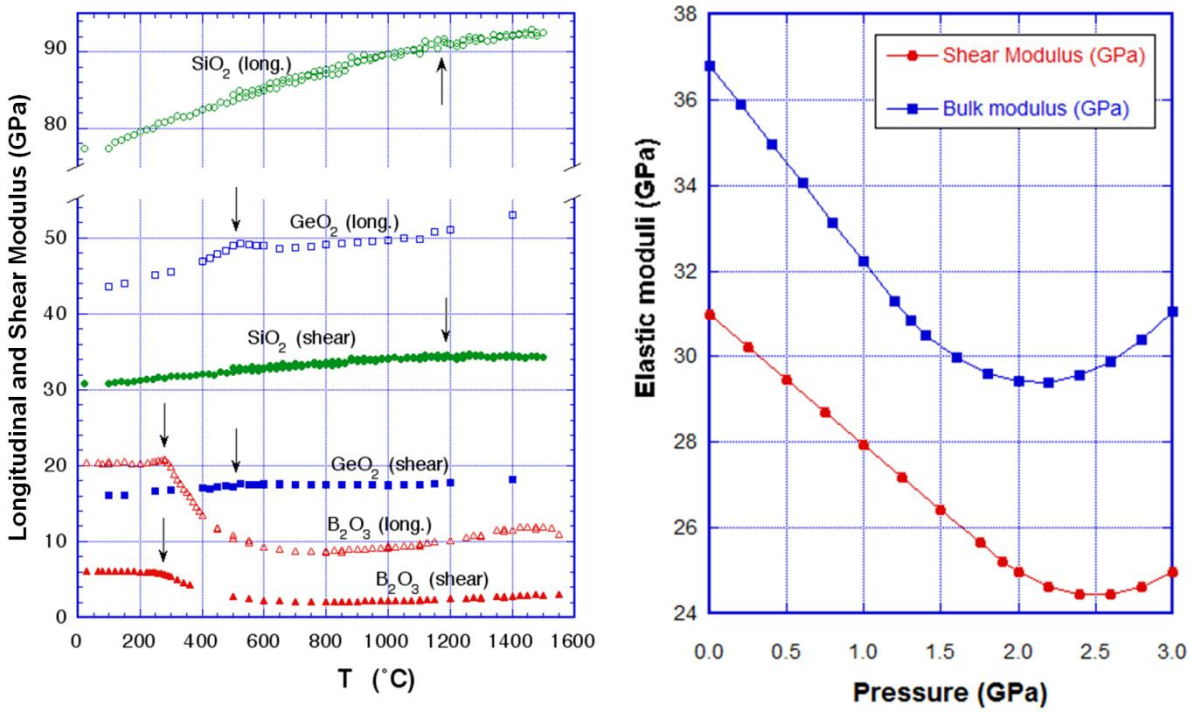

Fig. 2-4. Temperature dependence of longitudinal and shear moduli in silica, boron oxide, and germania glasses (left) [40]. Bulk and shear moduli of silica glass as a function of pressure (right) [41].

Through the addition of other components, anomalous glasses can be made to exhibit normal behavior. In between, intermediate glasses exhibit neither normal nor anomalous behavior, in other words, their elastic moduli don't change with temperature/pressure. These intermediate glasses are of particular interest because of their unique properties. Zhao et al. showed that Na_2O-SiO_2 glasses exhibit temperature independent Young's and shear moduli at 15% Na_2O–85% SiO_2 (Fig. 1-5). The intermediate behavior was shown to arise from two competing structural changes.

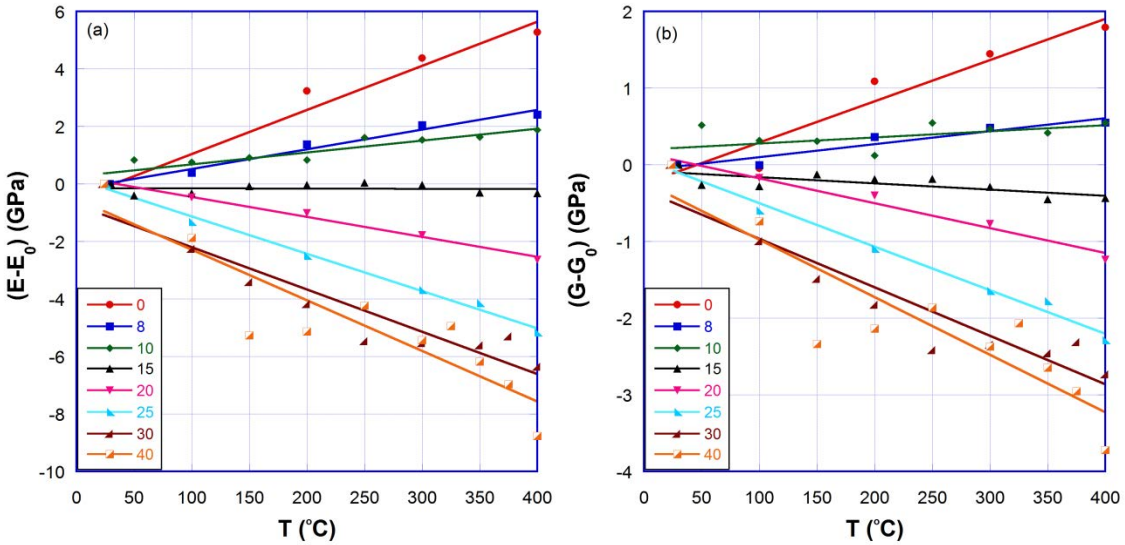

Fig. 2-5. Normalized temperature dependence of Young's modulus (E) (a) and shear modulus (G) (b) for sodium silicate glasses. E_0 and G_0 are the room temperature values. Sodium silicate glasses switch from anomalous to normal behavior with increasing sodium content, with intermediate behavior occurring around 15% Na_2O [19].

Under load, glasses typically deform through a combination of densification and shear flow. Anomalous glasses tend to favor densification and normal glasses favor shear flow. Both kinds of glasses exhibit high brittleness and are readily susceptible to cracking. Sehgal and Ito [42] developed a less brittle glass that exhibits little to no cracking under indentation (Fig. 1-6). When we examined the less brittle glass with Brillouin light scattering over a range of temperatures, its elastic moduli were found to have little response to temperature (Fig. 1-6). During the indentation process, the glass is plastically deformed in an area around the indentation approximately three times the indentation diagonal in radius. In this area, the elastic moduli change in accordance with the behavior type of the glass. Larger strains will cause a decrease in elastic moduli for abnormal glasses, and increase for normal glasses, and will remain constant for intermediate glasses (Fig. 1-7). By examining the elastic constants in less brittle glasses in the area surrounding the indentation, the presence of a relationship between the less brittle behavior and the intermediate behavior can be determined.

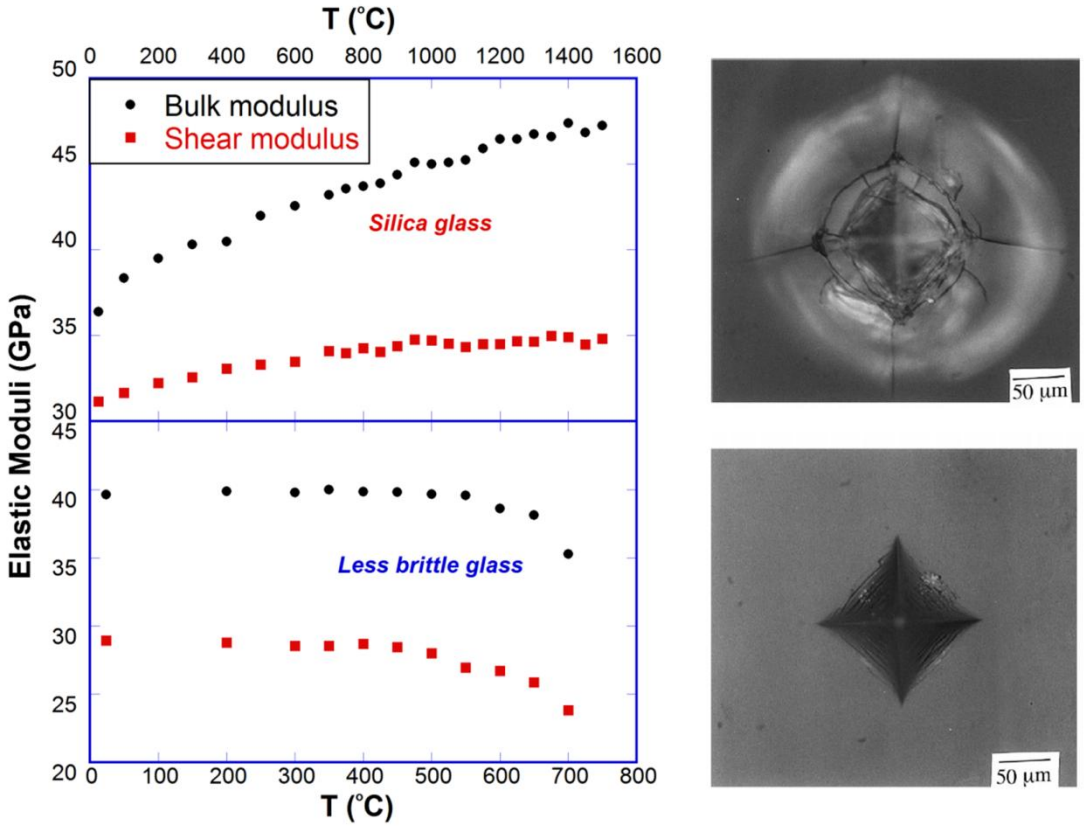

Fig. 2-6. (Left) Elastic moduli of Corning 7980 silica glass and Asahi less brittle glass as a function of temperature. (Right) Indentation pattern of silica glass (top) and less brittle glass (bottom) under 9.8 N load. Silica glass showed large amounts of surface damage and cracking around the indentation site while the less brittle glass with intermediate behavior showed almost no surface damage and no cracking around the indentation site. [42]

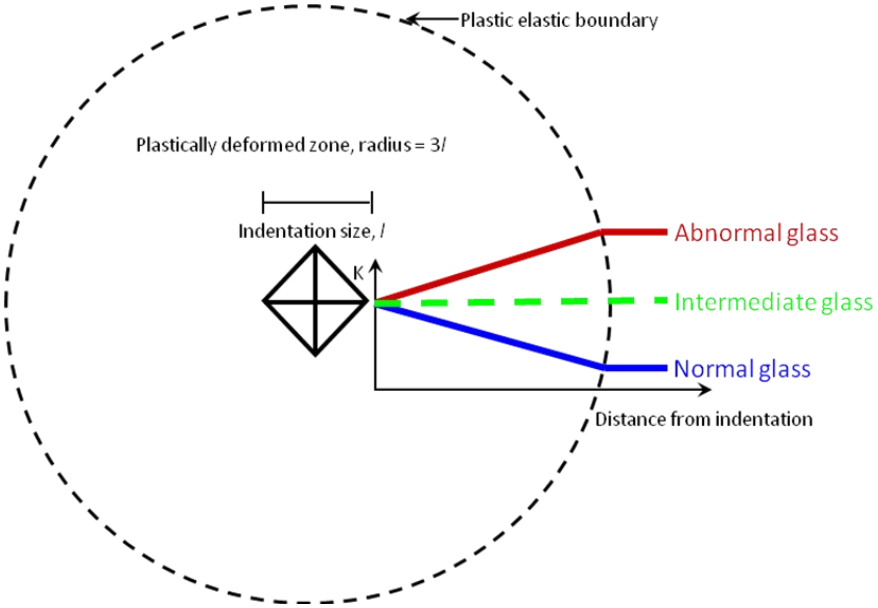

Fig. 2-7. Schematic of a Vicker's hardness indentation. During the indentation, the surrounding glass is plastically deformed up to three times the indentation diagonal. In this indentation region, the bulk modulus increases for abnormal glass, decreases for normal glass, and remains constant for intermediate glass with the distance away from the center of the indentation.

1.2: Silicate Glasses Containing Titania

1.2.1: TiO_2-SiO_2Glasses

Up to 10-12 mol% TiO_2 can be added to silica to form glasses, depending on the method employed to make the glass. The addition of titania to silica has interesting effects on the density, coefficient of thermal expansion, and elastic moduli of glass (detailed below). While the property changes with composition of TiO_2-SiO_2 glasses have been studied extensively [43-50] and numerous studies have been conducted on their structure [40, 51-55], there has been little done to establish satisfactory structure-property relationships that explain why these properties occur.

Ti is a significantly heavier element than Si, and the density of pure TiO_2 is 4.23 g/cm^3. Thus, it might be expected that the density of SiO_2 glass, normally 2.2 g/cm^3, would increase with increasing TiO_2 content. Instead, density measurements show that the density of these glasses remains more or less constant with changing composition (Fig. 1-8) [46, 47, 49]. Possible explanations for this behavior include the larger weight of the titanium being offset by the larger TiO_4 tetrahedron and increases in the free volume [43, 49]. This invariance of the density to

composition has been found only to exist in glasses with up to ~9 mol% TiO_2 concentration, after which the density increases with increasing TiO_2 content [49].

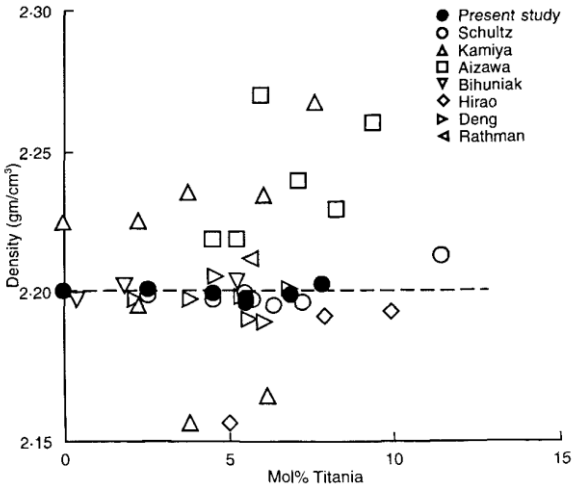

Fig. 2-8. Density of TiO_2-SiO_2 glasses versus TiO_2 content. Density remains constant with increasing concentration for most studies [46].

TiO_2-SiO_2 glasses are well known for their low coefficients of thermal expansion. Increasing concentration of TiO_2 appears to have an inverse, linear relationship with the coefficient of thermal expansion (Fig. 1-9) [45, 47, 49]. This causes the glass to change from normal to anomalous behavior, with the intermediate composition occurring at approximately 5 mol%. Around 10 mol% TiO_2 this trend reverses and the coefficient of thermal expansion increases sharply with increasing TiO_2 content. Kamiya and Sakka suggested that the low coefficients of thermal expansion are related to the presence of 4-coordinated Ti^{4+} ions, as opposed to 6-coordinated Ti^{4+} ions [45]. Other proposed explanations for the decrease in coefficient of thermal expansion include a decrease in the average cation root mean squared displacement due to the increased mass of the Ti^{4+} ions, an increase in the free volume available to oxygen atoms, which allows them to move more with the same change in length, and that the Ti^{4+} increases the number of low frequency modes, which reduces the distortion of the SiO_4 tetrahedra and reduces their thermal expansion [49].

The addition of TiO_2 to silica lowers the elastic moduli without affecting its anomalous behavior. The dependence of the shear wave velocity on pressure was found to be similar in both TiO_2-SiO_2 and pure SiO_2 glasses [44]. Similarly, the dependence of the shear wave speed [44] and of the Young's modulus [49] on temperature was found to be similar for both glasses. Meng et al. found that after a critical pressure was reached, TiO_2-SiO_2 glasses

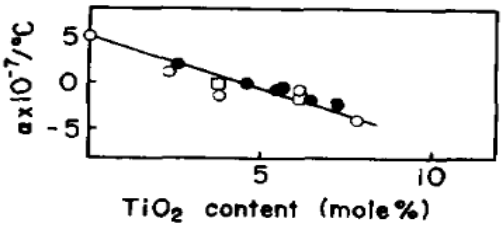

Fig. 2-9. Coefficient of thermal expansion with changing TiO_2 content. Open marks indicate glasses formed through the sol-gel process while black circles indicate glasses formed through flame hydrolysis [45].

transitioned to a normal behavior and their elastic moduli increased with increasing pressure [50]. The pressure needed to affect this transition increased and became partially irreversible at larger TiO_2 contents.

Titania-doped silica glasses have been used in a wide range of applications, including large telescope mirror blanks, windows for space vehicles, sight glasses for high temperature/high pressure chambers for combustion research, liquid halogen trays for linear accelerators, and in optical fibers, couplers, amplifiers and cables [49]. It is of scientific and technological importance to understand whether these thermo-mechanical anomalies share some common structural origins.

1.2.2: Ti Coordination in Silicate Glasses Containing Titania

Titanium atoms generally adopt a six-fold coordination with oxygen in most crystalline silicates [48]. In low Ti concentration silicate glasses, however, Ti^{4+} has been observed to take on a four-fold coordination [52]. Sandstrom et al. reported that for very small concentrations of TiO_2 in SiO_2 (up to 0.05 wt%), Ti^{4+} occupies primarily six-fold coordination sites [51, 53]. At higher concentrations, Ti^{4+} atoms are primarily four-fold coordinated, with a small concentration of them in six-fold coordination. The ratio of six-fold coordinated to four-fold coordinated Ti atoms was found to increase with Ti concentration. Above approximately 9 wt% the Ti^{4+} atoms begin primarily to adopt six-fold coordination again [51]. This unusual four-fold coordination is likely responsible for the unusual properties observed in TiO_2-SiO_2 glasses.

Farges et al. found that in alkali-titanosilicate glasses, Ti^{4+} atoms primarily adopted a five-fold coordination, forming a $(Ti{=}O)O_4$ square pyramid, and the four-fold tetrahedral and six-fold octahedral structures were only present in small quantities [55]. By bonding with both bridging and non-bridging oxygen (NBO) the titanium cations act as both network formers and network modifiers. Similar results were obtained through micro-Raman analysis by Hendersen and Fleet [51]. They observed primarily four-fold coordination with some six-fold coordination in TiO_2-SiO_2 glasses, primarily five-fold coordination in alkali-titania-silica glasses, and a mixture of four-fold and five-fold coordination in alkaline earth-titania-silica glasses.

The precise compositions at which different coordination states of Ti^{4+} occur in the TiO_2-SiO_2 glass system seem to vary depending upon the synthesis method and analysis technique used. Sokolov et al. provided a summary of the different results as well as the Raman positions associated with the different coordination states. Peaks at 900-945 cm^{-1} and 960-1115 cm^{-1}, at

800-860 cm^{-1}, and at 700-750 cm^{-1} were assigned to four-fold, five-fold, and six-fold coordination states, respectively [54]. The 900-945 cm^{-1} and 960-1115 cm^{-1} peaks can be seen in Fig. 1-10 for 8.3 mol% TiO_2 - 91.7 mol% SiO_2 glass synthesized through flame hydrolysis deposition by the Asahi Glass Company in Japan.

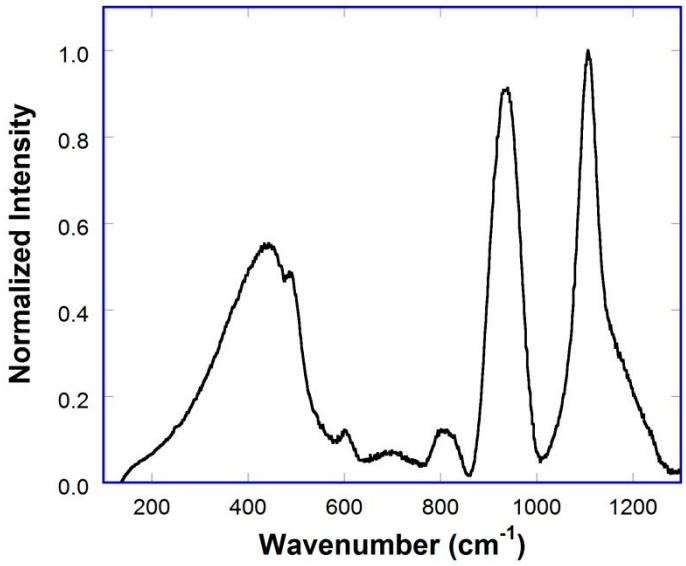

Fig. 2-10. Room temperature Raman spectrum of 8.3 mol% TiO_2–91.7 mol% SiO_2 glasses from the Asahi Glass Company. Peaks at 950 cm^{-1} and ~1100 cm^{-1} correspond to anti-symmetric Ti-O vibrations.

1.2.3: Na_2O-TiO_2-SiO_2 Glasses

Na_2O-TiO_2-SiO_2 glass system has been the subject of considerable study and has been found to possess numerous anomalous properties. TiO_2 also appears to have a different effect on the properties of glass than in the binary TiO_2-SiO_2 system. The coefficient of thermal expansion increases with increasing TiO_2 concentration (Fig. 1-11). The density of the glasses is no longer constant with increasing TiO_2 content, but rather increases [57, 58]. These changes in behavior are likely due to changes in the Ti^{4+} coordination state from four-fold in the binary system to five-fold in the ternary system [51, 54].

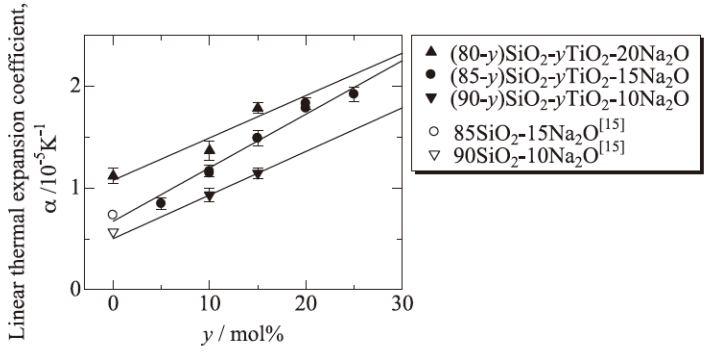

Fig. 2-11. Coefficient of thermal expansion versus TiO_2 content in Na_2O-TiO_2-SiO_2 glasses [56].

The temperature and pressure dependence of elastic moduli of Na_2O-TiO_2-SiO_2 glasses have been studied up to 0.8 GPa and up to 300°C by Manghnani [59]. Glasses studied range from 17.5-30 mol% Na_2O and 20-25 mol% TiO_2. The negative temperature and positive or slightly negative pressure dependence of the elastic moduli were observed. Both temperature and pressure dependence of the bulk modulus decrease in magnitude with decreasing Na_2O, approaching zero for the glasses with 17.5 mol% Na_2O. The temperature dependence of the shear modulus does not seem to change with the Na_2O content, while glasses with 17.5 mol% Na_2O have slightly negative dependence on pressure in shear modulus (Fig. 1-12).

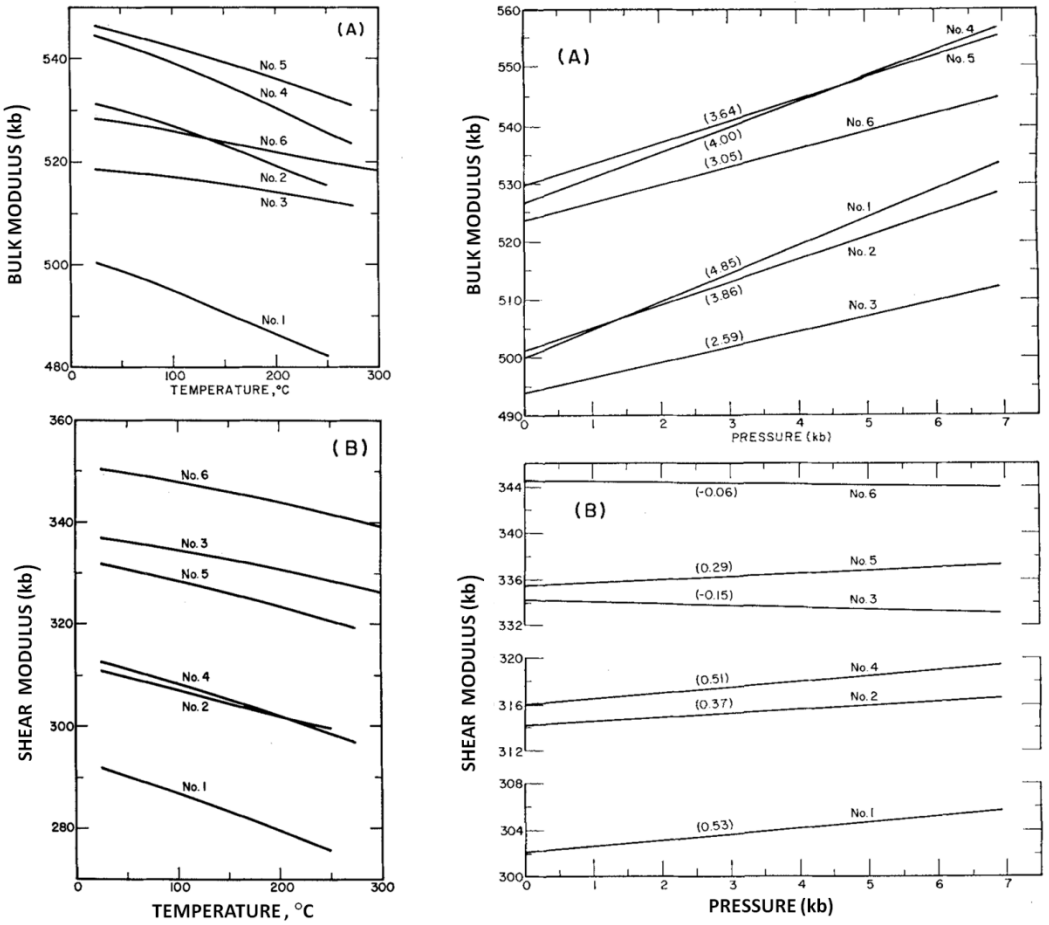

Fig. 2-12. Bulk and shear modulus versus temperature (left) and pressure (right). No. 1: 30 Na_2O - 20 TiO_2 - 50 SiO_2 ; No. 2: 25 Na_2O - 20 TiO_2 - 55 SiO_2; No. 3: 17.5 Na_2O - 20 TiO_2 - 62.5 SiO_2; No. 4: 27.5 Na_2O - 25 TiO_2 - 47.5 SiO_2; No. 5: 22.5 Na_2O - 25 TiO_2 - 52.5 SiO_2; No. 6: 17.5 Na_2O - 25 TiO_2 - 57.5 SiO_2. Compositions are given in mol% [59].

This appears similar to the findings of Zhao et al., where the intermediate elastic behavior was observed in Na_2O-SiO_2 glasses at approximately 15 mol% Na_2O [19]. This trend also

appears to continue at high temperatures. Liu et al. found that the acoustic speeds in Na_2O-TiO_2-SiO_2 liquids at temperatures up to 1800 K remained constant with increasing temperature for glasses with 14.3 and 19 wt% Na_2O [60]. The continuation of the intermediate behavior at high temperature implies that the structural mechanisms responsible continue to function in the high temperature regime, at least for glass melts. Whether these behaviors continue for glasses at higher pressures and temperature, or if there is a point where they revert to normal behavior (such as how silica changes from anomalous to normal behavior at pressures above 7 GPa [24]), remains to be investigated. Na_2O-TiO_2-SiO_2 will also serve as a model system to investigate relationships between the intermediate behavior and the less brittle behavior.

Liu et al. also found that at high temperatures, the Ti component in Na_2O-TiO_2-SiO_2 glasses significantly increased the thermal expansivity and compressibility of the glass melts [60]. This effect was strongest for glasses where the percentage of five-fold coordinated Ti atoms was largest. Their conclusion was that the square pyramid geometry of five-fold coordinated Ti atoms allows for a large number of different configurations in liquids. This is because Ti atoms act as bridges between areas with large numbers of network modifiers (alkalis) and areas with large numbers of network formers (silicon), allowing for a large possible variation in liquid density depending on temperature and pressure. These configurations are not possible at lower temperatures, as seen by the small contribution of TiO_2 to the thermal expansion in glasses.

1.3: Research Goals

In summary, the major goals of my thesis research are:

1) to examine the elastic moduli and their variations induced by external stimuli such as temperature and pressure to study the structure and bonding of glass
2) to examine the deformation and crack initiation behavior around indentations to study whether Poisson's ratio can be used as a determinant parameter for damage resistant glass
3) to examine whether a relationship between the less brittle behavior and the intermediate behavior of glass exists

1.4: References

[1] T. Rouxel, Thermodynamics of viscous flow and elasticity of glass forming liquids in the glass transition range, J. Chem. Phys. 135 (2011) 184501.
[2] L. Wondraczek, J. Mauro, J. Eckert, U. Kuhn, J. Horbach, J. Deubener, T. Rouxel, Towards Ultrastong Glasses, Adv. Mater. 23 (2011) 4578–4586.
[3] B.A. Proctor, I. Whitney, J.W. Johnson, Strength of Fused Silica, Proc. R. Soc. Lond. A. 297 (1967) 534–557.
[4] M. Tomozawa, Stress Corrosion Reaction of Silica Glass and Water, Phys. Chem. Glasses. 39 (1998) 65–69.
[5] A. Makishima, J. Mackenzie, Direct calculation of Young's modulus of glass, J. Non-Cryst. Solids. 12 (1973) 35–45.
[6] A. Makishima, J. Mackenzie, Calculation of Bulk Modulus, Shear Modulus and Poisson's Ratio of Glass, J. Non-Cryst. Solids. 17 (1975) 147–157.
[7] B. Bridge, A model for estimating the bulk modulus of polycomponent inorganic oxide glasses, J. Mater. Sci. 24 (1989) 804–810.
[8] B. Bridge, N. Patel, A model of elastically and anelastically produced temperature derivatives of acoustic wave velocities in inorganic oxide glasses, J. Mater. Sci. 22 (1987) 781–790.
[9] B. Bridge, N. Patel, Correlations between low-temperature ultrasonic relaxation parameters and other physical properties for the oxide glasses, J. Mater. Sci. Lett. 5 (1986) 1255–1257.
[10] B. Bridge, N. Patel, D. Water, On the elastic constants and structure of the pure inorganic oxide glasses, Phys. Status Solidi A. 77 (1983) 655–668.
[11] S. Bhatti, S. Singh, Calculation of Elastic and Thermodynamic Properties of Alkali-Earth Silicate Glasses, Acustica. 65 (1988) 261–263.
[12] K. Annapurna, A. Tarafder, K. Phani, Compositional dependence of ultrasonic velocities in glasses, J. Appl. Phys. 102 (2007) 083542.
[13] S. Iftekhar, J. Grins, M. Eden, Composition-property relationships of the La_2O_3-Al_2O_3-SiO_2 glass system, J. Non-Cryst. Solids. 356 (2010) 1043–1048.
[14] M. Matecki, S. Rogard, C. Ecolivet, Elastic Moduli of halide glasses: experimental determinations and application of the Makishima and Mackensie's theory, Eur. J. Solid State Inorg. Chem. 32 (1995) 483–492.
[15] J. Phillips, Topology of Covalent Non-Crystalline Solids I: Short-range order in chalcogenide Alloys, J. Non-Cryst. Solids. 34 (1979) 153–181.
[16] P. McMillan, B. Poe, P.H. Gillet, B. Reynard, A study of SiO_2 glass and supercooled liquid to 1950 K via high-temperature Raman spectroscopy, Geochim. Cosmochim. Acta. 58 (1994) 3653–3664.
[17] W.H. Wang, The Elastic Properties, Elastic Models and Elastic Perspectives of Metallic Glasses, Prog. Mater. Sci. 57 (2012) 487–656.
[18] T. Rouxel, Elastic Properties and Short-to Medium-Range Order in Glasses, J. Am. Ceram. Soc. 90 (2007) 3019–3039.
[19] Q. Zhao, M. Guerette, G. Scannell, L. Huang, In-situ high temperature Raman and Brillouin light scattering studies of sodium silicate glasses, Journal of Non-Crystalline Solids. 358 (2012) 3418–3426.
[20] M. Smedskjaer, L. Huang, G. Scannell, J. Mauro, Elastic Interpretation of the Glass Transition in Aluminosilicate Liquids, Phys. Rev. B. 85 (2012) 144203.

[21] H. Fukui, M. Kanzaki, N. Hiraoka, X-ray Raman scattering for structural investigation of silica/silicate minerals, Phys. Chem. Miner. 36 (2009) 171–181.
[22] M. Dove, D. Keen, A. Hannon, I. Swainson, Direct measurement of the Si-O bond length and orientation disorder in the high-temperature phase of cristobalite, Phys. Chem. Miner. 24 (1997) 311–317.
[23] V. Prokopenko, L. Dubrovinski, V. Dmitriev, H.-P. Weber, In-situ characterization of phase transitions in cristobalite under high pressure by Raman spectroscopy and X-ray diffraction, J. Alloys Compd. 327 (2001) 87–95.
[24] L. Huang, J. Kieffer, Amorphous-amorphous transitions in silica glass. I. Reversible transitions and thermomechanical anomalies, Phys. Rev. B. 69 (2004) 224203.
[25] L. Huang, J. Kieffer, Amorphous-amorphous transitions in silica glass. II. Irreversible transitions and densification limit, Phys. Rev. B. 69 (2004) 224204.
[26] L. Huang, L. Duffrene, J. Kieffer, Structural transitions in silica glass: thermal-mechanical anomalies and polyamorphism, J. Non-Cryst. Solids. 349 (2004) 1–9.
[27] A. Takada, P. Richet, C. Catlow, G. Price, Molecular dynamics simulation of temperature-induced structural changes in cristobalite, coesite, and amorphous silica, J. Non-Cryst. Solids. 354 (2008) 181–187.
[28] S. Rau, S. Baebler, G. Kasper, G. Weiss, S. Hunklinger, Brillouin Scattering of Vitreous Silica under High Pressure, Ann. Phys. 4 (1995) 91–98.
[29] T. Deschamps, C. Martinet, D. de Ligny, B. Champagnon, Elastic anomalous behavior of silica glass under high pressure: In-situ Raman study, J. Non-Cryst. Solids. 355 (2009) 1095–1098.
[30] C. Bernard, V. Keryvin, J.-C. Sangleboeuf, T. Rouxel, Indentation creep of window glass around glass indentation, Mech. Mater. 42 (2010) 196–206.
[31] R. Bruckner, Structural Aspects of Highly Deformed Glass Melts, J. Non-Cryst. Solids. 95-96 (1987) 961–968.
[32] T. Rouxel, J.-C. Sangleboeuf, The brittle to ductile transition in a soda-lime-silica glass, J. Non-Cryst. Solids. 271 (2000) 224–235.
[33] H. Shang, T. Rouxel, M. Buckley, C. Bernard, Viscoelastic behavior of soda-lime-silica glass in the 293-933 K range by micro-indentation, J. Mater. Res. 21 (2006) 632–638.
[34] X. Liu, R. Wang, W. Wang, Poisson's ratio of metallic glasses under pressure and low temperature, Scr. Mater. 62 (2010) 254–257.
[35] M. Hojamberdiev, H. Stevens, Indentation recovery of soda-lime silicate glasses containing titania, zirconia, and hafnia at low temperatures, Mater. Sci. Eng., A. 532 (2012) 456–461.
[36] T. Rouxel, H. Ji, T. Hammouda, A. Moreac, Poisson's Ratio and the densification of glass under high pressure, Phys. Rev. Lett. PRL 100 (2008) 225501.
[37] G. Greaves, A. Greer, R. Lakes, T. Rouxel, Poisson's Ratio and Modern Materials, Nat. Mater. 10 (2011) 823–837.
[38] T. Rouxel, H. Ji, J. Guin, F. Augereau, B. Ruffle, Indentation Deformation Mechanism in Glass: Densification versus Shear Flow, J. Appl. Phys. 107 (2010) 094903.
[39] J. Lewandowski, W. Wang, A. Greer, Intrinsic Plasticity or Brittleness of Metallic Glasses, Philos. Mag. Lett. 85 (2005) 77–87.
[40] R. Youngman, J. Kieffer, J. Bass, L. Duffrene, Extended structural integrity in network glasses and liquids, J. Non-Cryst. Solids. 222 (1997) 190–198.

[41] K. Kondo, S. Lio, A. Sawaoka, Nonlinear pressure dependence of the elastic moduli of quartz up to 3 GPa, J. Appl. Phys. 52 (1981) 2826–2831.
[42] J. Sehgal, S. Ito, Brittleness of glass, J. Non-Cryst. Solids. 253 (1999) 126–132.
[43] J. Shelby, Fictive Temperature and Density of Doped Vitreous Silica, Phys. Chem. Glasses: Eur. J. Glass Sci. Technol., Part B. 50 (2009) 7–14.
[44] P. Andreatch, H. McSkimin, Pressure dependence of ultrasonic wave velocities and elastic stiffness moduli for a TiO_2-SiO_2 glass (Corning 7971), J. Appl. Phys. 47 (1976) 1299–1301.
[45] K. Kamiya, S. Sakka, Thermal Expansion of TiO_2-SiO_2 and TiO_2-GeO_2 glasses, J. Non-Cryst. Solids. 52 (1982) 357–363.
[46] J. Shelby, Density of TiO_2-doped vitreous silica, Phys. Chem. Glasses. 46 (2005) 494–499.
[47] Z. Deng, E. Breval, C. Pantano, Colloidal sol/gel processing of ultra-low expansion TiO_2-SiO_2 glasses, J. Non-Cryst. Solids. 100 (1988) 364–369.
[48] J. Arndt, Densification of glasses of the system TiO_2-SiO_2 bulk glasses and fibers, Physics and Chemistry of Glasses. 24 (1983) 104–110.
[49] S. Gulati, Mechanical Properties of SiO_2 vs. SiO_2-TiO_2 Bulk Glasses and Fibers, Mat. Res. Soc. Symp. Proc. 244 (1992) 67–83.
[50] Y. Meng, M. Manghnani, L. Ming, Investigation on the elastic behavior of TiO_2-SiO_2 glasses under high pressure using Brillouin scattering, Eos. 68 (1987) 1470.
[51] G. Henderson, M. Fleet, The structure of Ti silica glasses by micro-Raman spectroscopy, Can. Mineral. 33 (1995) 399–408.
[52] H. Chandrasekhar, M. Chandrasekhar, M. Manghnani, Phonons in TiO_2-SiO_2 glasses, J. Non-Cryst. Solids. 40 (1980) 567–575.
[53] D. Sandstrom, F. Lytle, P. Wei, R. Greegor, J. Wong, P. Schultz, Coordination of Ti in TiO_2-SiO_2 glass by X-ray absorption spectroscopy, J. Non-Cryst. Solids. 41 (1980) 201–207.
[54] V. Sokolov, V. Plotnichenko, E. Dianov, Quantum-Chemical Modeling of Titanium Centers in Titanosilicate Glass, Inorg. Mater. 42 (2006) 1273–1288.
[55] F. Farges, G. Brown, A. Navrotsky, H. Gan, J. Rehr, Coordination chemistry of Ti(IV) in silicate glasses and melts: II. Glasses at ambient temperature and pressure, Geochim. Cosmochim. Acta. 60 (1996) 3039–3053.
[56] Y. Kobayashi, S. Shimizu, S. Miyashita, R. Endo, M. Susa, Determination of refractive indices and linear coefficients of thermal expansion of silicate glasses containing titanium oxides, ISIJ Int. 51 (2011) 186–192.
[57] R. Johnston, C. Babcock, Composition dependence of elastic moduli in Na_2O-TiO_2-SiO_2 glasses, J. Am. Ceram. Soc. 58 (1975) 85–87.
[58] E. Hamilton, G. Cleek, Properties of sodium titanium silicate glasses, J. Res. Natl. Bur. Stand. (U.S.). 61 (1958) 89–94.
[59] M. Manghnani, Pressure and Temperature dependence of the elastic moduli of Na_2O-TiO_2-SiO_2 glasses, J. Am. Ceram. Soc. 55 (1972) 360–365.
[60] Q. Liu, R. Lange, Y. Ai, Acoustic velocity measurements on Na_2O-TiO_2-SiO_2 liquids: Evidence for a highly compressible TiO_2 component related to five-coordinated Ti, Geochim. Cosmochim. Acta. 71 (2007) 4314–4326.

Chapter 2 : Structure and Thermo-mechanical Response of TiO_2-SiO_2 Glasses to Temperature

2.1: Abstract

Structure and elastic moduli of $xTiO_2$ - (1-x) SiO_2 (x=0-10 mol%) glasses prepared via the sol-gel process have been investigated through *in-situ* high temperature Raman and Brillouin light scattering from room temperature to 1200 °C. Three other synthetic glasses prepared by the flame hydrolysis deposition (FHD) process, namely, synthetic silica glass (Corning 7980) and two titania silicate glasses (x=5.4 and 8.3), were also examined under the same conditions. The coefficients of thermal expansion of sol-gel glasses were measured up to 800 °C. Differences in properties of sol-gel glasses, FHD glasses, and literature values are presented and discussed. Changes in elastic moduli and Raman peak positions with composition and temperature are discussed. Young's modulus, bulk modulus, and shear modulus were found to decrease with increasing TiO_2 content and increase with temperature. A possible explanation for the anomalies in TiO_2-SiO_2 glasses is suggested based on the response of elastic moduli, Raman spectra, and coefficients of thermal expansion to temperature.

2.2: Introduction

Titania is added to silica to produce ultra-low expansion (ULE) glasses, i.e., glasses that have zero or even negative coefficient of thermal expansion (CTE) at room temperature [1,2]. This unique characteristics has made them very useful in many applications, such as machine tool reference blocks, mirror blanks for telescopes and space satellites, and mask substrates for extreme ultra-violet lithography (EUVL) in the semiconductor industry [3]. However, the role titanium plays in the glass structure to give the ultra-low CTE is still under much speculation despite the extensive studies in the past few decades [1,2,4, and 5].

This chapter has been submitted to: G. Scannell, A. Koike, L. Huang, Structure and Thermo-mechanical response of TiO_2-SiO_2 glasses to temperature, J. Non-Cryst. Solids, (2016).

In addition, other properties of titania silicate glasses have been found to behave anomalously with increasing TiO_2 content. Shelby showed that the density is almost independent of the TiO_2 content below 10 wt% (7.7 mol%) TiO_2, while the sensitivity of density to fictive temperature increases with increasing TiO_2 [6,7]. An anomalous response of transverse sound velocity to temperature has been shown in several titania silicate glasses from 0 to 300 K, where a minimum occurs around 80 K, above which it increases with increasing temperature [8]. Young's modulus and Poisson's ratio were shown to increase with temperature from room temperature to 900 °C for Corning 7971 ULE™ glass [9]. Young's modulus, bulk modulus and shear modulus of a TiO_2-SiO_2 glass with 8.4 wt% of TiO_2 were observed to decrease with pressure up to 2 GPa [10]. It has been suggested that the anomalous response of elastic moduli to temperature is connected to low thermal expansion of titania silicate glasses [8].

The structure of TiO_2-SiO_2 glasses has been studied frequently over the last several decades. Sandstrom et al. examined the glasses through extended X-ray absorption fine structure (EXAFS) and X-ray absorption near edge spectroscopy (XANES) to measure the coordination of Ti in the glass [11]. They showed that Ti^{4+} occupies primarily four-fold coordination, with a small concentration of six-fold coordinated atoms. More recent XANES experiments by Henderson et al. [12] showed that Ti^{4+} actually occupies five-fold coordinated sites at concentrations below 3.6 wt% with further additions of Ti occupying primarily four-fold coordinated sites. Chandrasekhar et al. [13] examined TiO_2-SiO_2 glasses through infrared (IR) and Raman spectroscopy. Henderson and Fleet provided a more detailed Raman peak analysis [14] for a variety of TiO_2 containing glasses. The structure of TiO_2-SiO_2 glasses has also been studied through neutron diffraction by Pickup et al. [15], and through quantum-chemical calculations by Sokolov et al., who estimated their vibrational frequencies, IR and Raman spectra [16]. These structural studies have generally been in agreement about the behavior of Ti^{4+} cations in the glass at room temperature. They replace Si^{4+} cations in the glass structure, initially with a higher coordinated state, either five- or six-fold. After approximately 2 mol%, Ti^{4+} becomes primarily four-fold coordinated until it phase separates into six-fold coordinated crystals above 10 mol%. To date, the structure of TiO_2-SiO_2 glasses under conditions other than ambient has been much less well studied.

In order to understand the role of TiO_2 in silica glass, particularly, to gain a fundamental understanding of the anomalous thermal and elastic responses to temperature from the structure

point of view, it is helpful to examine how the structure of the glass changes over a large composition and temperature range. In this study, we examined TiO_2-SiO_2 glasses from 0 - 10 mol% TiO_2 produced through the sol-gel process and three synthetic glasses with 0, 5.4, and 8.3 mol% TiO_2 prepared by the flame hydrolysis deposition (FHD) process by using *in-situ* high temperature Raman and Brillouin light scattering from room temperature to 1200 °C. Density and CTE up to 800°C of these glasses were also measured. Glasses produced through the sol-gel method are compared to other synthetic glasses by FHD in terms of density, thermal expansion, elastic moduli, and Raman spectra. Correlations are drawn between changes in Raman peak shifts with temperature, and changes in responses of elastic moduli and thermal expansion to temperature. A possible explanation for the anomalous responses of TiO_2-SiO_2 glasses to temperature is suggested.

2.3: Methods

TiO_2-SiO_2 glasses were synthesized through the sol-gel process over the range of 0-10 mol% TiO_2, based on the procedure used by Huang et al. [17]. Tetraethyl orthosilicate (TEOS) and titanium butanate were used as the silica source and the titania source, respectively. Methanol was used as the solvent, water and 0.1 M hydrochloric acid were used as catalysts for the hydrolysis process, and dimethyl formamide (DMF) was used as a drying control agent. Molar ratios of chemicals are 1: 12.8: 0.0025: 4.75: 0.85 for alkoxides: methanol: HCl: H_2O: DMF. Methanol and TEOS were mixed together, then the HCl and about half of the water were added to start the hydrolysis process. Titanium butanate was added dropwise with continuous stirring. Then the second portion of the water was added along with the DMF. The sol was stirred for approximately 30 minutes before being transferred to sample molds (plastic tubes with caps). The sols were gelled for one day at room temperature and then three days at 60°C. The gelled samples were removed from the molds and soaked in methanol for three days to remove any remaining water.

After soaking, the gels were dried under atmospheric conditions for one week. They were then heated at 60 °C for three days to remove any remaining methanol/water. The dried gels were sintered in a programmable tube furnace from room temperature to 1100 °C through the following steps: ramp from room temperature to 70 °C at 1.5 °C/min; dwell at 70 °C for 60 minutes; ramp from 70 °C to 150 °C at 0.5 °C/min; dwell at 150 °C for 120 minutes; ramp from

150 °C to 200 °C at 0.2 °C/min; dwell at 200 °C for 120 minutes; ramp from 200 °C to 300 °C at 0.1 °C/min; dwell at 300 °C for 60 minutes; ramp from 300 °C to 350 °C at 0.2 °C/min; ramp from 350 °C to 400 °C at 0.5 °C/min; ramp from 400 °C to 700 °C at 1.0 °C/min; dwell at 700 °C for 240 minutes; ramp from 700 °C to 900 °C at 0.5 °C/min; ramp from 900 °C to 1100 °C at 6.0 °C/min; dwell at 1100 °C for 20 minutes; cool to room temperature in the furnace. Between 150 °C and 700 °C oxygen was flowed through the tube furnace at a rate of 60 ml/min to facilitate the decomposition of residual organics in the glass. Through this process cylindrical, bulk glass samples of up to 20 mm in length and 3 mm in diameter were prepared. As a reference, commercial synthetic silica glass (Corning 7980) and two TiO_2-SiO_2 glasses (x=5.4 and 8.3) prepared by FHD were used. The commercial synthetic silica glass was produced by the direct deposition of combusted silica precursor to transform into glass boule. On the other hand, TiO_2-SiO_2 glasses in this study were prepared through soot process. Fine soot particles of TiO_2-SiO_2 were produced by hydrolysis of gaseous silicon tetrachloride and titanium tetrachloride in oxygen-hydrogen flame. The porous soot preform was heat-treated at 1200 °C for 3 h in air, at 1400 °C for 4 h in vacuum, and at 1700 °C for 4 h in vacuum. Then, the glasses were annealed at 1100 °C for x=5.4 and 1040 °C for x=8.3.

Density of samples was measured through the Archimedes method, using water as the liquid medium. Each sample was measured ten times, resulting in standard deviations between 0.005 and 0.01 g/cm^3. Sintered sol-gel samples have densities between 2.15 and 2.18 g/cm^3, very close to the values of TiO_2-SiO_2 glasses prepared through other methods [6-8], but lower than the 2.20 g/cm^3 of other synthetic glasses produced by FHD that were measured using the same method. Shelby [6] summarized densities of TiO_2-SiO_2 glasses from eight studies, where the majority of measured values are between 2.19-2.21 g/cm^3 with the rest between 2.15 and 2.28 g/cm^3. Densities of TiO_2-SiO_2 glasses prepared through the sol-gel process have been reported in the range of 2.10 to 2.36 g/cm^3 [15], so the densities of our sol-gel samples seem reasonable, if generally slightly low.

Electron microprobe analysis (EMPA) was used to determine the composition and the homogeneity of four sol-gel TiO_2-SiO_2 glasses. Quartz and rutile were used as the Si and Ti references, respectively. Compositions were measured at 40 points across the surface for each sample. Nominal compositions, measured compositions, and standard deviations are shown in

Table 2-1. Compositions are within 0.3 mol% of the nominal values, and have standard deviations of 0.04 mol% or less.

Table 2-1. Compositions and standard deviations (in mol%) of TiO_2-SiO_2 sol-gel glasses.

Sample	SiO_2	SiO_2 Std	TiO_2	TiO_2 Std
4 TiO_2 - 96 SiO_2	96.28	0.026	3.72	0.026
5.4 TiO_2 - 94.6 SiO_2	94.51	0.039	5.49	0.039
8.3 TiO_2 - 91.7 SiO_2	91.68	0.034	8.32	0.034
10 TiO_2 - 90 SiO_2	90.23	0.043	9.77	0.043

Fourier transform infrared spectroscopy (FTIR) was used to measure the water content in the glasses produced through the sol-gel process (Table 2-2). Hydroxyl concentrations were determined using the Beer-Lambert law, following procedures used in literature [18-20]. The water content in our sol-gel glasses is more than 2000 ppm, higher than that in Corning 7980 (800 ppm) and much higher than that in TiO_2-SiO_2 glasses (50 ppm) by FHD.

Table 2-2 OH content in three FHD synthetic glasses and two sol-gel glasses. Values for FHD synthetic glasses are the published values.

Material	OH content (ppm)
Synthetic silica glass by direct deposition	800
5.4 TiO_2 - 94.6 SiO_2 by soot process	50
8.3 TiO_2 - 91.7 SiO_2 by soot process	50
5.4 TiO_2 - 94.6 SiO_2 by sol-gel	2250
8.3 TiO_2 - 91.7 SiO_2 by sol-gel	2965

In-situ high temperature Raman spectra and Brillouin spectra were collected using the procedure described by Guerette and Huang [21]. A 532.18 nm Verdi V2 DPSS green laser was used as the probing light source. Brillouin measurements were collected every 100 °C from room temperature to 1200 °C. Spectra were collected until the longitudinal peak from the emulated platelet geometry reached a minimum of 600 counts to ensure a good peak fit. Raman spectra were collected every 100 °C from room temperature up to 800 °C. Raman spectra were averaged over six 50 second collections. Above 800 °C, the thermal background becomes more and more significant with increasing temperature, and peaks become increasingly more difficult to be determined.

Elastic moduli and Poisson's ratio were calculated from the sound velocities measured through Brillouin light scattering and the density of the glasses using Equations 2-(1-4).

$$E = \rho V_T^2(3V_L^2-4V_T^2)/(V_L^2-V_T^2) \quad (2\text{-}1)$$

$$\mu = \rho V_T^2 \quad (2\text{-}2)$$

$$\nu = (V_L^2-2V_T^2)/2(V_L^2-V_T^2) \quad (2\text{-}3)$$

$$K = E/(3(1-2\nu)) \quad (2\text{-}4)$$

where V_L and V_T are longitudinal and transverse sound velocities, ρ is sample density, E is Young's modulus, μ is shear modulus, ν is Poisson's ratio, K is bulk modulus. Standard deviations for Brillouin light scattering experiments at room temperature have been reported at 0.2 to 0.5 GPa for glasses of different compositions [21-23]. No error bars are presented for high temperature experiments as only one sample was measured for each composition.

The thermal expansion of several sol-gel samples were measured using a dilatometer between room temperature and 800 °C at a rate of 4 °C/min.

2.4: Results:

Elastic moduli of TiO_2-SiO_2 glasses at room temperature are shown in Fig. 2-1. In FHD synthetic glasses, Young's modulus, bulk modulus, and shear modulus decrease with increasing TiO_2 content. Sol-gel glasses follow this trend, but tend to have slightly lower values than FHD synthetic glasses, with the difference being larger at low content of TiO_2.

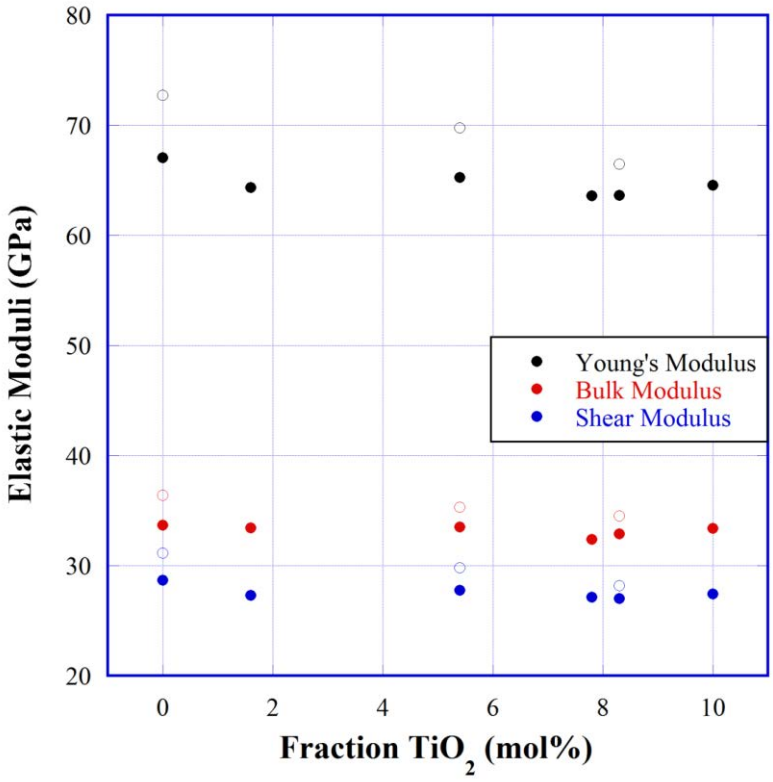

Fig. 2-1. Elastic moduli of TiO_2-SiO_2 glasses with respect to the TiO_2 content. Solid symbols represent values of sol-gel glasses, while open circles are for FHD synthetic glasses.

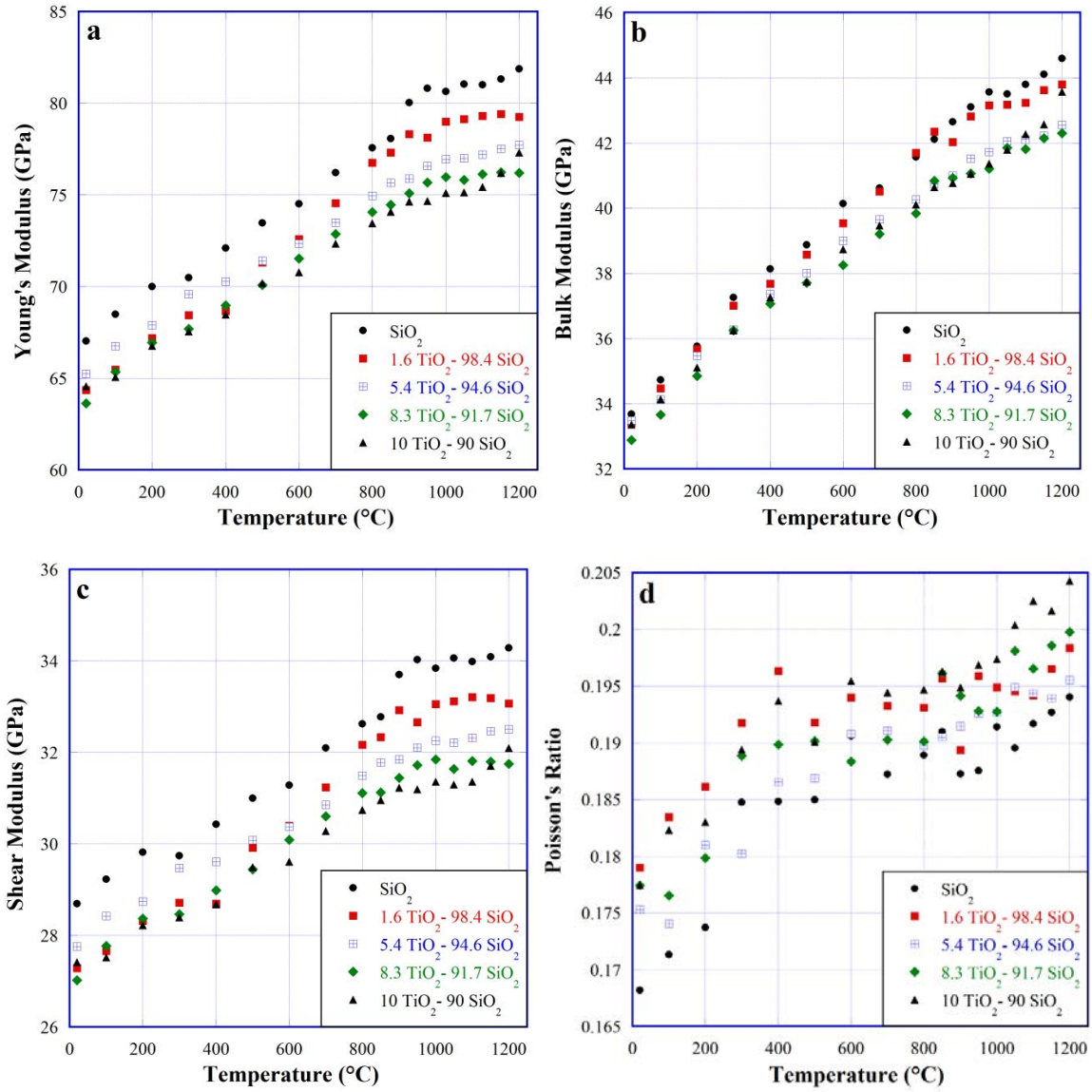

Fig. 2-2. Change of a) Young's modulus, b) bulk modulus, c) shear modulus, and d) Poisson's ratio with temperature for TiO_2-SiO_2 glasses produced through the sol-gel process.

Response of elastic moduli to temperature for sol-gel glasses and TiO_2-SiO_2 glasses by FHD are presented in Figs. 2-2 and 2-3. For sol-gel glasses, the Young's modulus changes from 66 GPa to 78 GPa for SiO_2 glass and from 64 GPa to 74 GPa for 10 TiO_2 - 90 SiO_2 when heated from room temperature to 800 °C. Values for bulk modulus are much closer, with SiO_2 and 10 TiO_2 - 90 SiO_2 differing by less than 1 GPa at room temperature, and by 2 GPa at 800 °C. Shear modulus differs by 2 GPa at both room temperature and at 800 °C. Change in elastic modulus with temperature is calculated from a least-squares linear fit to curves in Figs. 2-2 and 2-3(a)-(c)

from room temperature to 800 °C and summarized in Table 2-3. The temperature dependence of Young's modulus generally decreases with increasing TiO_2. Temperature dependence of the bulk modulus shows a decrease between 1.6 TiO_2 and 5.4 TiO_2, but not between SiO_2 and 1.6 TiO_2 or between 5.4 TiO_2 and 10 TiO_2. Change in the temperature dependence of the shear modulus is less than the noise between samples. Overall, elastic moduli appear to have a slightly reduced anomalous response to temperature with increasing TiO_2 content.

Table 2-3. Change of elastic modulus with respect to temperature between 23 °C and 800 °C.

Composition	d(ΔE)/dT (GPa/100 °C)	d(ΔK)/dT (GPa/100 °C)	d(Δμ)/dT (GPa/100 °C)
SiO_2	1.35	1.03	0.47
1.6 TiO_2 - 98.4 SiO_2, sol-gel	1.47	1.04	0.54
5.4 TiO_2 - 94.6 SiO_2, sol-gel	1.21	0.89	0.46
8.3 TiO_2 - 91.7 SiO_2, sol-gel	1.29	0.92	0.51
10 TiO_2 - 90 SiO_2, sol-gel	1.09	0.88	0.39
Synthetic silica, FHD	1.05	0.86	0.38
5.4 TiO_2 - 94.6 SiO_2, FHD	1.08	0.98	0.37
8.3 TiO_2 - 94.6 SiO_2, FHD	0.81	0.79	0.27

Poisson's ratio increases by approximately 0.01 with the addition of 10 mol% TiO_2. The change in Poisson's ratio with temperature appears constant across all compositions (increase by 0.025 from room temperature to 1200 °C). An interesting feature is that in the range of 400 - 800 °C Poisson's ratio appears to remain constant with increasing temperature for sol-gel TiO_2-SiO_2 glasses (Fig. 2(d)). This is unexpected and does not appear in the FHD synthetic glasses (Fig. 3(d)).

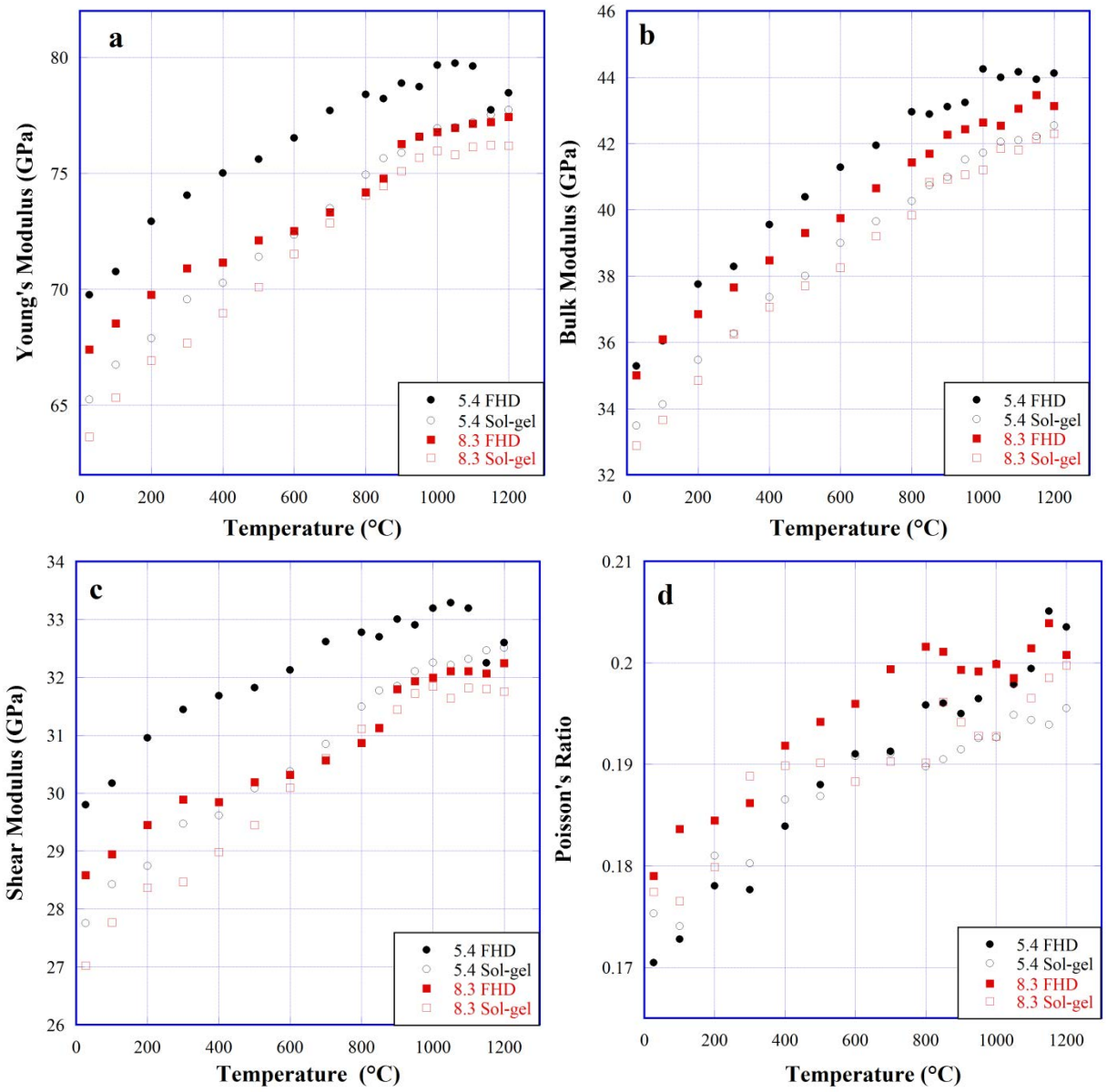

Fig. 2-3. Change of a) Young's modulus, b) bulk modulus, c) shear modulus, and d) Poisson's ratio with temperature for sol-gel and FHD synthetic TiO_2-SiO_2 glasses.

Raman spectra of sol-gel and FHD synthetic glasses at room temperature are shown in Fig. 2-4. Intensities were normalized to the maximum of the 450 cm^{-1} peak. Peak positions are reported in Table 2-4 with those of synthetic silica glass, and 5.4 TiO_2 and 8.3 TiO_2 FHD synthetic glasses included as references. Peak positions of the sol-gel glasses agree quite well with FHD synthetic samples. The 450 cm^{-1} peak and peaks in the 900-1200 cm^{-1} range have been shown to be sensitive to sintering temperature, with the 450 cm^{-1}, 1060 cm^{-1}, 1100 cm^{-1},

and 1200 cm^{-1} peaks shifting to higher frequencies with increasing sintering temperature (thus, increasing density) and the 950 cm^{-1} peak shifting to lower frequencies with increasing sintering temperature [24].

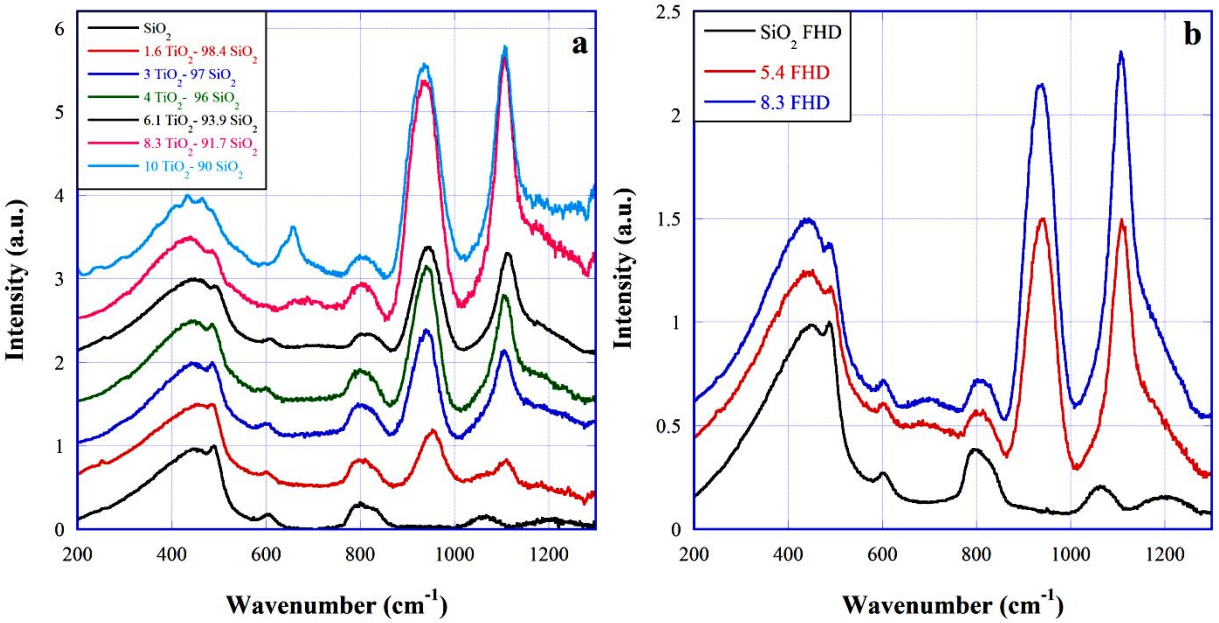

Fig. 2-4. Room temperature Raman spectra of a) sol-gel and b) FHD synthetic glasses. Spectra intensity was frequency corrected and normalized to the intensity of the 450 cm^{-1} peak. Spectra are offset vertically for clarity.

Changes in intensity of Raman peaks in sol-gel TiO_2-SiO_2 glasses at room temperature in Fig. 2-4(a) are similar to those observed in FHD synthetic glasses in Fig. 2-4(b) and in literature [14,24]. With the addition of TiO_2, two new peaks appear at ~950 cm^{-1} and at ~1100 cm^{-1}. The intensity of these peaks increases with TiO_2 content. Peaks at ~1060 cm^{-1} and 1200 cm^{-1} remain visible with 1.6 mol% TiO_2, but become indiscernible above 3 mol% TiO_2 as the ~1100 cm^{-1} peak grows in intensity. A peak at ~650-700 cm^{-1} appears in 6.1, 8.3, and 10 mol% TiO_2 sol-gel glasses and in both FHD synthetic glass. Most of the peak positions in the 8.3 mol% TiO_2 sol-gel sample are lower than those in the FHD synthetic sample of the same composition, suggesting that the sol-gel sample did not densify fully during the sintering process. The 10 TiO_2 sol-gel sample shows several small peaks in the 400-700 cm^{-1} range. This sample is uniformly clear and transparent, so these peaks are likely due to slight crystallization of both rutile and anatase phases [14].

Table 2-4. Positions of Raman peaks at room temperature in sol-gel and FHD synthetic glasses.

Peak (cm^{-1})	SiO_2	1.6 TiO_2 98.4 SiO_2	3 TiO_2 97 SiO_2	4 TiO_2 96 SiO_2	6.1 TiO_2 93.9 SiO_2	8.3 TiO_2 91.7 SiO_2	10 TiO_2 90 SiO_2	FHD silica	FHD 5.4 TiO_2	FHD 8.3 TiO_2
450	450	456	450	443	449	436	437	449	443	442
490	490	485	485	481	492	486	484	491	490	488
600	605	601	599	600	609	-	-	604	601	602
665	-	-	-	-	-	683	656	-	695	702
800	801	802	798	796	810	803	804	794	806	809
950	-	953	944	938	942	936	936	-	939	936
1060	1062	-	-	-	-	-	-	1061	-	-
1100	-	1110	1108	1106	1112	1106	1105	-	1108	1107
1200	1203	-	-	-	-	-	-	1200	-	-

In-situ high temperature Raman spectra from room temperature to 800 °C are shown in Fig. 2-5 for sol-gel glasses. For sol-gel SiO_2 in Fig. 2-5(a), peak shifts are quite small with increasing temperature, in good agreement with previous studies in literature [21, 25]. The 450 cm^{-1} peak shifts slightly toward higher frequencies, while the 490, 605, 1060, and 1200 cm^{-1} peaks shift toward lower frequencies. The 800 cm^{-1} peak does not appear to move with increasing temperature. With the addition of TiO_2, the change in peak position with temperature increases for the majority of peaks. The shift in the 450 cm^{-1} peak increases with increasing TiO_2 content. The 490 cm^{-1} and 605 cm^{-1} peaks show little change in their temperature response with the addition of TiO_2. The 800 cm^{-1} peak initially remains insensitive to temperature with the addition of up to 4 mol% TiO_2, but at higher TiO_2 contents shows a significant shift to lower frequencies. The two new high frequency peaks that appear at 950 and 1100 cm^{-1} with the addition of TiO_2 show a much stronger temperature dependence than the 1060 and 1200 cm^{-1} SiO_2 peaks, shifting by ~30 cm^{-1} and ~20 cm^{-1} to lower frequency, respectively.

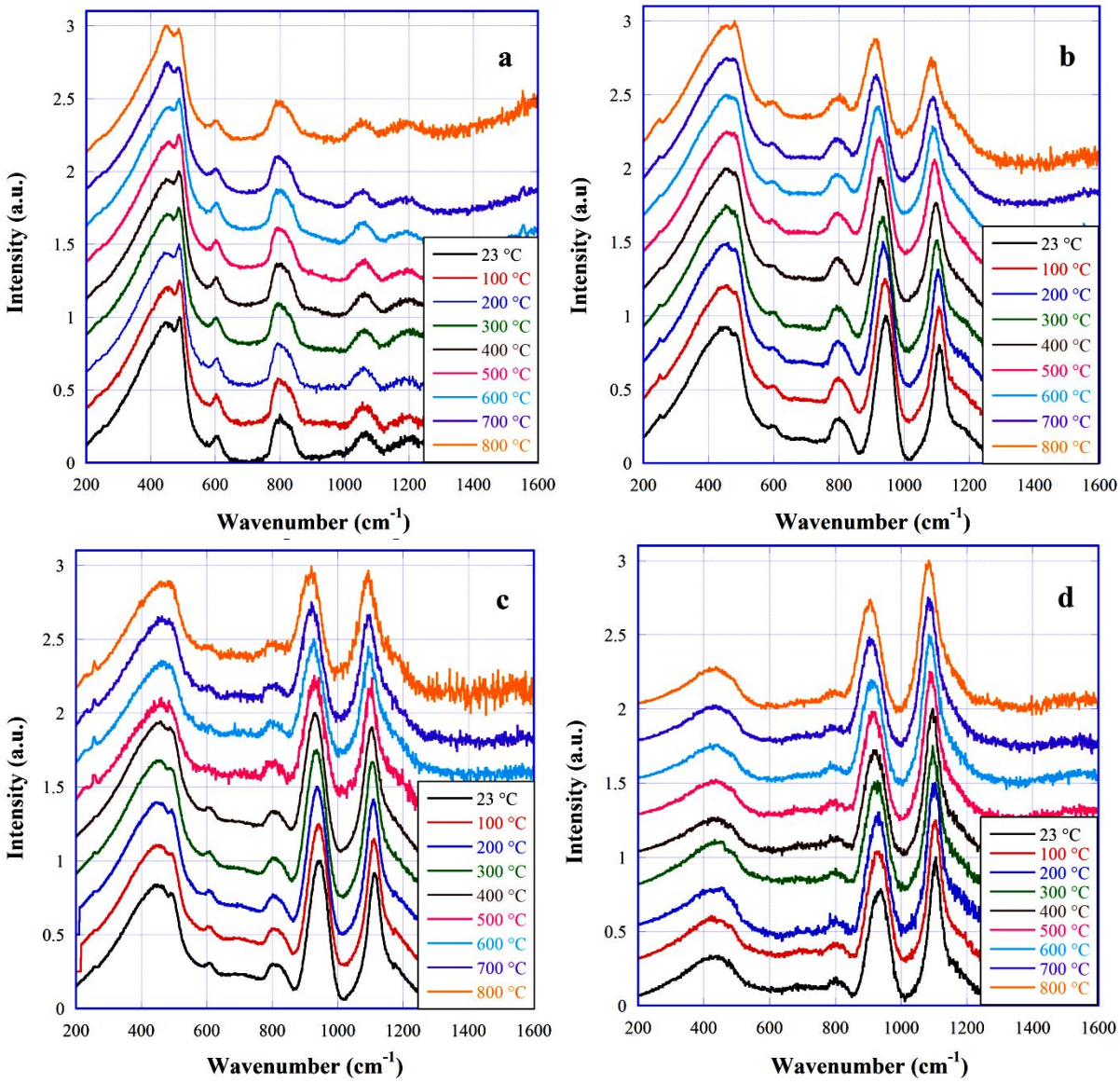

Fig. 2-5. Raman spectra of a) SiO_2, b) 3 TiO_2 - 97 SiO_2, c) 6.1 TiO_2 - 93.9 SiO_2, and d) 8.3 TiO_2 - 91.7 SiO_2 sol-gel glasses from room temperature to 800 °C. The intensity of Raman spectra was corrected for frequency and temperature, and then normalized to the intensity of the 450 cm^{-1} peak. Spectra are offset vertically for clarity.

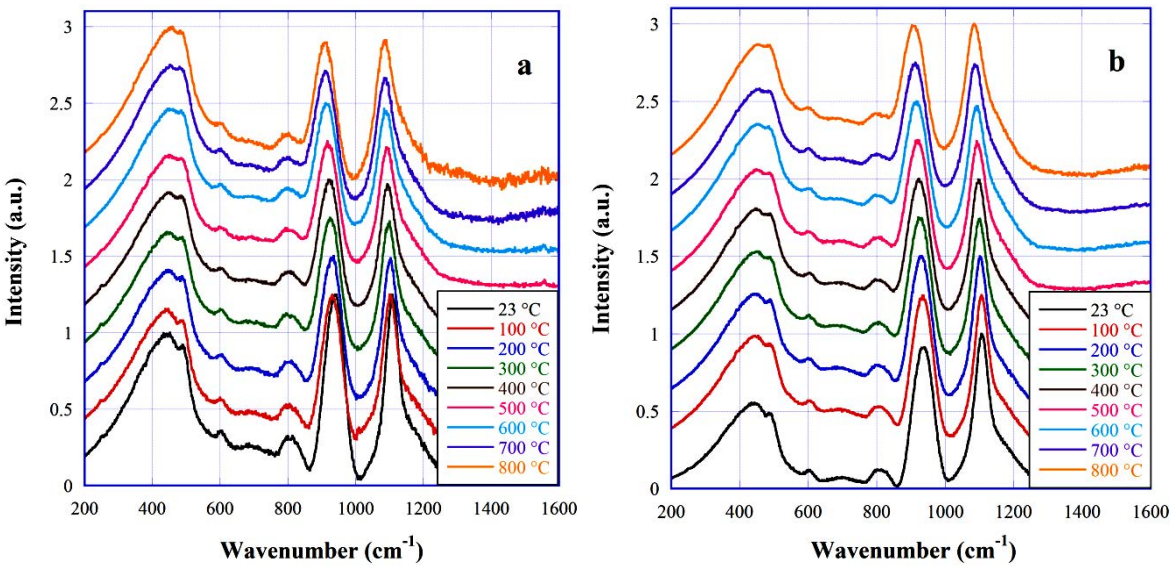

Fig. 2-6. Raman spectra of a) 5.4 TiO_2 and b) 8.3 TiO_2 FHD synthetic glasses from room temperature to 800 °C. The intensity of Raman spectra was corrected for frequency and temperature, and then normalized to the intensity of the 450 cm^{-1} peak. Spectra are offset vertically for clarity.

In-situ high temperature Raman spectra for the two FHD synthetic TiO_2-SiO_2 glasses are presented in Fig. 2-6. Compared to Raman spectra of sol-gel glasses, the 450 cm^{-1} peak tends to be higher in intensity in the FHD synthetic glasses, and the 490 cm^{-1} and 600 cm^{-1} peaks tend to be better defined, particularly at high temperatures. The 800, 950, and 1100 cm^{-1} peaks are basically identical to the sol-gel glasses in terms of relative intensity, shape, and how the shape changes with temperature. The positions of peaks and the shift in position in response to temperature shows similarity between the FHD synthetic glasses and the sol-gel glasses.

The shift in peak positions from room temperature to 800 °C are summarized in Table 2-5. For the FHD synthetic samples, from room temperature to 800 °C, the 450 cm^{-1} appears to shift further to higher frequencies with increasing TiO_2 content. The 490, 605, 800, 950, and 1100 cm^{-1} peaks all appear to shift by the same amount in response to temperature regardless of the TiO_2 concentration. At room temperature, the peak positions of the FHD synthetic silica glass are similar to those of the sol-gel silica glass. However, the peak shifts are drastically different, particularly those of the 800, 1050, and 1200 cm^{-1} peaks. Frequency shift from room temperature to 800 °C differs in magnitude by 14, 17, and 19 cm^{-1} for these peaks, respectively. The smaller shift to lower frequency with increasing temperature in the sol-gel silica glass may indicate additional densification during high temperature Raman measurements.

Table 2-5: Raman peak shifts for TiO_2-SiO_2 glasses from room temperature to 800 °C. Blanks indicate that the peak is not expected or not distinguishable for that composition.

Peak Shift	SiO_2	3 TiO_2 97 SiO_2	4 TiO_2 96 SiO_2	6.1 TiO_2 93.9 SiO_2	7.8 TiO_2 92.2 SiO_2	8.3 TiO_2 91.7 SiO_2	FHD silica	FHD TiO_2	FHD TiO_2
450	3	10	19	19	8	-4	1	12	17
490	-3	-3			-2		-2	-5	-5
600	-4	-3	-3	-7	-1		2	-2	-3
800	-1	-3	0	-13	-9	-13	-15	-12	-13
950		-35	-27	-24	-39	-28		-30	-28
1060	-6						-23		
1100		-23	-24	-19	-24	-21		-22	-22
1200	-9						-28		

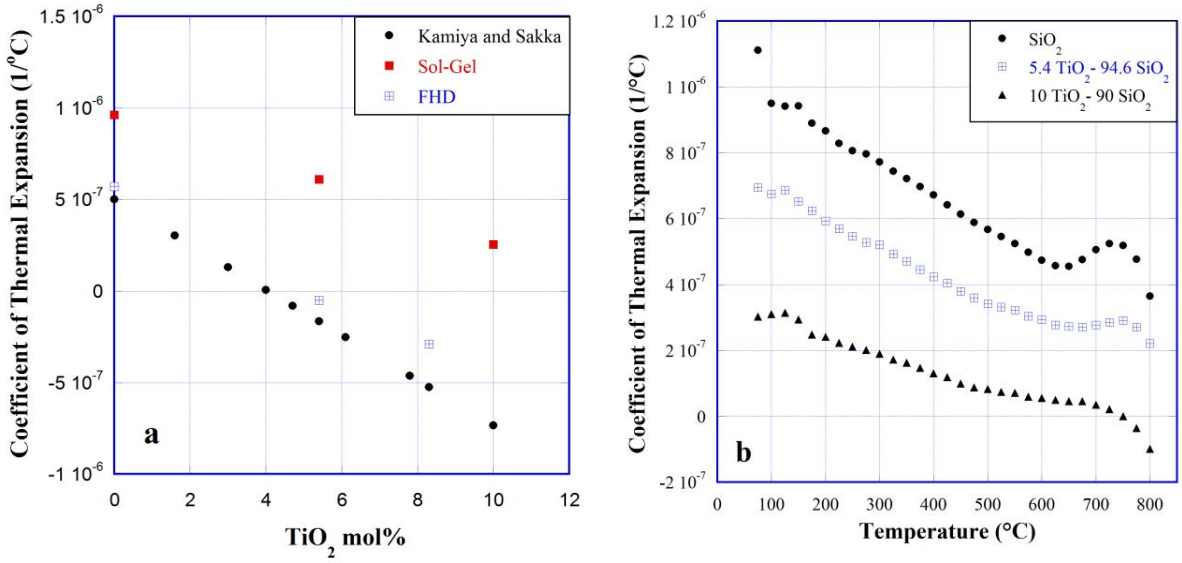

Fig. 2-7. a) CTE versus TiO_2 content for FHD synthetic glasses and sol-gel glasses from our and from Kamiya and Sakka's study [2], and b) CTE versus temperature for sol-gel glasses from our study. CTE values in part a) are average values from room temperature to 300 °C for our sol-gel glasses and FHD synthetic glasses, and from room temperature to 700 °C for Kamiya and Sakka's values [2].

CTE of our sol-gel glasses as a function of TiO_2 content is shown in Fig. 2-7(a), in comparison with those of FHD synthetic glasses and sol-gel glasses from Kamiya and Sakka's study [2]. Values of our sol-gel glasses are higher than FHD synthetic glasses and literature values for these glasses, which is likely caused by the lower density of sol-gel glasses and the higher water content in them compared to those produced through other methods [6-8]. However, the change in thermal expansion with composition matches literature quite well. By

adding 10 mol% TiO_2, the CTE decreases by $7x10^{-7}$ 1/°C, while in literature the change by adding ~8 mol% TiO_2 is $8x10^{-7}$/°C [2]. Change of the CTE for sol-gel glasses with temperature is shown in Fig. 2-7(b) for 0, 5.4, and 10 mol% TiO_2. The change in CTE with temperature also matches well with literature. Schultz and Smyth [1] reported CTE values for TiO_2-SiO_2 glasses with 0 - 9.45 wt% TiO_2 in the temperature range from 0 to 750 °C. For these glasses the CTE decreases with increasing TiO_2, and shows a reduced response to temperature with increasing TiO_2 up to 7.4 wt%; i.e., the CTE changes less with temperature, similar to the trend seen in Fig. 2-7(b).

2.5: Discussion:

Sol-gel TiO_2-SiO_2 glasses have comparable structure and properties to those of glasses of similar composition synthesized through other methods [1, 8, 9], as seen from results presented above, although it is not trivial to control the sol-gel process to get fully densified and/or homogenous glasses. Hirao et al. [8] measured the acoustic velocities of TiO_2-SiO_2 glasses in the low temperature region. Their samples were prepared by sintering powders at 1400 °C and acoustic velocities were measured by using the cube resonance method (a type of ultrasonic measurement). Hirao et al.'s measurements are plotted together with our measurements of sol-gel and FHD synthetic samples in Fig. 2-8(a). Values for 8.3 TiO_2 FHD synthetic glass line up with those of the 8 TiO_2 glass by Hirao et al., better than sol-gel values, while this is reversed for the 5.4 TiO_2 samples. The explanation for this is that the 5 TiO_2 sample prepared by Hirao has a density of 2.157 g/cm^3, which is much closer to that of our sol-gel sample (2.16 g/cm^3) than FHD synthetic sample (2.2 g/cm^3). While the 8 TiO_2 sample prepared by Hirao has a density of 2.193 g/cm^3, so it matches the FHD synthetic sample (2.2 g/cm^3) more closely than our sol-gel sample (~2.18 g/cm^3). The same trend is seen in Fig. 2-8(b), where the Young's modulus of our sol-gel sample is lower than FHD synthetic sample and Gulati's sample (2.2 g/cm^3) due to the lower density. Fig. 2-8(b) also shows the elastic response of TiO_2-SiO_2 glass to temperature is very sensitive to the subtle difference in sample preparation even using the same synthesis technique. Gulati's sample has TiO_2 content (5.7 mol%) close to that of the 5.4 TiO_2 FHD synthetic sample, the difference in Young's modulus and its variation with temperature seem beyond what can be explained by the small composition difference. On the other hand, it cannot be completely ruled

out that different techniques for measuring elastic moduli may contribute to the discrepancy, especially at high temperatures.

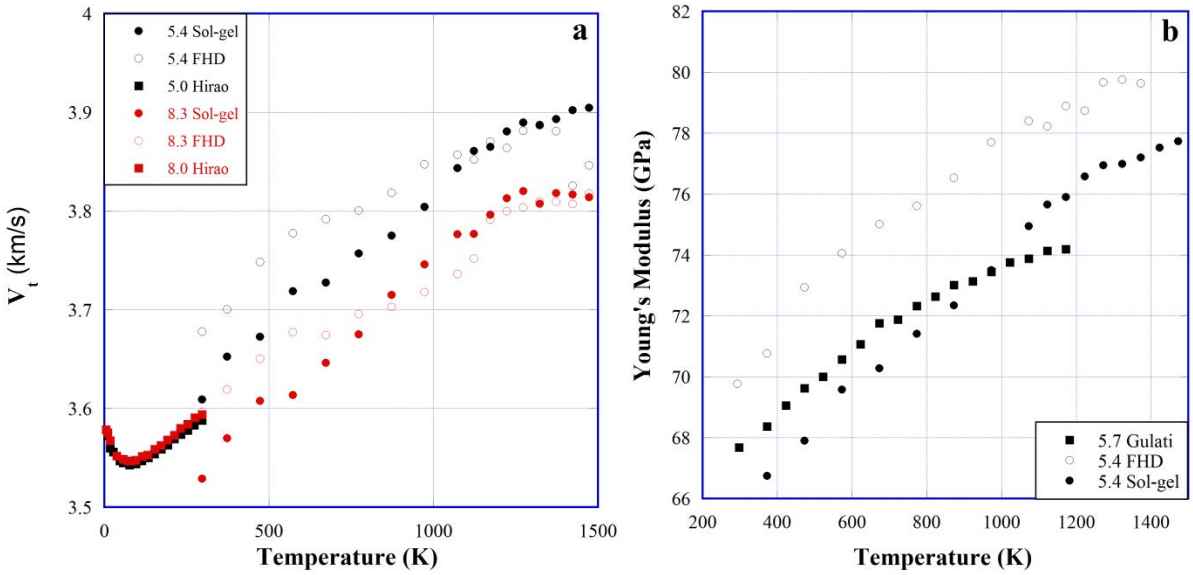

Fig. 2-8. a) Transverse acoustic velocity and b) Young's modulus versus temperature in TiO_2-SiO_2 glasses prepared by different methods. Hirao's data in a) were taken from [8] and Gulati's data in b) were taken from [9].

This sensitivity of elastic properties to density in TiO_2-SiO_2 glasses is also apparent in their Raman spectra. Raman peak positions of sol-gel glasses at room temperature and the shifts from room temperature to 800 °C, presented in Tables 2-4 and 2-5 respectively, generally match those of FHD synthetic glasses, but show significantly more scatter with changes in composition. A shift to lower frequencies would be expected with decreasing density; however, the observed shifts are a mix of lower and higher frequencies, indicating some level of non-uniformity of sol-gel glasses. It is highly likely that the fictive temperatures of the sol-gel glasses vary significantly, which would also contribute to the significant scatter observed. While the general trend in response to both composition and temperature are the same as FHD synthetic glasses, the scatter in sol-gel glasses makes discussion of structure-property relations difficult. Thus, the focus of the rest of the discussion will be mostly on the results of the FHD synthetic glasses and available data from literature.

To further discuss the changes in properties with structure in titania silicate glasses, it is necessary to briefly review the Raman peak assignments in silicate glass. McMillan et al.

[26,27] summarized numerous Raman studies for silica and the effects of many different additives to the silica spectra. The high frequency bands at 1060 cm^{-1} and 1200 cm^{-1} are assigned to non-symmetric Si-O-Si stretching vibrations within the three dimensional network of cornering sharing tetrahedra. The mid-range peak at 800 cm^{-1} is associated with motion of Si within its tetrahedral cage. The peaks in the low frequency range are generally associated with bridging oxygens or the Si-O-Si bonds. The 450 cm^{-1} peak is assigned to symmetric stretching of bridging oxygens and the 490 cm^{-1} and 600 cm^{-1} peaks are attributed to breathing vibrations of 3- and 4-member ring defects within the glass. These assignments are rather simplistic, as many of the peaks in the Raman spectra are not symmetric, suggesting that they are a combination of multiple peaks. Kalampounias et al. provided a more thorough analysis of the SiO_2 Raman peaks, including weaker peaks and deconvoluting the non-symmetric peaks [25].

Raman peaks in the TiO_2-SiO_2 system have been discussed by Chandrasekhar et al. [13], Perry et al. [24], and Henderson and Fleet [14], among others. The 450, 490, 600, and 800 cm^{-1} peaks remain largely unchanged in shape and intensity with the addition of TiO_2, indicating that TiO_2 does not significantly disrupt the silica network. The two new bands that appear at 950 and 1100 cm^{-1} with the addition of TiO_2 are difficult to assign with certainty. Their positions match those of Q^2 and Q^3 species of non-bridging oxygen present in sodium silicate glasses, respectively [23]. However, in sodium silicate glasses the Q^2 peak does not become significant relative to the SiO_2 main band until the Na_2O content is more than 30 mol%. Additionally, the disruption in the 450, 490, and 600 cm^{-1} silica bands observed in sodium silicate glasses is not present in TiO_2-SiO_2 system. Henderson and Fleet [14] noted that these bands could be due to Ti-O vibrations if the motion is mainly caused by the oxygen atom. Sokolov et al. [16] found through quantum-chemical calculations that the band near 1050 cm^{-1} is due to single $^{[4]}$Ti atoms (Ti-O-Si) and that the band near 940 cm^{-1} is from both single (Ti-O-Si) and double $^{[4]}$Ti (Ti-O-Ti). In TiO_2-SiO_2 system with low TiO_2 content, the population of Ti-O-Ti linkages is negligibly small [28], so these bands are assigned to anti-symmetric Ti-O and Si-O stretches in the Ti-O-Si bridges. This corresponds to the low disruption of the silica network with the addition of TiO_2.

The addition of TiO_2 to SiO_2 causes a shift in position of the 450 cm^{-1} and 800 cm^{-1} peaks as seen in Raman spectra of the three FHD synthetic glasses in Fig. 2-4(b). The main band at 450 cm^{-1} shifts to lower frequencies with increasing TiO_2, which is expected with substitution of heavier Ti for Si within the glass network. This shift may also be partially attributed to an

opening up and increased flexibility of the glass structure. Sandstrom et al. [11], measured bond length of the Ti-O bond as 1.81 ± 0.02 Å through EXAFS. This matches the bond lengths measured by Pickup et al. [15] through neutron diffraction, where the Ti-O is 1.84±0.01 Å and the Si-O is 1.61 ± 0.01 Å for 8 TiO_2 - 92 SiO_2 glass. Farges et al. [29] reported the Ti-O bond as 1.84 Å with a bond valence 0.95 v.u. and the Si-O bond as 1.62 Å with a bond valence of 1.00 v.u. The increased bond length and related entropy with addition of TiO_2 to SiO_2 network are also manifested in the systematic decrease in strain and annealing points up to ~10wt% TiO_2 content [30] and the smearing of silica's scattering features [28].

The 800 cm^{-1} peak shifts to higher frequencies with increasing TiO_2. Kalampounias et al. [25] deconvoluted this peak in silica to two bands at 790 and 830 cm^{-1}, which were assigned to apex-bridged tetrahedra and four membered supertetrahedra substructures, respectively. As the TiO_2 content increases the peak appears to become more symmetric, resulting in a shift of the peak to higher frequencies. So the addition of TiO_2 may promote more organized substructures within the glass network.

The addition of TiO_2 to SiO_2 reduces the elastic moduli of the glass as seen in Fig. 2-2 and in Gulati's study [9]. This can be attributed to the longer length and the weaker strength of Ti-O bonds compared to Si-O bonds. Response of silica glass to temperature is characterized by an anomalous increase in elastic moduli and an unusually low CTE. The addition of TiO_2 has a minor effect, if any, on the thermal response of the elastic moduli, but reduces the CTE. This change in thermal expansion due to the addition of TiO_2 is relatively small, compared to the difference between silica glass and quartz [25], but is technologically important as it causes the CTE to pass through zero [2,9].

The anomalous response of elastic moduli to temperature in silica glass has been attributed to transitions between α- and β-like six member rings [31-33], similar to ring structure in α- and β'-cristobalite [34], respectively. This transition is accompanied by a slight increase in the intra-ring Si-O-Si angles [35] as the bonds rotate into a more symmetric and stiffer conformation. However, the main 450 cm^{-1} Raman band shifts to higher frequencies with increasing temperature. This suggests that O moves further from the Si-Si line as the Si-O bond length increases with temperature, in order to have a smaller average Si-O-Si angles [27]. This can occur through cooperative rotation of adjacent tetrahedra, which allows for conformational

changes to occur below the glass transition temperature (T_g) due to the small energy barrier between different ring conformations [34].

Adding TiO_2 to silica glass appears to preserve the transition between α-like and β-like rings with increasing temperature, based on the response of elastic moduli to temperature in Figs. 2-2 and 2-3. Raman spectra show that while the 450 cm^{-1} band shifts to lower frequencies with increasing TiO_2 at room temperature, the peak shift to higher frequencies in response to temperature increases faster with TiO_2 content (Table 2-5). The shift in the 490 and 600 cm^{-1} peaks with temperature remains at approximately -3 and -5 cm^{-1}, respectively, after the addition of TiO_2, suggesting that there is little change in the response of the breathing mode vibrations of 3- and 4-member rings with temperature. This makes sense given that the peak shifts in this temperature range are due primarily to conformation changes. 3- and 4-member rings are much tighter than the 6-member rings that undergo the transition between α- and β-ring conformations. It is reasonable that these small rings would only expand slightly with temperature and be resistant to significant rearrangement below the glass transition temperature.

The 800 cm^{-1} peak shifts by 15 cm^{-1} to lower frequency from room temperature to 800 °C in silica and by 12-13 cm^{-1} in the FHD synthetic glasses. As these peaks occur from the motion of Si or Ti in Si-O or Ti-O stretching modes, the shift in these peaks corresponds to either an increase in the motion of Si and Ti with temperature or a change in the local structure to more open arrangements. As Ti is significantly more massive than Si, it is more likely to promote smaller cation motions, which corresponds to the observed change in peak shift with temperature. It is also possible that the glass experiences a change in population from more organized structures (such as supertetrahedra suggested by Kalampounias) to more open apex-bridged tetrahedra, which requires only small angular changes [25] and is possible at temperatures below T_g.

The high frequency bands at 950 and 1100 cm^{-1} in TiO_2-SiO_2 glasses shift to lower frequencies quickly with increasing temperature. The total shift of these peaks is approximately equal to those for the 1050 and 1200 cm^{-1} bands in pure silica (Table 2-5). If these peaks correspond to the anti-symmetric vibrations of oxygen in Si-O-Ti triplets, this suggests that the oxygen atom is moving further off the Si-Ti line, resulting in a decrease in the average inter-tetrahedral angles with temperature. This agrees with the change in symmetric vibrations of the oxygen atoms; the shift of the 450 cm^{-1} peak to higher frequencies with temperature. The

addition of TiO_2 increases the free volume of the glass and reduces the stiffness of the network, which results in a significantly larger shift in the 450 cm^{-1} peak than in pure silica, due to a larger reduction in the average inter-tetrahedral angles with temperature.

Both anomalous responses of elastic moduli and thermal expansion in TiO_2-SiO_2 glasses to temperature can be explained through this enhanced conformational and angular changes. It is important to remember that actual changes that occur with the addition of TiO_2 are relatively small compared to the differences that already exist between amorphous and crystalline silica. The CTE changes from $35x10^{-6}$ $°C^{-1}$ to $0.5x10^{-6}$ $°C^{-1}$ between quartz and silica glass [35]. It changes from $0.5x10^{-6}$ $°C^{-1}$ to $-0.5x10^{-6}$ $°C^{-1}$ with the addition of 8 mol% TiO_2 [2]. Thus, the addition of 8 mol% TiO_2 increases the difference in CTE between silica glass and quartz by slightly less than 3%. Based on the observed responses of elastic moduli, Raman spectra, and CTE to temperature, we propose the following explanation for the anomalous behaviors in TiO_2-SiO_2 glasses.

It has been shown that Ti enters the silica network in primarily a five-fold coordination for the first 2.7 mol%, above which it primarily adopts a four-fold coordination [12]. Henderson et al. proposed that it is necessary to increase the flexibility and the open nature of the network in order to incorporate Ti in the tetrahedral network [12]. The lack of a change in density with the addition of heavier Ti agrees with the opening up of the network and increasing the free volume in the glass. This increase in free volume, lower Ti-O bond strength, and the heavier mass of the Ti atom all contribute to reduction of the stiffness of the glasses seen in room temperature elastic moduli (Fig. 2-1) and the shift of 450, 490, and 600 cm^{-1} Raman peaks to lower frequencies with addition of TiO_2 to SiO_2 (Table 2-4). The resulting opening up and increased flexibility of the glass structure promotes the conformational transitions between softer α-like and stiffer β-like rings, to compensate the sensitivity of weaker bonds to temperature, which explains the almost constant increase in the stiffness of the network with increasing temperature, regardless of TiO_2 content, as observed in *in-situ* high temperature Brillouin light scattering study. β-like rings occupy larger volumes than the α-like rings, so it would be expected that these conformational transitions would cause an increase in expansion. However, these conformational expansions occur in the relatively open tetrahedral network and can take advantage of the large free volume in the glass. While the inter-tetrahedral angles increase slightly within these rings, the cooperative rotation of adjacent tetrahedra results in a net decrease in the average inter-

tetrahedral angle throughout the network, which explains the increased shift in the 450 cm^{-1} peak to higher frequencies in response to temperature in glasses with increasing TiO_2 content. These rotations effectively allow the glass to counter balance the normal thermal expansion by rearranging the tetrahedron packing to reduce the free volume when temperature is increased.

2.6: Conclusions:

Structure and elastic moduli of TiO_2-SiO_2 glasses have been studied with regards to compositions and in their response to temperature through *in-situ* high temperature Raman and Brillouin light scattering. Glasses produced through both the sol-gel process and the FHD process were examined. Glasses produced through the sol-gel process were found to be clear, transparent, and homogeneous. Sol-gel glasses have lower elastic moduli than the FHD synthetic glasses, which can be attributed to the slightly lower densities, in the range of 2.15-2.18 g/cm^3 as opposed to 2.20 g/cm^3 for the FHD synthetic glasses. Sol-gel glasses are also characterized by a shift in Raman peaks to lower frequencies and an increased coefficient of thermal expansion, both of which match a lower density glass.

In the composition range where $^{[4]}$Ti atoms are four-fold coordinated in silica network, the addition of TiO_2 reduces the elastic moduli and shifts Raman peaks at room temperature to low frequencies due to the heavier mass of Ti atoms, more importantly, resulting from a more open and flexible network given by the longer and weaker Ti-O bonds. The balance between increased mass and free volume from the addition of TiO_2 results in an almost constant density of TiO_2-SiO_2 glasses, independent of TiO_2 content.

Our *in-situ* high temperature studies show that the anomalies in TiO_2-SiO_2 glasses are similar to those in pure SiO_2 glass, which can be explained by the conformational and angular changes with temperature. The incorporation of TiO_2 into silica increases the network flexibility and the free volume of the glass while preserving the tetrahedral network structure, and thus facilitates the ring conformational transitions given enough thermal energy to overcome the energy barrier. The increased conformational transitions between softer α-like and stiffer β-like rings compensate the sensitivity of weaker bonds to temperature, so the amount of stiffening of the network with increasing temperature does not change obviously with TiO_2 content. The resulting opening up and increased flexibility of the glass structure promotes the cooperative rotation of adjacent tetrahedra, resulting in a net decrease in the average inter-tetrahedral angles.

The larger change (reduction) of the average inter-tetrahedral angles with temperature is the underlying mechanism for the Raman band at 450 cm^{-1} to shift further to higher frequencies with increasing TiO_2. The normal thermal expansion due to bond elongation with temperature is counter balanced by the free volume reduction facilitated by the cooperative rotation of adjacent tetrahedra assisted by thermal energy. As the network flexibility increases with the amount of TiO_2 addition to silica, the coefficient of thermal expansion decreases with TiO_2 content, as long as the silica tetrahedral network is preserved, i.e., in the composition range where $^{[4]}Ti$ atoms adopt four-fold coordinated sites.

2.7: References:

[1] P. Schultz, H. Smyth, Ultra-Low Expansion Glasses and their structure in the SiO_2-TiO_2 system, in: Amorphous Materials, Wiley Interscience, 1970: pp. 453–461.

[2] K. Kamiya, S. Sakka, Thermal Expansion of TiO_2-SiO_2 and TiO_2-GeO_2 glasses, J. Non-Cryst. Solids. 52 (1982) 357–363.

[3] A.P. Carapella, C.A. Duran, K.E. Hrdina, D.J. Sears, J.E. Tingley, ULE® Glass for EUVL applications, a fictive temperature correlation, J. Non-Cryst. Solids. 367 (2013) 37–42.

[4] P. Schultz, W. Dumbaugh, Silica-rich glasses in the TiO_2-Al_2O_3-SiO_2 system, J. Non-Cryst. Solids. 38 & 39 (1980) 33–37.

[5] R. Roy, D. Agrawal, H. McKinstry, Very Low Thermal Expansion Coefficient Materials, Annu. Rev. Mater. Sci. 19 (1989) 59–81.

[6] J. Shelby, Density of TiO_2-doped vitreous silica, Phys. Chem. Glasses. 46 (2005) 494–499.

[7] J. Shelby, Fictive Temperature and Density of Doped Vitreous Silica, Phys. Chem. Glasses: Eur. J. Glass Sci. Technol., Part B. 50 (2009) 7–14.

[8] K. Hirao, K. Tanaka, S. Furukawa, N. Soga, Anomalous temperature dependence of the sound velocities of SiO_2-TiO_2 glasses, J. Mater. Sci. Lett. 14 (1995) 697–699.

[9] S. Gulati, Mechanical Properties of SiO_2 vs. SiO_2-TiO_2 Bulk Glasses and Fibers, Mat. Res. Soc. Symp. Proc. 244 (1992) 67–83.

[10] F.Y. Li, S.S. Fu, R.J. Wang, M. Manghnani, Elastic properties of float glass and TiO_2- SiO_2 glass under high pressure, Acta Phys. Sin. 49 (2000) 2129–2132.

[11] D. Sandstrom, F. Lytle, P. Wei, R. Greegor, J. Wong, P. Schultz, Coordination of Ti in TiO_2-SiO_2 glass by X-ray absorption spectroscopy, J. Non-Cryst. Solids. 41 (1980) 201–207.

[12] G. Henderson, X. Liu, M. Fleet, A Ti L-edge X-ray absorption of Ti-silicate glasses, Phys. Chem. Miner. 29 (2002) 32-42.

[13] H. Chandrasekhar, M. Chandrasekhar, M. Manghnani, Phonons in TiO_2-SiO_2 glasses, J. Non-Cryst. Solids. 40 (1980) 567–575.

[14] G. Henderson, M. Fleet, The structure of Ti silica glasses by micro-Raman spectroscopy, Can. Mineral. 33 (1995) 399–408.

[15] D. Pickup, F. Sowrey, R. Newport, P. Gunawidjaja, K. Drake, M. Smith, The Structure of TiO_2-SiO_2 Sol-Gel Glasses from Neutron Diffraction with Isotropic Substitution of

Titanium and 17 O and 49 Ti Solid-State NMR with Isotropic Enrichment, J. Phys. Chem. B. 108 (2004) 10872–10880.
[16] V. Sokolov, V. Plotnichenko, E. Dianov, Quantum-Chemical Modeling of Titanium Centers in Titanosilicate Glass, Inorg. Mater. 42 (2006) 1273–1288.
[17] R.L. Huang, S.K. Ruan, Z.C. Kang, M.Z. Su, Radial Gradient-Index Glass Prepared by the Sol-Gel Process, Mater. Res. Bull. 30 (1995) 543–548.
[18] K. Davis, A. Agarwal, M. Tomozawa, K. Hirao, Quantitative infrared spectrascopic measurements of hydroxyl concentrations in silica glass, J. Non-Cryst. Solids. 203 (1996) 27–36.
[19] B. Sloots, Measuring the low OH content in quartz glass, Vib. Spectrosc. 48 (2008) 158–161.
[20] B. Schmidt, F. Holtz, J.-M. Beny, Incorporation of H_2 in vitreous silica, qualitative and quantitative determination from Raman and infrared spectroscopy, J. Non-Cryst. Solids. 240 (1998) 91–103.
[21] M. Guerette, L. Huang, A simple and convenient set-up for high-temperature Brillouin light scattering, J. Phys. D: Appl. Phys. 45 (2012) 275302.
[22] G. Scannell, L. Huang, T. Rouxel, Elastic properties and indentation cracking behavior of Na_2O-TiO_2-SiO_2 glasses, J. Non-Cryst. Solids. 429 (2015) 129–142.
[23] Q. Zhao, M. Guerette, G. Scannell, L. Huang, In-situ high temperature Raman and Brillouin light scattering studies of sodium silicate glasses, Journal of Non-Crystalline Solids. 358 (2012) 3418–3426.
[24] C. Perry, X. Li, D. Waters, Structural studies of gel phases--IV. An infrared reflectance and Fourier transform Raman study of silica and silica/titania gel glasses, Spectrochim. Acta. 47A (1991) 1487–1494.
[25] A. Kalampounias, S. Yannopoulos, G. Papatheodorou, Temperature-induced structural changes in glassy, supercooled molten silica from 77 to 2150 K, J. Chem. Phys. 124 (2006) 014504.
[26] P. McMillan, Structural studies of silicate glasses and melts--applications and limitations of Raman spectroscopy, Am. Mineral. 69 (1984) 622–644.
[27] P. McMillan, B. Poe, P.H. Gillet, B. Reynard, A study of SiO_2 glass and supercooled liquid to 1950 K via high-temperature Raman spectroscopy, Geochim. Cosmochim. Acta. 58 (1994) 3653–3664.
[28] D. Evans, Glass Structure: The bridge between the molten and crystalline states, J. Non-Cryst. Solids. 52 (1982) 115–128.
[29] F. Farges, G. Brown, A. Navrotsky, H. Gan, J. Rehr, Coordination chemistry of Ti(IV) in silicate glasses and melts: II. Glasses at ambient temperature and pressure, Geochim. Cosmochim. Acta. 60 (1996) 3039–3053.
[30] P. Schultz, Binary Titania-Silica Glasses Containing 10 to 20 wt% TiO_2, J. Am. Ceram. Soc. 59 (1976) 214–219.
[31] L. Huang, J. Kieffer, Molecular dynamics study of cristobalite silica using a charge transfer three-body potential: Phase transformation and structural disorder, J. Chem. Phys. 118 (2003) 1487–1498.
[32] L. Huang, J. Kieffer, Amorphous-amorphous transitions in silica glass. I. Reversible transitions and thermomechanical anomalies, Phys. Rev. B. 69 (2004) 224203.
[33] L. Huang, J. Kieffer, Amorphous-amorphous transitions in silica glass. II. Irreversible transitions and densification limit, Phys. Rev. B. 69 (2004) 224204.

[34] F. Yuan, L. Huang, α-β transformation and disorder in β-cristobalite silica, Phys. Rev. B. 85 (2012) 134114.
[35] R. Vukcevich, A new interpretation of the anomalous properties of vitreous silica, J. Non-Cryst. Solids. 11 (1972) 25–63.

Chapter 3 : Structure and Properties of Na_2O-TiO_2-SiO_2 Glasses: Role of Na and Ti on Modifying the Silica Network

3.1: Abstract:

Changes in the structure and properties of xNa_2O-$yTiO_2$-$(1-x-y)SiO_2$ glasses have been studied with regards to composition through Raman spectroscopy, Brillouin light scattering, and dilatometry. Twelve glasses with nominal compositions x=10, 15, 20, and 25, and y=4, 7, and 10 were prepared through a traditional melt quench method. Na_2O was found to increase the density, refractive index, coefficient of thermal expansion (CTE), bulk modulus, and Poisson's ratio of glasses, and to decrease Young's modulus and shear modulus. Density, refractive index, Young's modulus, shear modulus, bulk modulus and Poisson's ratio increase with the increase of TiO_2 content. CTE was found to increase with the initial addition of 4 mol% TiO_2 and to remain constant with further additions, regardless of the Na_2O content. Changes in the Raman spectra with composition have been discussed and related to the changes in resulting properties.

3.2: Introduction:

Titanium dioxide is a common minor additive in minerals and natural glasses, and it is used in commercial glasses for its optical and thermal expansion properties. It is of interest to both geologists and glass scientists because of the strong impact small quantities of TiO_2 can have on mechanical, optical, and thermodynamic properties [1-13]. Understanding the role TiO_2 plays in glass systems is complicated by the fact that Ti^{4+} can occupy four-, five-, and six-fold coordination states, in tetrahedral, square pyramidal, and octahedral geometries, respectively. The coordination state that Ti adopts is dependent on the chemistry of the surrounding glass, and a change of coordination can result in TiO_2 having a completely different effect on the resulting properties.

This chapter has been submitted to: G. Scannell, S. Barra, L. Huang, Structure and Properties of Na_2O-TiO_2-SiO_2 Glasses: Role of Na and Ti on Modifying the Silica Network, J. Non-Cryst. Solids. (2016).

Alkali-TiO_2-SiO_2 glasses provide a convenient composition space to observe the change in behavior of TiO_2 from the binary TiO_2-SiO_2 [14]. Glasses of these compositions have been the subject of numerous studies designed to explore the structural environment around Ti. The coordination and local structure of TiO_2 containing glasses and minerals were extensively examined through XANES and XAFS by Farges et al. [15-19]. The structure of these glasses has also been examined through other means, including infrared spectroscopy [20-22], Raman spectroscopy [20,23-27], pulsed neutron scattering [28], and a variety of X-ray techniques [29-31]. A general agreement has emerged from these studies that many of the property changes caused by TiO_2 can be explained through an increase in the medium-range order.

Farges et al. proposed a percolation model for a Na_2O-TiO_2-$2SiO_2$ glass with pockets of 3-6 Å in size of high alkali concentration surrounded by a $^{[5]}$Ti-rich region, which is then surrounded by areas with lower concentrations of network modifiers [16]. Henderson et al.'s later study of the same system, $xTiO_2$-$(1-x)Na_2SiO_3$ glasses, showed that $^{[4]}$Ti occurs at low Ti contents and gradually transitions to $^{[5]}$Ti as the Ti content is increased to ~14 wt% [31]. Inoue et al.'s study included glasses with TiO_2 contents up to approximately 40% and found that Ti coordination increases from 4 to 5 to 6 as the concentration of Ti is increased [1].

As our understanding of how TiO_2 behaves in glasses has improved, there have been numerous studies on the connections between compositional, structural behavior and optical properties, such as index of refraction and dispersion [1,2], or thermodynamics properties, such as viscosity, heat capacity, and configurational entropy [3-5]. However, studies on the thermo-mechanical properties of these glasses, such as elastic moduli and thermal expansion, generally dated from before much of the structural studies were done [6-8], had a much more general focus [9,10], or focused primarily on glass melts [11-13].

In this work, we examined the structure through Raman spectroscopy, elastic moduli through Brillouin light scattering, and thermal expansion through dilatometry, of glasses with nominal compositions of xNa_2O-$yTiO_2$-$(1-x-y)SiO_2$, where x=10, 15, 20, and 25, and y=4, 7, and 10. These compositions were chosen to provide complementary structural information to existing literature, as most glasses studied have large Na_2O or TiO_2 contents (>30 mol%). This composition range also allows for a direct comparison to glasses from the binary systems, TiO_2-SiO_2 and Na_2O-SiO_2, as previously studied [2,9,10,32-36].

3.3: Methods:

Glasses were prepared in 80 g batches in a Pt or 10%Rh - 90%Pt crucible through a traditional melt-quench method. Compositions prepared include $(x)Na_2O$-$(y)TiO_2$-$(1-x-y)SiO_2$, where x=10, 15, 20, and 25 and y=4, 7, and 10 mol%. Powders were mixed for 30 minutes and then melted at 1400-1500 °C for three hours. The mixed powder was added in three to four stages during the first hour, and the glass melt was stirred five to six times during the last two hours to improve homogeneity. The glass melt was held at 1600-1700 °C for 10 minutes immediately prior to pouring. The poured glasses were then annealed at 550-600 °C, slightly above their glass transition temperatures, for 1 hour before furnace cooling overnight. Glasses were checked for residual stresses using a polarizer, and crushed and re-melted if significant residual stresses were observed.

Samples were cut from the prepared bulk glasses using an abrasive cutting wheel. Samples were ground using 240, 400, and 600 grit Al_2O_3 papers and then polished to an optical finish using a CeO_2 slurry. For Raman light scattering and Brillouin light scattering experiments, sample dimensions were approximately 2 mm x 1 mm x 100 μm, with both surfaces parallel and polished to an optical finish.

Light scattering experiments were conducted by using a 532.18 nm Verdi V2 DPSS green laser as the probing light source. The experimental setup used for Brillouin light scattering (BLS) and Raman light scattering experiments is similar to that described by Guerette and Huang [37], which allows a simultaneous measurement of longitudinal peak from the backscattering geometry, longitudinal and shear peak from the emulated platelet geometry. BLS spectra were collected until the longitudinal peak from the emulated platelet geometry reached a minimum of 600 counts to ensure a good peak fit.

Elastic moduli, including Poisson's ratio, were calculated from the sound velocities measured through BLS and the density of the glasses using Equations 3-(1-4).

$$E = \rho V_T^2(3V_L^2-4V_T^2)/(V_L^2-V_T^2) \quad (3\text{-}1)$$

$$\mu = \rho V_T^2 \quad (3\text{-}2)$$

$$K = E/(3(1-2\nu)) \quad (3\text{-}3)$$

$$\nu = (V_L^2 - 2V_T^2)/2(V_L^2 - V_T^2) \quad (3\text{-}4)$$

where V_L and V_T are longitudinal and transverse sound velocities, ρ is sample density, E is Young's modulus, K is bulk modulus, μ is shear modulus, v is Poisson's ratio.

Densities of samples were measured through the Archimedes method using water as the liquid medium. Sample weight was measured ten times each in air and water and the density was calculated from average weight values in each medium. Standard deviations were calculated through error propagation of standard deviations of weight in air and in water. Average standard deviation across the 12 compositions examined was 0.0026 g/cm^3, and the maximum standard deviation of compositions measured was 0.0047 g/cm^3.

The index of refraction was measured for each composition using a thin sample, around 0.5-1 mm thick, with two optically polished, parallel surfaces. Index of refraction measurements were performed using a Metricon Model 2010/M Prism Coupler. Five measurements were made for each sample. Average standard deviation for the twelve compositions was 0.000381, and the maximum standard deviation was 0.000646. Error bars plotted on figures for index of refraction are smaller than the symbols.

Thermal expansion of samples was measured with a dual pushrod differential dilatometer at Corning, Inc. Glass bars with dimensions of 2″ by 0.25″ by 0.25″ and finely ground ends and coarsely ground sides were prepared. Measurements were done using a 4 °C/min heating and cooling rate from room temperature to 480 °C, and 5 minutes hold at the top temperature. Sapphire was used as a reference material.

Electron microprobe analysis (EMPA) was used to determine the composition and the homogeneity of Na_2O-TiO_2-SiO_2 glasses. Albite and jadeite were used as Na references; titanite, Ti metal, and rutile were used at Ti references; and quartz was used as the Si reference. Compositions were measured at 7 points across the surface of each sample. Nominal compositions, measured compositions, and standard deviations are shown in Table 3-1 for the 12 glasses examined here and two glasses provided by Corning to use for comparison. The 10 Na_2O - 10 TiO_2 - 80 SiO_2 and 25 Na_2O - 4 TiO_2 - 71 SiO_2 glasses were measured at 40 points across the sample to provide a measure of homogeneity. The 20 Na_2O - 10 TiO_2 - 70 SiO_2 glass deviates the most from the nominal composition, with 2.5 mol% less Na_2O and 2.8 mol% less

TiO_2 than nominal. The 25 Na_2O - 7 TiO_2 - 68 SiO_2 sample also has quite low TiO_2, with 2 mol% less than nominal.

Table 3-1. Compositions and standard deviations (in mol%) of Na_2O-TiO_2-SiO_2 glasses.

Nominal Composition (Na_2O-TiO_2-SiO_2)	Na_2O	Na_2O Std	TiO_2	TiO_2 Std	SiO_2	SiO_2 Std
10-4-86	10.26	0.33	3.90	0.12	85.84	0.28
10-7-83	10.35	0.35	6.52	0.14	83.13	0.46
10-10-80	8.59	0.44	10.29	0.30	81.12	0.65
15-4-81	15.32	0.26	3.93	0.12	80.75	0.22
15-7-78	15.69	0.42	6.77	0.14	77.54	0.45
15-10-75	15.71	0.23	9.59	0.13	74.70	0.26
20-4-76	20.61	0.28	3.92	0.10	75.46	0.23
20-7-73	20.42	0.27	6.70	0.09	72.89	0.28
20-10-70	17.53	1.27	7.17	1.33	75.30	2.56
25-4-71	24.99	0.70	3.79	0.12	71.22	0.74
25-7-68	25.12	0.29	5.08	0.05	69.80	0.29
25-10-65	25.74	0.30	9.27	0.29	64.99	0.46
Corning 10-10-80	10.68	0.25	9.34	0.14	79.97	0.24
Corning 25-10-65	26.95	0.43	10.28	0.17	62.77	0.39

Fourier transform infrared spectroscopy (FTIR) was used to measure the water content in Na_2O-TiO_2-SiO_2 glasses (Table 3-2). Hydroxyl concentrations were determined using the Beer-Lambert law, following procedures used in literature [38-40]. The water content in most of our glasses was $\leq$ 50 ppm, with the 15 Na_2O - 10 TiO_2 - 75 SiO_2 sample having an OH concentration of 92.8 ppm.

Table 3-2. OH content in Na_2O-TiO_2-SiO_2 glasses.

Nominal Composition (Na_2O-TiO_2-SiO_2)	OH Concentration (ppm)
10-4-86	
10-7-83	50.2
10-10-80	38.8
15-4-81	46.8
15-7-78	46.8
15-10-75	92.8
20-4-76	34.8
20-7-73	30.9
20-10-70	24.9

25-4-71	23.5
25-7-68	27.5
25-10-65	29.8

3.4: Results:

Fig. 3-1 shows the density of glasses versus the number of bridging oxygen per network forming cation. Calculation for the number of bridging oxygen is given in Equation 3-5, more detail can be found elsewhere [41]. Equation 3-5 assumes that Ti has a 50-50 mixture of four- and five-fold coordination state. In this case, a $^{[4]}$Ti forms four bridging bonds, acting to remove one sodium from the network, effectively restoring one Si bridging oxygen, and a $^{[5]}$Ti forms four bridging bonds and one non-bridging bond, with the non-bridging oxygen being charge-balanced by two sodium atoms.

$$n_{BO} = (4([Si] + [Ti]) - ([Na] - [Ti]))/([Si] + [Ti]) \quad (3\text{-}5)$$

The density generally increases with increasing TiO_2 and increasing Na_2O, in good agreement with Hamilton's study of similar compositions [34]. The slightly lower densities of the 20 Na_2O - 10 TiO_2 - 70 SiO_2 and the 25 Na_2O -7 TiO_2 - 68 SiO_2 glasses match the lower than expected TiO_2 contents.

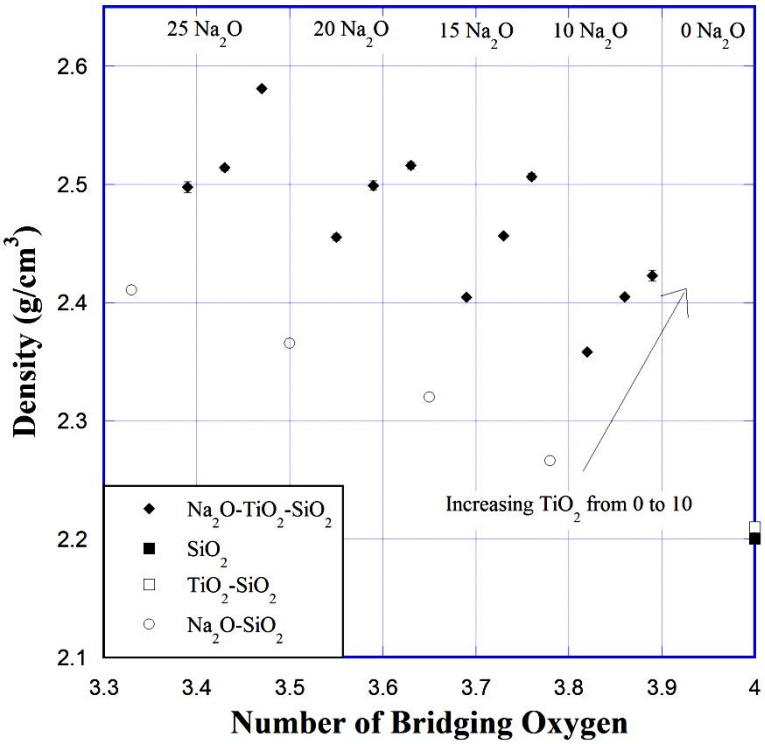

Fig. 3-1. Density of Na_2O-TiO_2-SiO_2 glasses versus the number of bridging oxygen per network forming cation. For each Na_2O composition, TiO_2 increases from left to right (4, 7, 10%). Density of TiO_2-SiO_2 glasses [33], Na_2O-SiO_2 [32], and SiO_2 glasses are also shown for comparison.

Refractive index versus the number of bridging oxygen per network forming cation is presented in Fig. 3-2. Refractive index increases with both increasing Na_2O and TiO_2 concentrations, although significantly more with the addition of TiO_2 than with Na_2O. Values measured are in good agreement with Hamilton's study of similar compositions [34]. The seemingly low index of refraction value for the 20 Na_2O - 10 TiO_2 - 70 SiO_2 glass corresponds with the TiO_2 content of 7.17 mol%, which is only slightly higher than the 6.70 mol% of TiO_2 in the 20 Na_2O -7 TiO_2 - 73 SiO_2 glass.

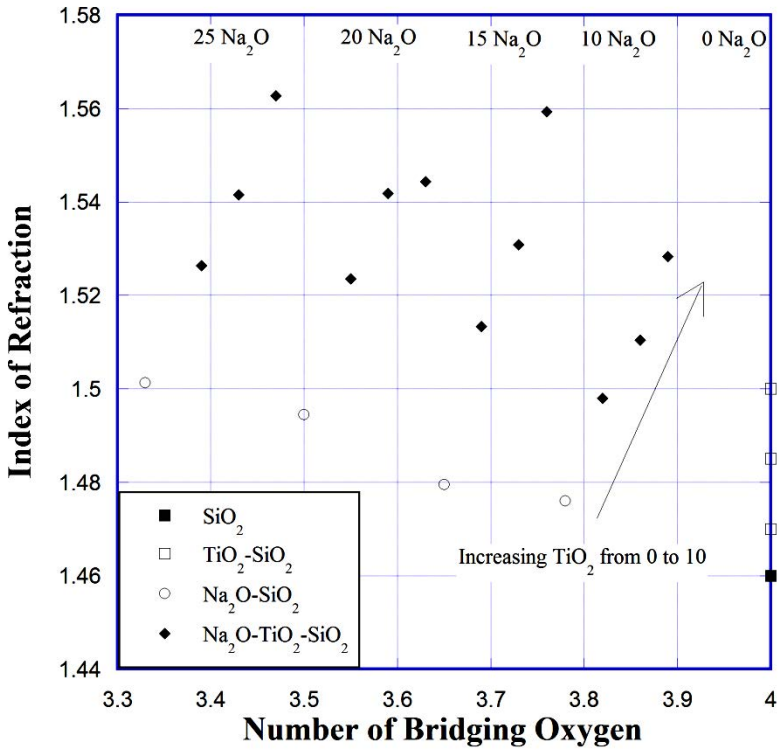

Fig. 3-2. Index of refraction versus the number of bridging oxygen per network forming cation for Na_2O-TiO_2-SiO_2 glasses. For each Na_2O composition, TiO_2 increases from left to right (4, 7, 10%). Values for TiO_2-SiO_2 [42], Na_2O-SiO_2 [32], and SiO_2 glasses are also shown for comparison.

Coefficients of thermal expansion (CTE) are plotted against the number of bridging oxygen per network forming cation in Fig. 3-3. CTE increases linearly with increasing Na_2O. With the initial addition of 4 TiO_2 the CTE increases by around $1x10^{-6}$ C^{-1}. Further additions of TiO_2 from 4 to 10 mol% only change the CTE very slightly.

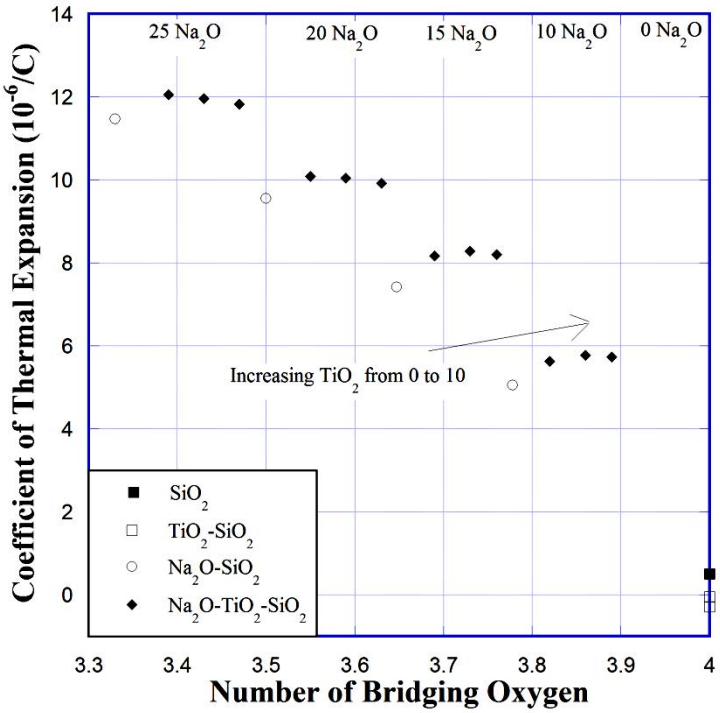

Fig. 3-3. Coefficient of thermal expansion versus number of bridging oxygen per network forming cation. For each Na_2O composition, TiO_2 increases from left to right (4, 7, 10%). CTE of Na_2O-TiO_2-SiO_2 samples represent the values at 50 °C. TiO_2-SiO_2 values are the average between room temperature and 300 °C, and Na_2O-SiO_2 values are the CTE between room temperature and 100 °C [43].

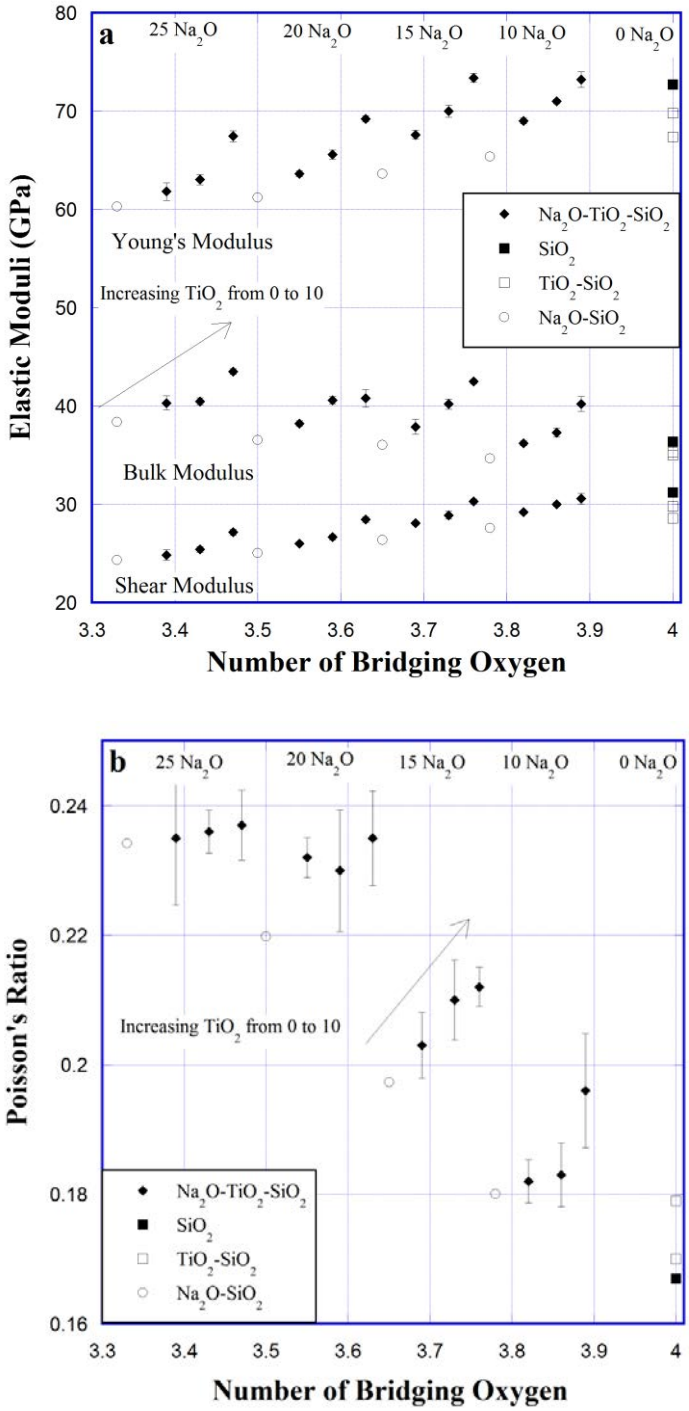

Fig. 3-4. a) Young's modulus, bulk modulus, and shear modulus, and b) Poisson's ratio versus the number of bridging oxygen per network forming cation. For each Na_2O composition, TiO_2 increases from left to right (4, 7, 10%). Na_2O-SiO_2 values are taken from previous research by Zhao et al. [32] and TiO_2-SiO_2 data by Scannell et al. [33]. Error bars are reported for all Na_2O-TiO_2-SiO_2 glasses and represent the standard deviation across five measurements.

Elastic moduli versus the number of bridging oxygen are presented in Figs. 3-4(a-b). Fig. 3-4a shows changes in Young's modulus, bulk modulus, and shear modulus with changes in composition and Fig. 3-4b shows the corresponding changes of Poisson's ratio. Relative to pure silica, Young's modulus decreases with the addition of either Na_2O or TiO_2. These changes are discussed in more detail for both Na_2O-SiO_2 [32] and TiO_2-SiO_2 [33] systems elsewhere. With the addition of both Na_2O and TiO_2, the observed change is quite different. In the presence of Na_2O, the effect of TiO_2 is directly opposite to the behavior observed in the binary system. With no Na_2O, adding 8.3 mol% TiO_2 decreases Young's modulus by 5.3 GPa from 72.7 to 67.4 GPa. With 10 Na_2O, adding 10 mol% TiO_2 increases Young's modulus by 4.2 GPa, from 69.0 to 73.2 GPa. And at 25 Na_2O, the same amount of TiO_2 increases Young's modulus from 64.5 GPa to 69.4 GPa, an increase of 4.9 GPa. A similar change in behavior can be observed with changes in Na_2O composition when TiO_2 is present. With no TiO_2, Young's modulus decreases by 5.1 GPa between 10 and 25 Na_2O. At 4 mol% TiO_2 this decrease is 4.5 GPa and at 10 mol% TiO_2 it is 3.8 GPa.

The shear modulus shows a similar behavior to Young's modulus. Holding the amount of Na_2O constant and changing TiO_2 from 0 to 10 (or 8.3 for the binary case), with no Na_2O, it decreases by 2.6 GPa, at 10 Na_2O it increases by 1.4 GPa, and at 25 Na_2O it increases by 2.0 GPa. In the reverse case, holding TiO_2 constant and changing Na_2O from 10 to 25, with no TiO_2 the shear modulus decreases by 3.2 GPa, at 4 TiO_2 it decreases by 3.1 GPa, and at 10 TiO_2 it decreases by 2.5 GPa. Thus, for both Young's modulus and shear modulus, in the presence of Na_2O, TiO_2 appears to stiffen the glass structure to both longitudinal and transverse vibrations while also making the integrity of the network more resistant to further increases in Na_2O.

Bulk modulus behaves differently with changes in Na_2O and TiO_2. In the Na_2O-SiO_2 system, there is a slight decrease from 0 to 10 Na_2O, but then the bulk modulus increases with further additions of Na_2O. In the TiO_2-SiO_2 system, it decreases in a similar fashion to Young's modulus and shear modulus but the change is much smaller, going from 36.4 to 35 GPa with the addition of 8.3 TiO_2. Increasing the TiO_2 from 0 to 10 mol% increases the bulk modulus in the presence of Na_2O, from 36.2 to 40.2 GPa at 10 Na_2O, from 40.5 to 44.1 GPa at 25 Na_2O. In this case, the change in bulk modulus with TiO_2 appears to remain relatively constant for different Na_2O contents, staying around 5 GPa. The change in bulk modulus with Na_2O while holding TiO_2 constant is more interesting. The minimum in bulk modulus that occurs in the Na_2O-SiO_2

system between 0 and 10 Na_2O diminishes at 4 TiO_2 and disappears completely at 7 and 10 TiO_2, where the bulk modulus increases with increasing Na_2O.

A similar behavior also appears in the response of Poisson's ratio to composition changes (Fig. 3-4b). Poisson's ratio increases with the addition of both TiO_2 and Na_2O. Adding Na_2O has the greatest effect between 10 and 20 Na_2O, and a lesser effect from 0 to 10 and 20 to 25 mol%. The initial 10 Na_2O only increases Poisson's ratio by 0.013, after which adding Na_2O in 5 mol% increment increases it by 0.017, 0.022, and then 0.014. The effect of adding TiO_2 is dependent on the Na_2O content, with a change of 0.016 at 10 Na_2O when 10 TiO_2 is added. This decreases to a change of 0.003 at 25 Na_2O over the same composition change for TiO_2.

The smaller increase in Young's and shear moduli between the 20 Na_2O - 7 TiO_2 - 73 SiO_2 and 20 Na_2O - 10 TiO_2 - 70 SiO_2 glasses matches the low TiO_2 content in the 20 Na_2O - 10 TiO_2 - 70 SiO_2 glass (Table 3-1). The low Na_2O content in this sample is reflected in the decrease of the bulk modulus and Poisson's ratio from the 20 Na_2O - 7 TiO_2 - 73 SiO_2 to the 20 Na_2O - 10 TiO_2 - 70 SiO_2 composition. This also appears in the 25 Na_2O glasses, where the 25 Na_2O - 7 TiO_2 - 68 SiO_2 glass has a low TiO_2 content, making the change from 25 Na_2O - 4 TiO_2 - 71 SiO_2 to 25 Na_2O - 7 TiO_2 - 68 SiO_2 small and from 25 Na_2O - 7 TiO_2 - 68 SiO_2 to 25 Na_2O - 10 TiO_2 - 65 SiO_2 large.

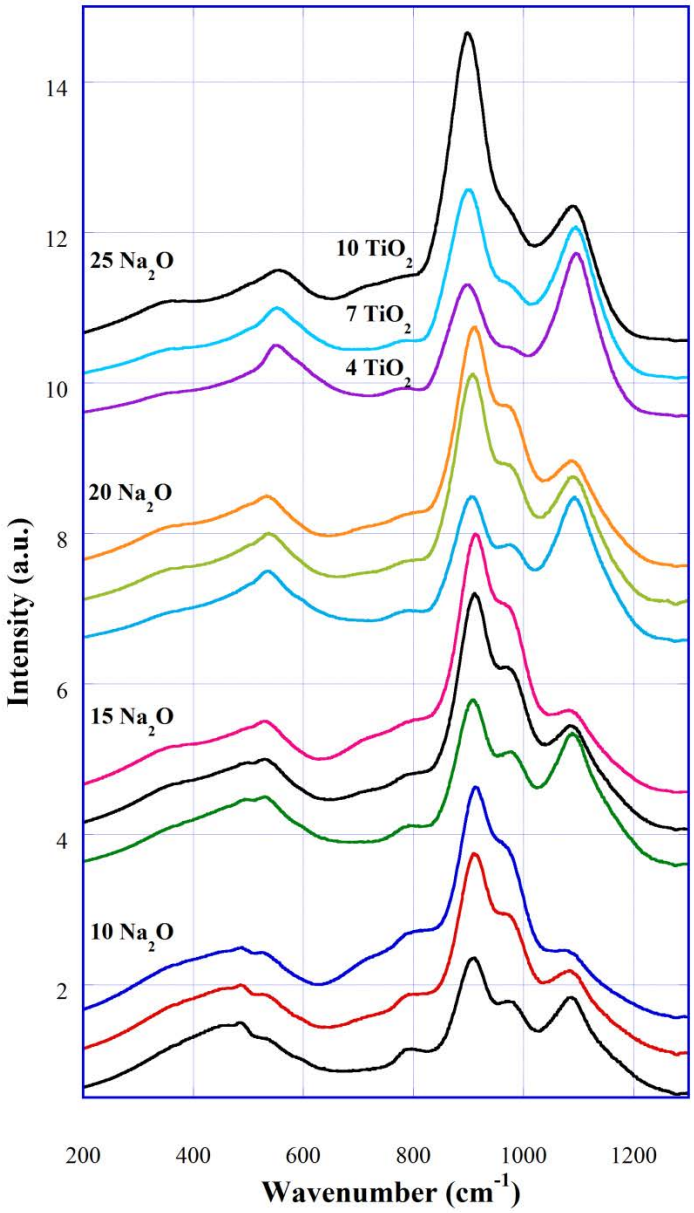

Fig. 3-5. Raman spectra of Na_2O-TiO_2-SiO_2 glasses at room temperature. Spectra are offset vertically for clarity, with Na_2O compositions of 10, 15, 20, and 25 in large offsets, and TiO_2 compositions of 4, 7, and 10 in small offsets.

Raman spectra for Na_2O-TiO_2-SiO_2 glasses are shown in Fig. 3-5. Spectra are offset vertically, with different Na_2O contents having large offsets and different TiO_2 contents having small offsets. Spectra were corrected for frequency and temperature [44] and then normalized to the maximum intensity in the 400-600 cm^{-1} range. These Raman spectra were then fit with Gaussian peaks using Fityk [45]. Peaks are observed at 340, 460, 490, 540, 600, 720, 800, 840,

900, 980, 1080, and 1100 cm^{-1}. The fitted peak positions are given in Table 3-3. The intensities of the peaks are shown in Table 3-4.

Table 3-3. Position of Raman peaks for Na_2O-TiO_2-SiO_2 glasses at room temperature.

Composition (Na_2O-TiO_2-SiO_2)	Wavenumber of Fitted Peaks (cm^{-1})												
	340	460	460 Small	490	540	600	720	800	840	900	980	1080	1100
10-4-86		457	458	488	539		730	794	841	906	977	1072	1087
10-7-83	336	458	455	488	536		725	797	848	907	973	1063	1086
10-10-80	332	458	453	487	533		728	802	851	908	970	1052	1082
15-4-81	341	476	458	490	534	590	720	794	849	906	975	1083	1090
15-7-78	342	470	457	491	535	576	718	799	851	908	976	1070	1091
15-10-75	336	474	462	493	533	571	722	802	852	908	973	1067	1088
20-4-76	343	498	459	490	537	592	720	794	851	905	975	1089	1094
20-7-73	340	494	462	491	540	592	722	790	849	906	975	1080	1094
20-10-70	337	484	450	491	537	580	724	795	849	908	976	1074	1093
25-4-71	340	528	452	500	548	589	725	788	848	897	973	1091	1099
25-7-68	341	529	465	497	552	600	717	790	849	899	972	1087	1098
25-10-65	336	534		493	557		715	791	843	897	969	1078	1099

Table 3-4. Intensity of Raman peaks for Na_2O-TiO_2-SiO_2 glasses at room temperature. Intensity is normalized to the maximum intensity in the 400-600 cm^{-1} range.

Composition (Na_2O-TiO_2-SiO_2)	Normalized Intensity of Fitted Peaks (a.u.)												
	340	460	460 small	490	540	600	720	800	840	900	980	1080	1100
10-4-86		0.91	0.07	0.13	0.04		0.27	0.48	0.35	1.72	0.66	0.98	0.38
10-7-83	0.02	0.92	0.05	0.12	0.09		0.42	0.67	0.54	2.43	1.23	0.98	0.25
10-10-80	0.05	0.92	0.04	0.10	0.13		0.68	0.86	0.69	2.62	1.60	0.86	0.16
15-4-81	0.02	0.82	0.05	0.13	0.25	0.04	0.19	0.52	0.37	2.16	1.01	1.38	0.48
15-7-78	0.05	0.83	0.04	0.13	0.25	0.05	0.33	0.68	0.46	2.93	1.46	1.23	0.28
15-10-75	0.08	0.79	0.04	0.11	0.27	0.07	0.49	0.81	0.56	3.11	1.84	1.03	0.17
20-4-76	0.03	0.65	0.05	0.10	0.40	0.09	0.06	0.35	0.27	1.93	0.90	1.48	0.53
20-7-73	0.06	0.69	0.05	0.06	0.36	0.05	0.19	0.47	0.55	3.00	1.32	1.48	0.33
20-10-70	0.06	0.74	0.02	0.11	0.31	0.06	0.32	0.56	0.53	3.06	1.48	1.30	0.22
25-4-71	0.04	0.51	0.02	0.11	0.38	0.26	0.02	0.23	0.17	1.69	0.74	1.73	0.50
25-7-68	0.07	0.59	0.02	0.10	0.40	0.13	0.05	0.32	0.34	2.42	1.01	1.69	0.40
25-10-65	0.12	0.70		0.06	0.31		0.25	0.56	0.49	3.85	1.37	1.62	0.29

In the low frequency region, the main band at 460 cm^{-1} decreases in intensity and shifts to higher frequencies with increasing Na_2O, and with increasing TiO_2 it increases in intensity and shifts to lower frequencies. Increasing TiO_2 increases intensity more at 20 and 25 Na_2O contents

and shift the position less at 10 and 25 Na_2O. The shoulder at 340 cm^{-1} increases in intensity with increasing TiO_2 and this increase is larger for higher Na_2O contents. The 490 cm^{-1} peak remains relatively unchanged in intensity and shifts slightly to higher frequencies with increasing Na_2O and does not change significantly with increasing TiO_2. The 540 cm^{-1} peak position does shifts only slightly between 10 and 20 Na_2O before shifting significantly to higher frequencies between 20 and 25 Na_2O. 540 cm^{-1} peak intensity does the opposite, increasing steadily between 10 and 20 Na_2O and then remaining almost constant between 20 and 25 Na_2O. Changes in the TiO_2 content have mixed effects on the peak position and intensity, increasing intensity and shifting to lower frequencies at 10 Na_2O and decreasing intensity and shifting to higher frequencies at 25 Na_2O. The 600 cm^{-1} peak was too small to fit in the 10 Na_2O glasses, and generally shifted slightly to higher frequencies with increasing Na_2O and to lower frequencies with increasing TiO_2. At 15 and 20 Na_2O, the intensity remains largely unaffected by Na_2O and TiO_2 content. A large increase in intensity occurs at 25 Na_2O, with increasing TiO_2 decreasing the intensity significantly.

The 720 cm^{-1} peak shifts to higher frequencies with increasing TiO_2 and to lower frequencies with increasing Na_2O. It also increases in intensity with increasing TiO_2 and decreases in intensity with increasing Na_2O. The 800 cm^{-1} peak shows the same response to the addition of TiO_2, increasing in both frequency and intensity, although the change in position is larger than that seen in the 720 cm^{-1} peak. The 840 cm^{-1} peak behaves in the same manner as the 720 and 800 cm^{-1} peaks in intensity, but does not shift in position with either Na_2O or TiO_2.

The high frequency peaks tend to have larger changes with composition. The 900 cm^{-1} peak shifts to higher frequencies with added TiO_2 and to lower frequencies with added Na_2O. Similar to the reaction of the 800 cm^{-1} peak, there is a large shift to lower frequencies between 20 and 25 Na_2O. It increases in intensity with increasing TiO_2. Increasing Na_2O decreases its intensity at low TiO_2 contents and increases the intensity at high TiO_2 contents. The 1100 cm^{-1} peak shows the opposite response to composition changes, decreasing in frequency with added TiO_2 and increasing in frequency with added Na_2O. With this peak the shift is fairly constant with Na_2O between 15 and 25 mol%. The 1100 cm^{-1} peak increases in intensity with Na_2O and decreases with TiO_2. The 1080 cm^{-1} peak decreases in intensity with increasing TiO_2 and increases in intensity slightly with increasing Na_2O. It shifts slightly to higher frequencies with increasing Na_2O and shifts significantly to lower frequencies with increasing TiO_2. The 980 cm^{-1}

peak experiences no significant peak shift with composition changes, but it does generally increase in intensity with increasing TiO_2.

To summarize the peak changes, adding TiO_2 increases the intensity of the 340, 460, 720, 800, 900, and 980 cm^{-1} peaks, while decreasing the intensity of the 1080 and 1100 cm^{-1} peaks. Na_2O increases the intensity of the 540 and 1080 cm^{-1} peaks while decreasing the intensities of the 460, 720, 800, and 840 cm^{-1} peaks. Adding Na_2O shifts the 460, 540, 1080, and 1100 cm^{-1} peaks to higher frequencies and the 720, 800, and 900 cm^{-1} peaks to lower frequencies. Adding TiO_2 shifts the 460, 1080, and 1100 cm^{-1} peaks to lower frequencies and the 720, 800, and 900 cm^{-1} peaks to higher frequencies. The 340, 490, 840, and 980 cm^{-1} peaks do not shift significantly with changes in either Na_2O or TiO_2 content.

3.5: Discussion:

The changes in properties with respect to the addition of Na_2O to the ternary system are basically the same as observed in the binary Na_2O-SiO_2 system. Density [9,32,34] and refractive index increase [2], Young's modulus and shear modulus decrease [9,32], bulk modulus and Poisson's ratio increase [32] (note: there is a shallow minimum in the bulk modulus around 10 Na_2O in the binary system), and thermal expansion increases [2,10]. The response to the addition of TiO_2 differs notably between the ternary and binary systems. In both cases the refractive index [34,42] and Poisson's ratio [33] increase with TiO_2; however, in the ternary system the density increases instead of remaining basically constant in the binary system [42], the elastic moduli increase instead of decreasing [34], and thermal expansion increases instead of decreasing [46,47].

Since Ti should be four-fold coordinated in a tetrahedral geometry in both the binary and ternary systems at low Ti contents [1,31], with square pyramidal $^{[5]}Ti$ beginning to appear in the ternary glasses above 5 mol% TiO_2 [31] (and dominate at 15 mol% [16]), this difference in response of material properties is somewhat non-intuitive. To unravel this mystery, we will begin with a review of the Raman peak assignments and a discussion of the implications of the shifts in position and the changes in intensity.

Peak assignments in the 400-600 cm^{-1} range are generally in agreement, with the 460 cm^{-1} peak assigned to symmetric oxygen vibrations in Si-O-Si bonds, the 490 cm^{-1} peak assigned to a breathing mode vibration in four-member Si-O rings, and the 540 cm^{-1} peak assigned to

delocalized vibrational modes arising from non-bridging oxygen in the silica network [48]. The peak occurring at 340 cm^{-1} is harder to assign. Kusabiraki et al. [20] suggested that it was due to antisymmetric bending of $^{[6]}$Ti; however, the population of $^{[6]}$Ti should be extremely small in our glasses [1,16,31].

The 1080 cm^{-1} and 1100 cm^{-1} peaks are likely associated with Ti and Si non-bridging oxygen, respectively. A similar peak appears at ~1100 cm^{-1} in both binary systems; assigned to Q^3 species in Na_2O-SiO_2 glasses [48] and to anti-symmetric oxygen vibrations in TiO_2-SiO_2 glasses (either Ti-O-Si bonds [33] or Si-O^- nBO caused by the added Ti [24]). The Q^3 peak appears at 1080 cm^{-1} for Si-O-Li nBOs [48] as opposed to at 1100 cm^{-1} for Si-O-Na. This suggests that the difference in position is caused by an increase in the range of motion available to the oxygen rather than a change in the Si-O bond. As $^{[4]}$Ti has a longer and weaker bond than $^{[4]}$Si, the Ti Q^3 species would tend to occupy a lower frequency than a Si Q^3.

In earlier studies, the 900 cm^{-1} peak was assigned to the bridging oxygen vibrations of TiO_2 tetrahedra [24,49]. This peaks shifts to lower frequencies as the TiO_2 content is increased. If it were caused by $^{[4]}$Ti, this could correspond to an increase in the amount of corner sharing Ti tetrahedra, which would tend to increase the free volume around the bridging oxygen, allowing for larger motions and a lower frequency. This would match Raman spectra for sodium titanates, which have peaks between 860 and 885 cm^{-1} depending on stoichiometry [50]. However, it has been observed that the fraction of $^{[4]}$Ti decreases and that of $^{[5]}$Ti increases as the TiO_2 content in the glass is increased [16,24,31]. $^{[5]}$Ti has four Ti-O bonds and one titanyl Ti=O bond. Farges et al. [15,17] predicted that the vibrations of this titanyl oxygen would have frequencies between 850-910 cm^{-1}. In a later high temperature Raman study by Reynard and Webb, the 900 cm^{-1} peak was assigned to the titanyl oxygen vibrations [25].

The 980 cm^{-1} peak is also difficult to assign, as peaks at ~950 cm^{-1} appear in both the TiO_2-SiO_2 and Na_2O-SiO_2 systems. In the Na_2O-SiO_2 system, this peak is assigned to the Q^2 species, which starts to become significant in intensity around 30 mol% Na_2O [32] and can shift towards 980 cm^{-1} as the Na_2O content reaches 40-50 mol% [48]. In the TiO_2-SiO_2 system, this peak has been assigned to either Si Q^2 species caused by the addition of TiO_2 [24] or Ti-O-Si bridging oxygens [33]. If it were due to the Q^2 species of Si caused by Na, then it would be expected that the peak intensity would be sensitive to the Na composition. As neither the peak intensity nor the position is sensitive to the Na_2O content (Tables 3-3 and 3-4), it makes more

sense to assign it to a Ti-O vibration. The intensity of the 980 cm^{-1} peak is sensitive to the TiO_2 content and the shift from 950 to 980 cm^{-1} between the binary and ternary systems.

The 720 and 800 cm^{-1} peaks have historically been difficult to assign for the ternary system. Inoue et al. assigned them to vibrations around $^{[6]}Ti$ and $^{[5]}Ti$, respectively [1]. Reynard and Webb assigned the 720 cm^{-1} peak to the motion of bridging oxygen in Q^2 and Q^3 species [25]. Reynard additionally pointed out that $^{[6]}Ti$ has peaks at ~600 cm^{-1} in rutile and anatase, with peaks at 720 cm^{-1} only appearing in crystals with edge-sharing $^{[6]}Ti$ octahedra [51]. If the 720 cm^{-1} peak was associated with the presence of Q^2 and Q^3 species, then it would be expected to increase with Na_2O content. As the intensity of this peak decreases with Na_2O and increases with TiO_2, that seems unlikely. Rather, if we suppose that the 800 cm^{-1} continues to correspond to the motions of Si within its tetrahedral oxygen cage [48], then it is possible that the 720 cm^{-1} peak corresponds to the motions of tetrahedral Ti. In this case we would expect the addition of Na_2O to create more nBO, which would break the symmetry around Q^4 species of Ti and Si, reducing the intensity of both peaks. The 720 cm^{-1} peak is reported at frequencies of ~750 cm^{-1} for higher TiO_2 contents [24,49] and has been compared to the 767 cm^{-1} TiO_4 band in Ba_2TiO_4 [24]. The 840 cm^{-1} peak was reported in pure SiO_2 glass by Kalampounias et al. [52], and assigned it to Si cation vibrations within "supertetrahedra" structures, with the 800 cm^{-1} peak assigned to Si cation vibrations within apex-bridged tetrahedra.

Accepting these peak assignments, we can compare them to the changes in material and mechanical properties. To make the changes in the spectra with changing TiO_2 content easier to see, Raman spectra for glasses from 0 to 10 TiO_2 are plotted for 10 and 25 Na_2O in Fig. 3-6. As Na_2O and TiO_2 concentrations become higher, the density increases. The effect of Ti on the structure to increase density can be seen in the broadening of the main 460 cm^{-1} peak. This broadening indicates a larger range of angles occupied by the network formers, which would allow for more efficient packing. This arises from the longer and lower strength Ti-O bonds, which preserve the silica network integrity while making rearrangement easier. The role of Na is to make the structure less rigid and fills available free volume, as seen in Fig. 3-7, where the Na_2O content is increased from 0 to 25 mol% for 4 and 10 TiO_2 glasses. This is most clearly seen in the changes in the 460 cm^{-1} peak, with the loss of symmetry and shift to higher frequencies.

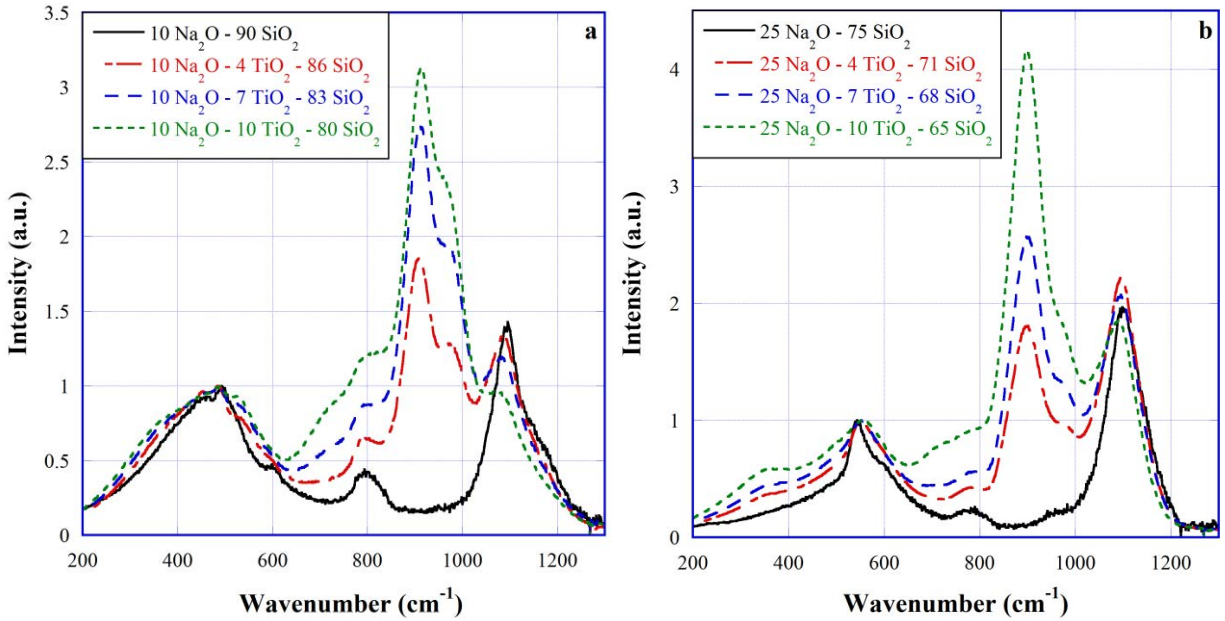

Fig. 3-6. Raman spectra of a) 10 Na_2O and b) 25 Na_2O glasses with TiO_2 contents between 0 and 10 mol%. Spectra are overlaid to make the differences in peak shape easier to observe. Spectra intensities are normalized to the peak maximum in the 400-600 cm^{-1} range.

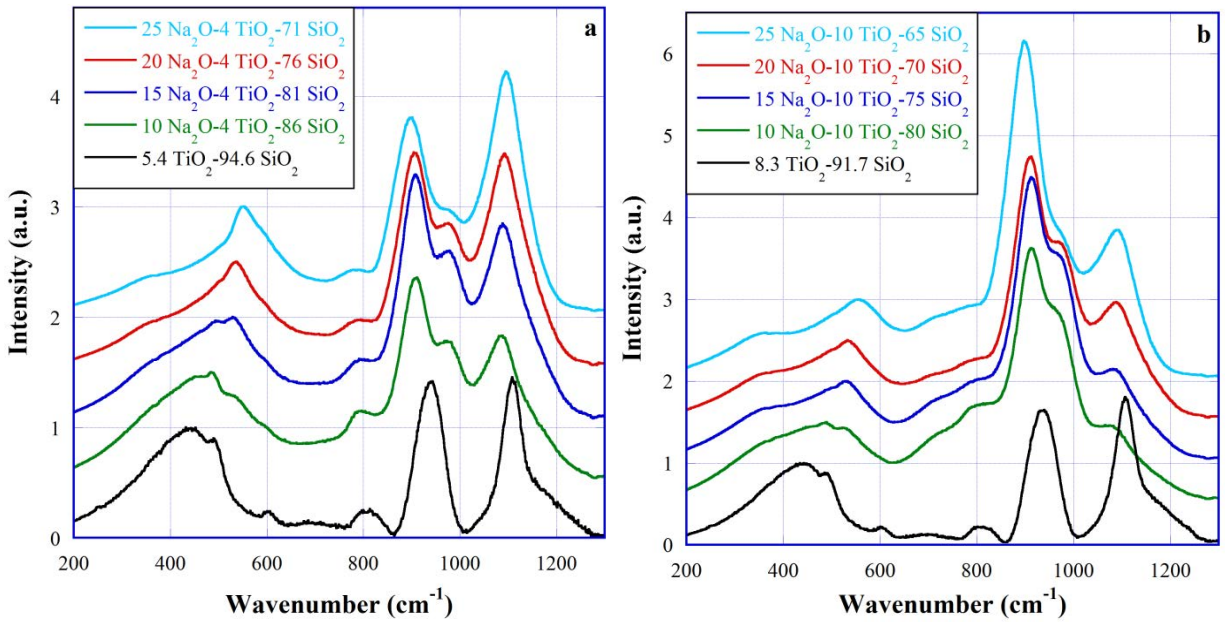

Fig. 3-7. Raman spectra of a) 4 TiO_2 and b) 10 TiO_2 glasses with Na_2O contents between 0 and 25 mol%. Spectra are offset vertically for clarity with increasing Na_2O. Spectra are normalized to the signal maximum in the 400-600 cm^{-1} range. Raman spectra of binary TiO_2-SiO_2 glasses with 5.4 and 8.3 TiO_2 are included in a) and b), respectively, for comparison.

If $^{[4]}$Ti is the primary species in these glasses, we might expect to see similar anomalous thermal expansion behavior to the binary system as we substitute Ti for Si. However, while

there is an initial increase in CTE between 0 and 4 mol% TiO_2, the CTE remains effectively constant between 4 and 10 TiO_2 (Fig. 3-3). Since the mechanism by which TiO_2 reduces the CTE in the binary system involves increasing the free volume [33], it might be expected that this effect would be hindered as the Na_2O content is increased. The increase in CTE with initial additions of Ti, which should be almost completely four-fold coordinated, supports this idea. The constant CTE between 4 and 10 mol% could be due to TiO_2 entering the glass as a combination of $^{[4]}$Ti and $^{[5]}$Ti. $^{[5]}$Ti should generally promote an increased flexibility in the network due to the titanyl nBO oxygen, but also removes Na from the silica network. The balance of these two effects could explain CTE remains relatively constant as TiO_2 is increased from 4 to 10 mol%.

This conjecture would support Farges et al.'s percolation model [16], where Ti atoms form clusters with localized high concentrations of Ti and Na. In these clusters ($^{[5]}$Ti=O)O_4 square pyramids are at the boundary between the Na-rich regions and the Si-rich regions, with the Ti=O titanyl oxygen on the Na-rich side of the boundary. If we adopt the percolation model into our explanation, the behavior of intensity of the 720, 800, 840, 900, 980, 1080, and 1100 cm^{-1} Raman peaks can be more easily explained. The addition of TiO_2 promotes further formation of these clusters, meaning that there will be less Na around Si. Thus the intensity of the 1100 cm^{-1} peak decreases, due to the reduced population of Si-O nBO contributing to this peak, consistent with the intensity increase in 800 and 840 cm^{-1} peaks, indicating that more Q^4 Si exists. And naturally, with more Ti the intensities of Ti related peaks, 720, 900, and 980 cm^{-1}, increase. Interestingly, the 1080 cm^{-1} peak decreases in intensity with increasing TiO_2. This would make sense if titanyl oxygens acted to charge balance Na^+ in the network, which would correspond to an increase in the $^{[5]}$Ti population.

Relating these peak changes to the mechanical properties, we see that as the TiO_2 content increases both Young's modulus and shear modulus. This can be related to a decrease in the number of nBO around Si. That is, as Ti enters the glass and preferentially attracts Na to form clusters, it leaves an interconnected network of silica tetrahedra with few nBO. This would act to increase the overall integrity of the network and stiffness of the glass structure. This mechanism of stiffening should be quite mild and certainly not increase the overall stiffness above that of pure silica. Inaba et al. reported Young's modulus for a 25 Na_2O - 15 TiO_2 - 60 SiO_2 glass of 74.2 GPa [9]. This follows the linear trend increase of Young's modulus with

added TiO_2 seen in our glasses, but also demonstrates that the stiffening aspect goes beyond shielding the SiO_2 network from Na. The further stiffening of the network is likely caused by an increase in the volume density of bonds in the network, tightening the network and increasing the packing density.

The shift in the 1080 and 1100 cm^{-1} peak positions match the free volume changes that would accompany the formation of these clusters. As Na_2O content increases, the peaks shift to higher frequencies, indicating that the free volume decreases as the amount of Q^3 species increases. With the addition of TiO_2, the peak shifts to lower frequencies as Na preferentially sits near titanyl oxygens and more free volume becomes available around nBO elsewhere in the glass. The fact that the 980 cm^{-1} peak changes its intensity but not its position with changes in either Na_2O or TiO_2 content suggests that the population of the Ti and Na rich clusters changes, but not their size. In the composition ranges we studied here, the population of clusters is not large enough for interactions between them to be appreciable; otherwise, the peak position would shift with the change of composition.

Both bulk modulus and Poisson's ratio increase with both TiO_2 and Na_2O content. This can generally be related to the reduction of free volume associated with both the number of nBOs and the formation of Ti and Na rich clusters. For both bulk modulus and Poisson's ratio, the observed increase is reduced between 20 and 25 mol% Na_2O than between other Na_2O contents. This corresponds to a significant increase in the frequency of the 460 and 540 cm^{-1} peaks. It is possible that at 25 mol% Na_2O there is enough Na in the network that the formation of Ti rich clusters does not significantly alter the free volume available to the surrounding silica network.

3.6: Conclusions:

The structure, material and mechanical properties of Na_2O-TiO_2-SiO_2 glasses have been studied with regards to composition through Raman spectroscopy, Brillouin light scattering, and dilatometry. Density, refractive index, elastic moduli, and Raman spectra agree well with literature values of similar glasses. The addition of Na_2O increases the density, refractive index, and CTE of glasses. It decreases Young's modulus and shear modulus while increasing the bulk modulus and Poisson's ratio. The addition of TiO_2 increases density, refractive index, Young's modulus, shear modulus, bulk modulus, and Poisson's ratio. CTE increases initially with TiO_2, and then remains constant with further additions of TiO_2.

Changes in the Raman spectra with composition have been discussed and related to the changes in properties. TiO_2 was observed to provide a stiffening effect by increasing the intensity and shifting to higher frequencies of peaks associated with network formers, namely the 720, 800, and 900 cm^{-1} peaks, while decreasing the intensity of the Si-O nBO peak at 1100 cm^{-1}. TiO_2 appears to reduce the effect of Na_2O on the silica network, and this shielding effect has been discussed in relationship to the percolation model proposed by Farges et al. [16]. TiO_2 stiffens the network by increasing the ordering and constraints in the network through the formation of clusters with higher local Ti and Na concentrations. While by increasing the number of nBO, Na_2O disrupts the network connectivity and fills available free volume.

3.7: References:

[1] K. Inoue, S. Sakida, T. Nanba, Y. Miura, Structure and optical properties of TiO_2 containing glasses, Materials Science and Technology 2006: Materials and Systems. 1 (2006) 583–593.

[2] Y. Kobayashi, T. Shimizu, M. Shigekazu, R. Endo, M. Susa, Determination of refractive indices and linear coefficients of thermal expansion of silicate glasses containing titanium oxides, ISIJ Int. 128 (1997) 6–10.

[3] M. Liska, P. Simurka, J. Antalik, P. Perichta, Viscosity of titania-bearing sodium silicate melts, Chem. Geol. 128 (1996) 199–206.

[4] M. Liska, V. Klyuev, J. Antalik, I. Stubna, Viscosity of $Na_2O{\cdot}2(TiO_2,SiO_2)$ glasses, Phys. Chem. Glasses. 38 (1997) 6–10.

[5] M. Bouhifd, A. Sipp, P. Richet, Heat Capacity, viscosity, and configurational entropy of alkali titanosilicate melts, Geochim. Cosmochim. Acta. 63 (1999) 2429–2437.

[6] M. Manghnani, Pressure and Temperature dependence of the elastic moduli of Na_2O-TiO_2-SiO_2 glasses, J. Am. Ceram. Soc. 55 (1972) 360–365.

[7] R. Johnston, C. Babcock, Composition dependence of the elastic moduli in Na_2O-TiO_2-SiO_2 glasses, J. Am. Ceram. Soc. 58 (1975) 85–87.

[8] G.K. White, J.A. Birch, M.H. Manghnani, Thermal-properties of sodium silicate glasses at low-temperatures, J. Non-Cryst. Solids. 23 (1977) 99–110.

[9] S. Inaba, S. Fujino, K. Morinaga, Young's modulus and compositional parameters of oxide glasses, J. Am. Ceram. Soc. 82 (1999) 3501–3507.

[10] V. Klyuev, Dependences of the dilatometric properties of glasses on their structure: II. silicate, phosphate, fluorine-containing, and titanium-containing glasses, Glass Phys. Chem. 32 (2006) 196–205.

[11] S. Webb, D. Dingwell, Compressibility of titanosilicate melts, Contrib. Mineral. Petrol. 118 (1994) 157–168.

[12] Q. Liu, R. Lange, The partial molar volume and thermal expansivity of TiO_2 in alkali silicate melts: systematic variation with Ti coordination, Geochim. Cosmochim. Acta. 65 (2001) 2379–2393.

[13] Q. Liu, R. Lange, Y. Ai, Acoustic velocity measurements on Na_2O-TiO_2-SiO_2 liquids: Evidence for a highly compressible TiO_2 component related to five-coordinated Ti, Geochim. Cosmochim. Acta. 71 (2007) 4314–4326.
[14] F. Glasser, J. Marr, Phase Relations in the system Na_2O-TiO_2-SiO_2, J. Am. Ceram. Soc. 62 (1979) 42–47.
[15] F. Farges, G.E.J. Brown, J.J. Rehr, Coordination Chemistry of Ti(IV) in Silicate Glasses and Melts: I. XAFS Study of Titanium Coordination in Oxide Model Compounds, Geochim. Cosmochim. Acta. 60 (1996) 3023–3038.
[16] F. Farges, G.E.J. Brown, A. Navrotsky, H. Gan, J.J. Rehr, Coordination Chemistry of Ti(IV) in Silicate Glasses and Melts: II. Glasses at Ambient Temperature and Pressure, Geochim. Cosmochim. Acta. 60 (1996) 3039–3053.
[17] F. Farges, G. Brown Jr., A. Navrotsky, H. Gan, J. Rehr, Coordination chemistry of Ti(IV) in silicate glasses and melts: III. Glasses and melts from ambient to high temperatures, Geochim. Cosmochim. Acta. 60 (1996) 3055–3065.
[18] F. Farges, G.E. Brown, Coordination chemistry of Ti(IV) in silicate glasses and melts: IV. XANES studies of synthetic and natural volcanic glasses and tektites at ambient temperature and pressure, Geochim. Cosmochim. Acta. 61 (1997) 1863–1870.
[19] F. Farges, A Ti K-edge EXAFS Study of the Medium Range Environment Around Ti in Oxide Glasses, J. Non-Cryst. Solids. 244 (1999) 25–33.
[20] K. Kusabiraki, Infrared and Raman spectra of vitreous silica and sodium silicates containing titanium, J. Non-Cryst. Solids. 95-96 (1987) 411–418.
[21] M. Manghnani, A study of Na_2O-TiO_2-SiO_2 glasses by Infrared spectroscopy, Appl. Spectrosc. 28 (1974) 256–259.
[22] G. Peng, S. Chen, H. Liu, Infrared absorption spectra and their correlation with Ti-O bond length variations for TiO_2 (rutile), Na-Titanates, and Na-Titanosilicates (Natisite, $NaTiO_2SiO_4$), Appl. Spectrosc. 49 (1995) 1646–1651.
[23] B. Mysen, D. Neuville, Effect of temperature and TiO_2 content on the structure of $Na_2Si_2O_5$-$Na_2Ti_2O_5$ melts and glasses, Geochimica et Cosmochimica Acta. 59 (1995) 325–342.
[24] G. Henderson, M. Fleet, The structure of Ti silica glasses by micro-Raman spectroscopy, Can. Mineral. 33 (1995) 399–408.
[25] B. Reynard, S. Webb, High-temperature Raman spectroscopy of $Na_2TiSi_2O_7$ glass and melt: coordination of Ti^{4+} and nature of the configurational changes in the liquid, Eur. J. Mineral. 10 (1998) 49–58.
[26] A. Osipov, G. Korinevskaya, L. Osipova, V. Muftakhov, Titanium coordination in TiO_2-Na_2O-SiO_2 glasses of $xTiO_2$ (100-x)[$2Na_2O$-$3SiO_2$] ($0 \leq x \leq 30$) composition based on Raman spectroscopy, Glass Phys. Chem. 38 (2012) 357–360.
[27] A. Sharma, M.S. Kerium, M. Abdel-Baki, F. El-Diasty, RDF analysis positron annihilation and Raman spectroscopy of $xTiO_2$-(60-x)SiO_2-$40Na_2O$ non-linear optical glasses: III. Non-bridging oxygen bonds tracing and structure analysis, J. Non-Cryst. Solids. 353 (2007) 2708–2716.
[28] H. Hidaka, N. Iwamoto, N. Umesaki, T. Fukunaga, K. Suzuki, Structural analysis of sodium silicate glasses containing TiO_2 by pulsed neutron scattering, J. Mater. Sci. 20 (1985) 2497–2502.
[29] S. Sakka, H. Hotta, The Si-O bonding in Na_2O-TiO_2-SiO_2 and K_2O-TiO_2-SiO_2 glasses as studied by Si K_β X-ray fluorescence and infra-red absorption spectroscopy, J. Mater. Sci. 14 (1979) 2335–2342.

[30] T. Hanada, N. Soga, Co-ordination of titanium in sodium titanium silicate glasses, J. Non-Cryst. Solids. 38-39 (1980) 105–110.
[31] G. Henderson, X. Liu, M. Fleet, A Ti L-edge X-ray absorption of Ti-silicate glasses, Phys. Chem. Miner. 29 (2002) 32–42.
[32] Q. Zhao, M. Guerette, G. Scannell, L. Huang, In-situ high temperature Raman and Brillouin light scattering studies of sodium silicate glasses, Journal of Non-Crystalline Solids. 358 (2012) 3418–3426.
[33] G. Scannell, A. Koike, L. Huang, Structure and Thermo-mechanical response of TiO_2-SiO_2 glasses to temperature, under review with Journal of Non-Crystalline Solids (2016).
[34] E. Hamilton, G. Cleek, Properties of sodium titanium silicate glasses, J. Res. Natl. Bur. Stand. (U.S.). 61 (1958) 89–94.
[35] J. Shelby, Fictive Temperature and Density of Doped Vitreous Silica, Phys. Chem. Glasses: Eur. J. Glass Sci. Technol., Part B. 50 (2009) 7–14.
[36] S. Gulati, Mechanical Properties of SiO_2 vs. SiO_2-TiO_2 Bulk Glasses and Fibers, Mat. Res. Soc. Symp. Proc. 244 (1992) 67–83.
[37] M. Guerette, L. Huang, A simple and convenient set-up for high-temperature Brillouin light scattering, J. Phys. D: Appl. Phys. 45 (2012) 275302.
[38] K. Davis, A. Agarwal, M. Tomozawa, K. Hirao, Quantitative infrared spectrascopic measurements of hydroxyl concentrations in silica glass, J. Non-Cryst. Solids. 203 (1996) 27–36.
[39] B. Sloots, Measuring the low OH content in quartz glass, Vib. Spectrosc. 48 (2008) 158–161.
[40] B. Schmidt, F. Holtz, J.-M. Beny, Incorporation of H_2 in vitreous silica, qualitative and quantitative determination from Raman and infrared spectroscopy, J. Non-Cryst. Solids. 240 (1998) 91–103.
[41] G. Scannell, L. Huang, T. Rouxel, Elastic properties and indentation cracking behavior of Na_2O-TiO_2-SiO_2 glasses, J. Non-Cryst. Solids. 429 (2015) 129–142.
[42] J. Shelby, Density of TiO_2-doped vitreous silica, Phys. Chem. Glasses. 46 (2005) 494–499.
[43] H. Shermer, Thermal Expansion of Binary Alkali Silicate Glasses, J. Res. Natl. Bur. Stand. (U.S.). 57 (1956) 97–101.
[44] P. McMillan, B. Poe, P.H. Gillet, B. Reynard, A study of SiO_2 glass and supercooled liquid to 1950 K via high-temperature Raman spectroscopy, Geochim. Cosmochim. Acta. 58 (1994) 3653–3664.
[45] M. Wojdyr, Fityk: a general-purpose peak fitting program, J. Appl. Crystallogr. 43 (2010) 1126–1128.
[46] S. Gulati, Mechanical Properties of SiO_2 vs. SiO_2-TiO_2 Bulk Glasses and Fibers, Mat. Res. Soc. Symp. Proc. 244 (1992) 67–83.
[47] K. Kamiya, S. Sakka, Thermal Expansion of TiO_2-SiO_2 and TiO_2-GeO_2 glasses, J. Non-Cryst. Solids. 52 (1982) 357–363.
[48] P. McMillan, Structural studies of silicate glasses and melts--applications and limitations of Raman spectroscopy, Am. Mineral. 69 (1984) 622–644.
[49] F. Miyaji, T. Yoko, H. Kozuka, S. Sakka, Structure of $Na_2O{\cdot}2TiO_2$ glass, J. Mater. Sci. 26 (1991) 248–252.
[50] C. Bamberger, G. Begun, Sodium Titanates: Stoichometry and Raman spectra, J. Am. Ceram. Soc. 70 (1987) 48–51.

[51] B. Reynard, F. Guyot, High temperature properties of geiklielite ($MgTiO_3$-ilmenite) from high-temperature high-pressure Raman spectroscopy - Some implications for $MgSiO_3$-ilmenite, Phys. Chem. Miner. 21 (1994) 441–450.
[52] A. Kalampounias, S. Yannopoulos, G. Papatheodorou, Temperature-induced structural changes in glassy, supercooled molten silica from 77 to 2150 K, J. Chem. Phys. 124 (2006) 014504.

Chapter 4 : Structure and Thermo-mechanical Response of Na_2O-TiO_2-SiO_2 Glasses to Temperature

4.1: Abstract:

In-situ high temperature Raman spectroscopy, Brillouin light scattering (BLS), and dilatometry have been used to study the structure and properties of xNa_2O-$yTiO_2$-$(1-x-y)SiO_2$ glasses. Glasses with nominal compositions x=10, 15, 20, and 25, and y=4, 7, and 10 were prepared through a traditional melt quench method. Addition of Na_2O decreases the temperature response of elastic moduli and increases the temperature response of the Poisson's ratio and the coefficient of thermal expansion (CTE). TiO_2 increases the magnitude of elastic moduli, but does not change their responses to temperature appreciably. TiO_2 has a much smaller effect in changing the CTE and the Poisson's ratio than Na_2O. Changes in the position and intensity of Raman peaks with temperature have been discussed. Changes in the temperature responses of mechanical and material properties have been correlated to changes in the temperature responses of Raman peaks.

4.2: Introduction:

Studying the response of glasses to external stimuli, such as temperature or pressure, can provide valuable insights into understanding the behavior of glasses. Especially, the elastic and vibrational properties of glass are directly related to the interatomic forces and potentials, embodying the local structure and bonding information [1]. Therefore, perturbing the glass with thermal or mechanical agitation (e.g., temperature, pressure or strain) and measuring the changes in its elastic and vibrational properties, can be used as a probe to gain insights into the atomic level structure of glass.

Vukcevich proposed a two-state model in 1972 for silica glass using changes in structure to explain the pressure and temperature dependence of compressibility, thermal expansion, and specific heat [2]. McMillan et al. and Kalampounias et al. studied how the structure of silica glass changed with *in-situ* high temperature Raman spectroscopy [3,4]. Deschamps et al. performed similar experiments with *in-situ* high pressure Raman spectroscopy [5]. However, our understanding of the behavior of glasses in response to external stimuli is still very limited outside of simple glass systems such as silica, and building this understanding is critical towards developing glasses with improved properties [6,7].

Understanding the response of structure and properties to temperature is of particular interest for Ti containing glasses. Binary TiO_2-SiO_2 glasses are well known for their extremely low coefficients of thermal expansion [8,9]. These glasses also show an anomalous increase of elastic moduli with temperature [10,11]. Alkali-titania-silicate glasses and melts have also been shown to have unusual responses to temperature, particularly in regards to their compressibility [12,13], shear viscosity [14], partial molar volume and thermal expansivity [15], and heat capacity, viscosity, and configurational entropy [16]. The coordination state of Ti is highly dependent on the surrounding glass composition [15,17,18], which has been attributed to be the origin of some of the unusual properties of titanate glasses [15].

Most of the *in-situ* high temperature measurements of the structure and elastic properties of the Na_2O-TiO_2-SiO_2 system has focused on melts, with less attention given to the behavior of the glass between room temperature and the glass transition temperature. High temperature Raman studies have been limited to either a single composition [19] or a constant Na_2O content [20]. Studies on the high temperature elastic properties are even more limited [21]. In this work we examined the high temperature response of the structure, elastic moduli, and thermal expansion of Na_2O-TiO_2-SiO_2 glasses. Structure was probed through *in-situ* high temperature Raman spectroscopy, elastic moduli through *in-situ* high temperature Brillouin light scattering (BLS), and thermal expansion through dilatometry. Glasses examined have nominal compositions of xNa_2O-$yTiO_2$-$(1-x-y)SiO_2$, where x=10, 15, 20, and 25, and y=4, 7, and 10. Room temperature data for this system has already been presented in a previous work [22]. Temperature responses of mechanical and material properties were correlated with the changes in the underlying structure reflected in the temperature responses of Raman peaks.

4.3: Methods/Experimental:

The sample preparation and room temperature experimental details were presented in the previous chapter. For high temperature light scattering experiments, Raman and Brillouin spectra were collected together. The sample was heated at 50 °C/min to the target temperature, held for five minutes to allow it to thermally equilibrate, then the Brillouin spectrum was collected, followed by the collection of the Raman spectrum. *In-situ* high temperature Raman spectra were collected at 50, 200, 400, 600, and 800 °C. Brillouin spectra were collect every 50 °C, with measurements taken every 10 °C between 450 °C and 650 °C to better observe the behavior around the glass transition temperature. Spectra were corrected for frequency and temperature [3], and then normalized to the maximum intensity of the main silica band (400-600 cm^{-1}).

Coefficient of thermal expansion (CTE) was measured using a dual pushrod differential dilatometer at Corning, Inc. Measurements were made from room temperature to 480 °C using a 4 °C/min heating rate and a 5 minute hold at the maximum temperature. Coefficients of thermal expansion were calculated every 25 °C from 50 °C to 475 °C. Sapphire was used as a reference material.

4.4: Results

The change of CTE with temperature is shown in Fig. 4-1. The CTE is almost constant for samples with 10 Na_2O between 50 and 475 °C. As the Na_2O content is increased, the CTE shows an increased sensitivity to temperature, increasing as the temperature is increased. Changes in the TiO_2 content have less effect on the CTE, and the small changes that are observed appear to shift from an increase in CTE at 10 Na_2O to a decrease at 25 Na_2O.

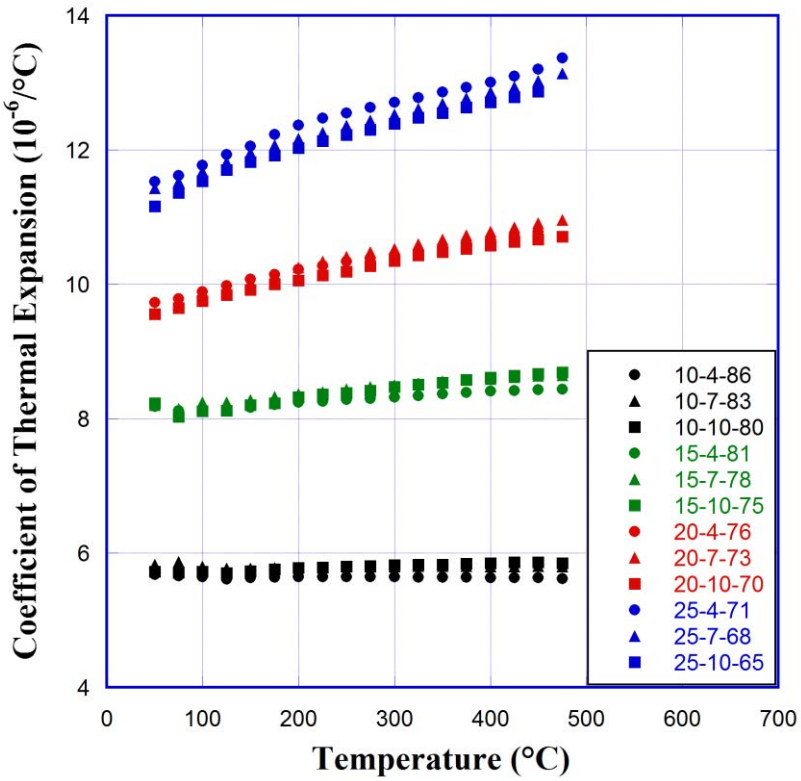

Fig. 4-1. CTE of Na_2O-TiO_2-SiO_2 glasses versus temperature.

Fig. 4-2(a-d) shows the response of elastic moduli to temperature for the Na_2O-TiO_2-SiO_2 glasses examined. Young's modulus (Fig. 4-2a) changes from anomalous behavior at 10 Na_2O to intermediate at 15 Na_2O and then normal at 20 and 25 Na_2O. The slope of Young's modulus with temperature decreases with increasing Na_2O content and weakly increases with increasing TiO_2 content. Increasing Na_2O significantly lowers the magnitude of Young's modulus from 10 to 15 to 20, but the change from 20 to 25 shows a smaller reduction. Increasing TiO_2 increases the magnitude of Young's modulus and increases the glass transition temperature.

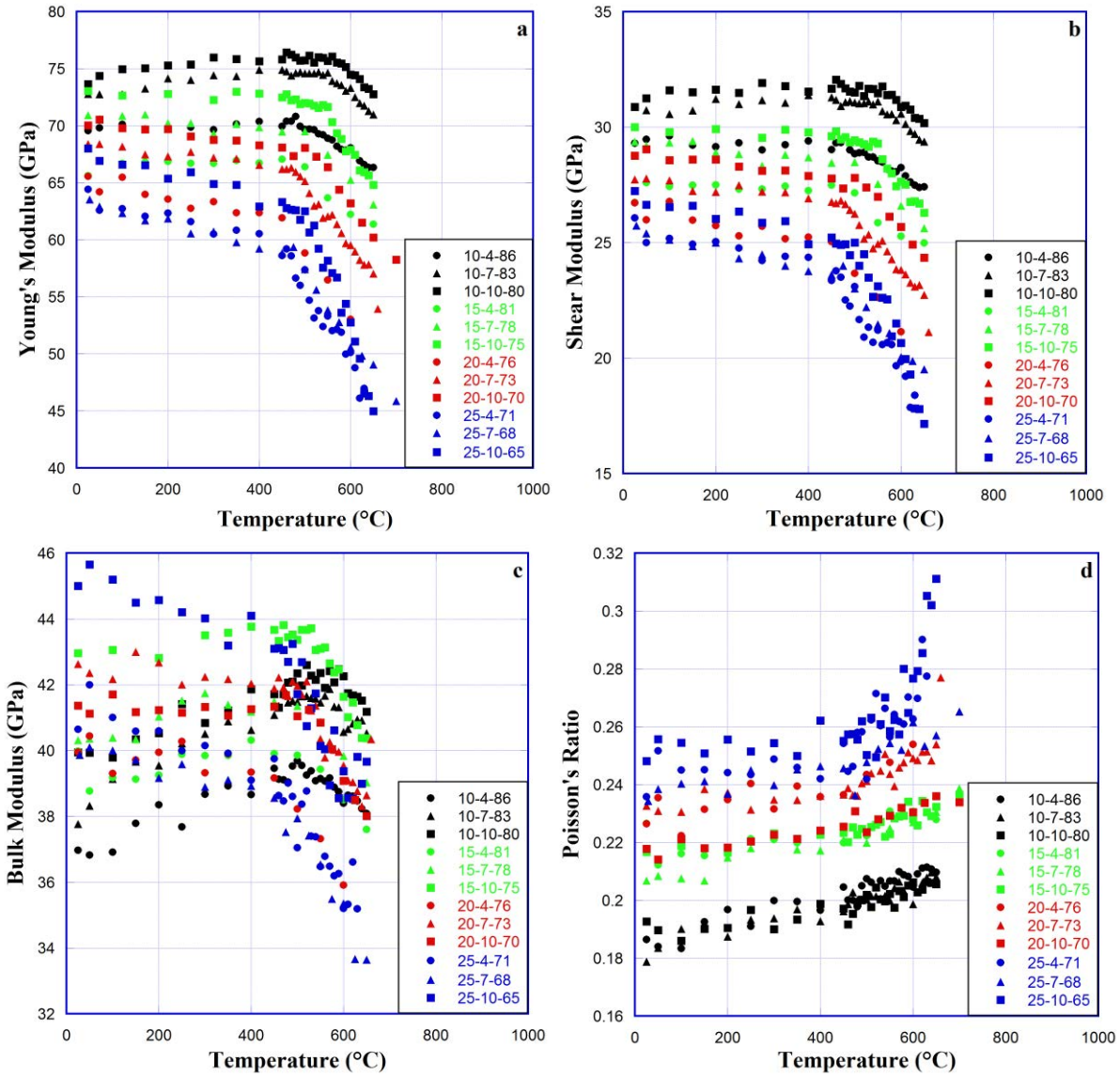

Fig. 4-2. Temperature response of a) Young's modulus, b) shear modulus, c) bulk modulus, and d) Poisson's ratio of Na_2O-TiO_2-SiO_2 glasses.

The shear modulus (Fig. 4-2b) behaves almost identically to Young's modulus, in that there is a decrease in magnitude, slope, and glass transition temperature with increasing Na_2O content, with the decrease in magnitude and slope only small between 20 and 25 Na_2O. Increasing the TiO_2 content increases the magnitude and the glass transition temperature without significantly changing the slope.

The bulk modulus (Fig. 4-2c) increases in magnitude with both increasing TiO_2 and increasing Na_2O. The increase with Na_2O is large between 10 and 15, and between 20 and 25,

but small between 15 and 20 mol%. Increasing the Na_2O content still decreases the slope, similar to Young's modulus and shear modulus. Bulk moduli for all twelve compositions fall within a 5 GPa range between 400 and 500 °C, down from the 10 GPa range observed at room temperature.

The Poisson's ratio (Fig. 4-2d) shows a strong increase with increasing Na_2O and a weak increase with increasing TiO_2. The increase in the Poisson's ratio with increasing Na_2O is reduced with each further addition of Na_2O, increasing by approximately 0.025, 0.02, and 0.015 when Na_2O content is increased from 10 to 15, from 15 to 20, and from 20 to 25, respectively. Additionally, the fragility of the glass, seen by the difference in slope from below to above the glass transition temperature, increases significantly with increasing Na_2O. Changing the TiO_2 content does not appear to affect the fragility much other than changing the glass transition temperature.

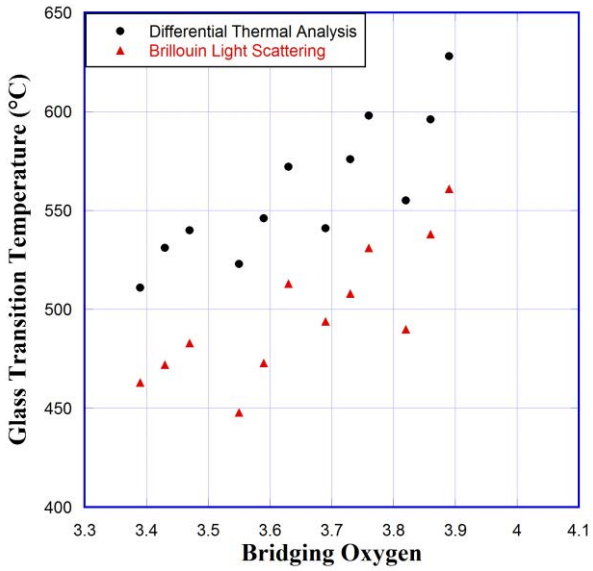

Fig. 4-3. Glass transition temperature versus number of bridging oxygen per network forming cation. Differential thermal analysis data is from Scannell et al. [23]. T_g values from BLS are measured as the temperature at which the slope of the shear modulus changes.

Fig. 4-3 shows the glass transition temperature (T_g) for Na_2O-TiO_2-SiO_2 glasses as fit from the temperature at which the slope of the shear modulus changes and from differential thermal analysis [23]. T_g from BLS experiments occurs at ~$0.9T_g$ of DTA measurements.

Between 20 and 25 Na_2O, or from 3.6 to 3.4 bridging oxygens per network forming cation, T_g becomes less sensitive to composition changes.

The temperature responses of the elastic moduli including Young's modulus, shear modulus, and bulk modulus and the Poisson's ratio are shown in Fig. 4-4. The slopes are obtained through a least squares linear fit to the elastic moduli between 100 °C and 400 °C. Slopes of Young's modulus and shear modulus decrease as the number of bridging oxygen per network cation decreases, but between 3.6 and 3.4 the changes in slopes become smaller, similar to the behavior of T_g in this composition range. The bulk modulus exhibits a continuous decrease in slope with decreasing number of bridging oxygen. Slopes of Poisson's ratio are extremely small and show significant scatter, but there is an overall trend of a decreasing slope with decreasing number of bridging oxygen.

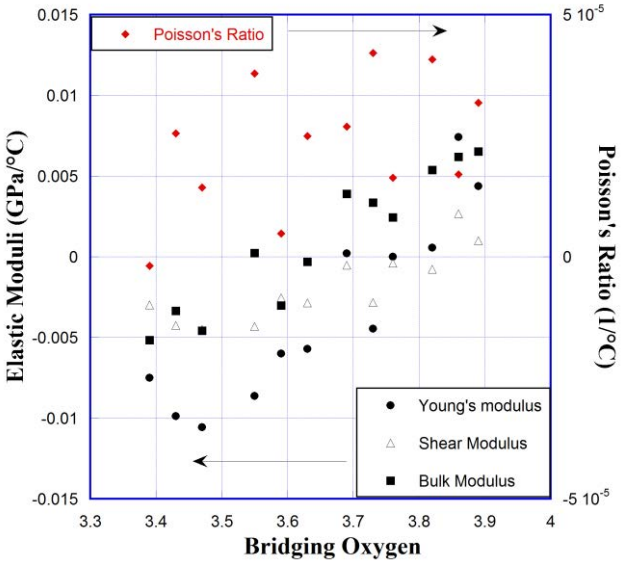

Fig. 4-4. Temperature response of elastic moduli versus the number of bridging oxygen per network forming cation.

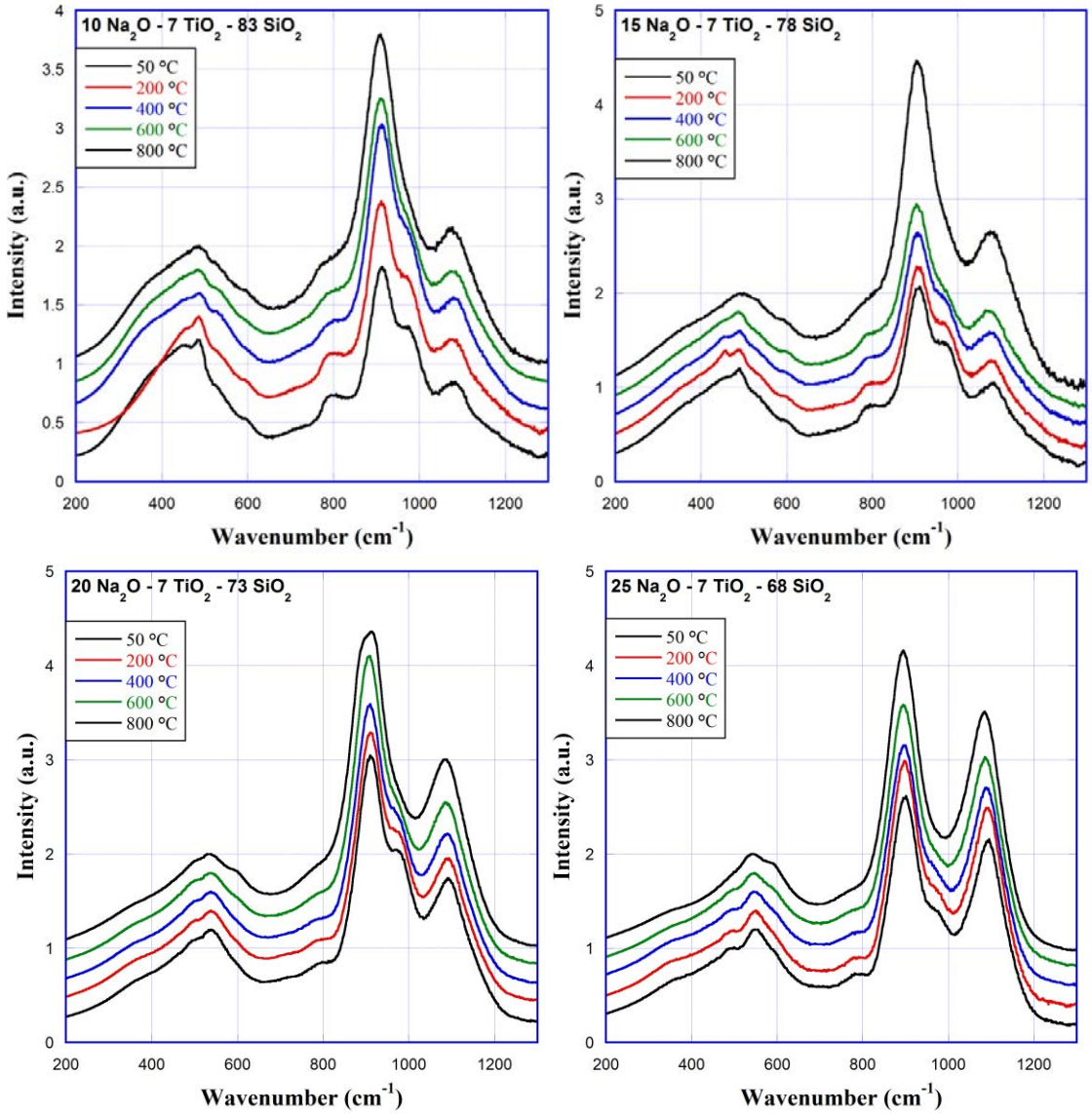

Fig. 4-5. Raman spectra for Na_2O - 7 TiO_2 - SiO_2 glasses at 50, 200, 400, 600, and 800 °C. Spectra intensities are normalized to the maximum intensity in the 400-600 cm^{-1} region and offset vertically with increasing temperature for clarity.

Raman spectra for Na_2O - 7 TiO_2 - SiO_2 glasses at 50, 200, 400, 600, and 800 °C are shown in Fig. 4-5(a-d). Spectra intensities are normalized to the maximum intensity in the 400-600 cm^{-1} region and offset vertically for clarity. The spectra were fit with Gaussian peaks using Fityk [24]. Peaks were fit at 460, 490, 540, 600, 720, 800, 840, 900, 980, 1080, and 1100 cm^{-1}. Additional, small peaks appear at ~340 and ~460 cm^{-1} in most, but not all samples. The position and intensity of the peaks are reported in Table 4-1.

The silica main band at 460 cm^{-1} increases in frequency from 450 to 510 cm^{-1} between 10 and 25 Na_2O. It also decreases in intensity from 0.88 to 0.65. The peak's response to temperature remains almost unchanged with changing Na_2O. From 50 to 800 °C, the peak shifts ~20 cm^{-1} to higher frequencies and increases by ~0.05 in relative intensity.

The 540 cm^{-1} peak shifts from 530 to 552 cm^{-1} and increases from 0.1 to 0.36 in intensity with increasing Na_2O. Most of the increase in intensity occurs between 15 and 20 Na_2O. In response to temperature, the peak position remains constant at 10, 15, and 20 Na_2O, and shifts from 552 to 538 at 25 Na_2O. The intensity is also approximately constant between 50 and 800 °C for 10 and 15 Na_2O, but decreases with increasing temperature at 20 and 25 Na_2O.

Peaks at 490 and 600 cm^{-1} are assigned to 4- and 3-member Si-O ring breathing modes, respectively. The position of these peaks does not change with either Na_2O composition or temperature. The relative intensity of the 490 cm^{-1} peak decreases from 0.18 to 0.14 with increasing Na_2O, while the intensity of the 600 cm^{-1} peak increases from 0.04 to 0.13. Both peaks' intensities are insensitive to temperature.

The 700, 800, and 840 cm^{-1} peaks are assigned to cation-oxygen vibrations, primarily due to the cation motion. The 700 cm^{-1} corresponds to the motion of Ti^{4+} with four bridging oxygen bonds. Fitting the position of this peak is less accurate than other peaks; however, the position generally remains between 720 and 730 cm^{-1} for all Na_2O compositions and the position appears relatively insensitive to temperature. The intensity of the 700 cm^{-1} peak changes significantly with increasing Na_2O, decreasing from 0.3 at 10 Na_2O to 0.26, 0.24, and 0.06 at 15, 20, and 25 Na_2O, respectively. Additionally, the temperature response of the intensity of the 700 cm^{-1} peak decreases with increasing Na_2O, with it changing from positive to negative between 15 and 20 Na_2O.

The 800 cm^{-1} corresponds to Si-O_4 silicon vibrations. For 10, 15, and 20 Na_2O the peak position is relatively insensitive to composition and temperature, remaining between 795 and 800 cm^{-1}. At 25 Na_2O it decreases to 792 cm^{-1} and then shifts to lower frequencies with increasing temperature, to 787 cm^{-1} at 800 °C. The intensity of the 800 cm^{-1} peak increases slightly, from 0.4 to 0.5 from 10 to 20 Na_2O, and 10, 15, and 20 Na_2O compositions see an intensity increase with temperature by ~0.2 between 50 and 800 °C. The 25 Na_2O has a peak intensity of 0.35, and the intensity decreases slightly with temperature, to 0.3 at 800 °C.

The 840 cm^{-1} peak is also associated with Si-O_4 silicon vibrations, when there is some local ordering with four tetrahedra forming a super-tetrahedra. The peak shifts slightly to lower frequencies with both increasing Na_2O and increasing temperature. The sensitivity to temperature increases with increasing Na_2O content, from a shift of -3 cm^{-1} at 10 Na_2O to -10 cm^{-1} at 25 Na_2O. The intensity of the 840 cm^{-1} peak generally decreases with increasing Na_2O content. The temperature response of the intensity changes from slightly negative at 10 Na_2O to slightly positive at 25 Na_2O.

The 900 cm^{-1} peak exhibits a weak, negative response to temperature which remains constant at all Na_2O contents. Increasing Na_2O causes a small shift to lower frequencies, from 908 cm^{-1} at 10 Na_2O to 906 cm^{-1} at 15 Na_2O to 896 cm^{-1} at 25 Na_2O. The intensity of the 900 cm^{-1} peak increases with increasing temperature and roughly with increasing Na_2O.

The 980 cm^{-1} peak's position is relatively insensitive to Na_2O content at 50 °C, but the response to temperature becomes increasingly negative with increasing Na_2O. The peak shifts from 973 to 978 cm^{-1} at 10 Na_2O and from 973 to 961 cm^{-1} at 25 Na_2O. The intensity of the 980 cm^{-1} peak has a weak, negative response to temperature and is fairly insensitive to Na_2O content, although at 20 Na_2O the intensity of the 980 cm^{-1} peak is significantly larger. The intensity at 25 Na_2O is comparable to 10 and 15 Na_2O.

The peak at 1080 cm^{-1} decomposes into two peaks, a large peak at 1080 and a smaller peak at 1100 cm^{-1}. The 1080 cm^{-1} peak shifts in position between 15 and 20 Na_2O, from 1070 to 1082 cm^{-1}. This shift is accompanied by an increase in intensity from 0.75 to 1.4. At 10 and 15 Na_2O, the peak position is relatively insensitive to temperature and the intensity increases only slightly between 50 and 800 °C at a constant rate. At 20 and 25 Na_2O, the peak position decreases with temperature, while the intensity increases slowly between 50 and 400 °C and then much faster between 400 and 800 °C.

The peak at 1100 cm^{-1} peak also changes behavior between 15 and 20 Na_2O. At 10 and 15 Na_2O, the position is 1082 cm^{-1} and is relatively constant with increasing temperature. The position increases to 1096 and 1098 cm^{-1} at 20 and 25 Na_2O, respectively, and decreases to 1091 cm^{-1} between 50 and 800 °C. The intensity increases from 0.14 to 0.18, 0.23, and 0.51 at 15, 20, and 25 Na_2O, respectively. With the large increase in intensity between 20 and 25 Na_2O, there is

also a significant change in the response to temperature, with the 1100 cm^{-1} peak increasing by 0.05 at 20 Na_2O and 0.32 at 25 Na_2O between 50 and 800 °C.

To summarize the effects of Na_2O on the peak positions, intensities, and their responses to temperature, increasing the Na_2O content from 10 to 25 mol% causes the 460, 540, 1080, and 1100 cm^{-1} peaks to shift to higher frequency and the 900 and 980 cm^{-1} peaks to shift to lower frequencies. These changes in composition have only small effects on the positions of the 490, 600, 720, 800, and 840 cm^{-1} peaks. For the temperature responses of these peaks, increasing the Na_2O content causes the 540, 980, and 1100 cm^{-1} peaks to have an increased negative dependence of peak position to temperature, with the temperature responses of the other peaks remaining unchanged.

In regard to intensity, increasing the Na_2O content decreases the intensities of the 460 and 720 cm^{-1} peaks, increases the intensities of the 540, 600, 1080, and 1100 cm^{-1} peaks, and either has no effect or an inconsistent effect on the intensities of the 490, 800, 840, 900, and 980 cm^{-1} peaks. The temperature response of the 720 cm^{-1} peak becomes more positive with increasing Na_2O, the response of the 540 cm^{-1} peak becomes more negative with increasing Na_2O, and all the other peaks remain largely unaffected by changing Na_2O content. An exception to this is the 800, 840, and 1100 cm^{-1} peaks, which see little change between 10 and 20 Na_2O but a large change between 20 and 25 Na_2O. The 800 cm^{-1} peak's response becomes more negative and the 840 and 1100 cm^{-1} peaks' responses become more positive.

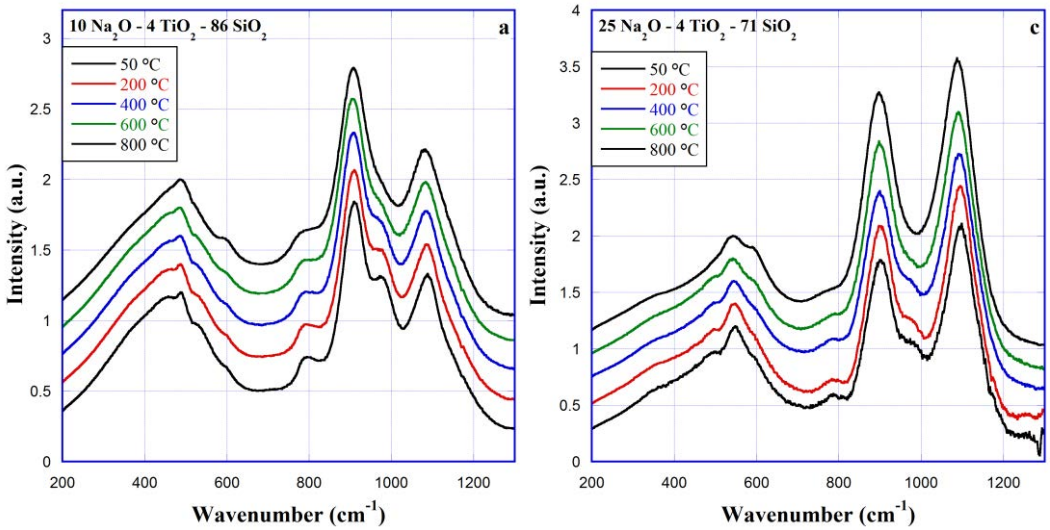

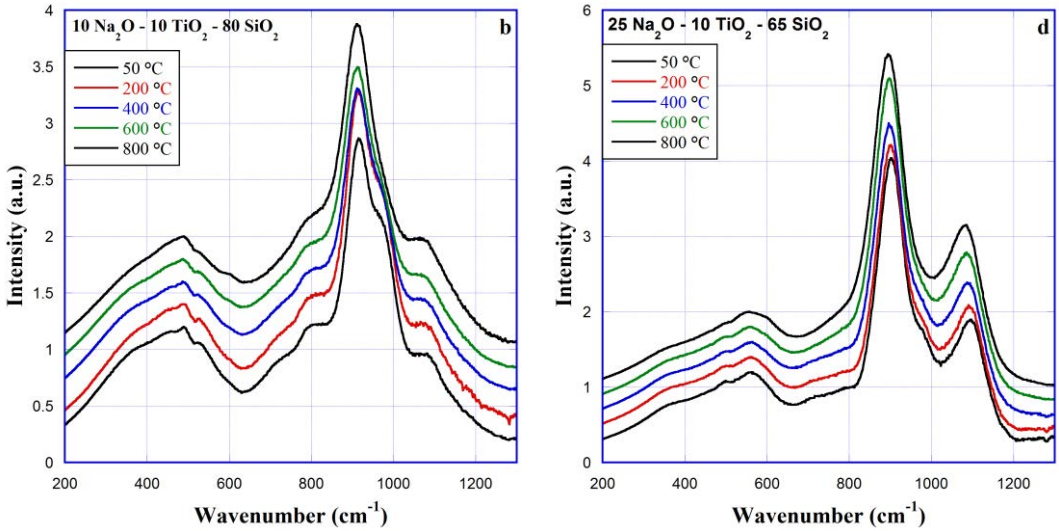

Fig. 4-6. High temperature Raman spectra for 10 Na_2O - TiO_2 - SiO_2 and 25 Na_2O - TiO_2 - SiO_2 glasses. Spectra are normalized to the maxima in the 400-600 cm^{-1} region and offset vertically with increasing temperature for clarity.

Changes in high temperature Raman spectra with changing TiO_2 content is shown in Fig. 4-6(a-d) for 10 and 25 Na_2O. Peak positions and intensities from Fityk peak fitting are given in Table 4-1.

The 460 cm^{-1} peak shifts slightly to higher frequencies when TiO_2 is increased from 4 to 10 mol%. At 10 Na_2O this shift is small, from 446 cm^{-1} at 4 TiO_2 to 452 cm^{-1} at 10 TiO_2, while at 25 Na_2O it shifts from 498 to 520 cm^{-1} between 4 and 10 TiO_2. For all Na_2O and TiO_2 contents, the 460 cm^{-1} peak shifts to higher frequencies linearly with temperature, by approximately 20 cm^{-1} between 50 and 800 °C. The intensity of the 460 cm^{-1} peak increases from 0.88 to 0.92 between 4 and 10 TiO_2 at 10 Na_2O, and from 0.65 to 0.77 at 25 Na_2O. For 10 Na_2O, at 4 TiO_2 the peak decreases in intensity with increasing temperature, from 0.88 to 0.83. This temperature response is reduced at 10 TiO_2, where a decrease from 0.92 to 0.90 is observed. A similar behavior occurs for 25 Na_2O contents, where 4 TiO_2 increases from 0.63 to 0.66 and 10 TiO_2 increases from 0.77 to 0.82. The addition of TiO_2 increases both the intensity and makes the intensity response to temperature more positive.

At 10 Na_2O, the 540 cm^{-1} peak is small, with an intensity around 0.05. Increasing the TiO_2 content has little effect on the peak intensity or position, and at both 4 and 10 TiO_2 the peak shifts slightly to lower frequencies. However, the 540 cm^{-1} peak sees a large change between 4

and 10 TiO_2 with 25 Na_2O. The peak position shifts from 551 cm^{-1} to 560 cm^{-1} at 50 °C, the shift in position with temperature decreases from -6 cm^{-1} to -4 cm^{-1}, and the intensity decreases from 0.37 to 0.23.

The position of the 490 and 600 cm^{-1} peaks are both insensitive to changes in temperature or TiO_2 content at 10 Na_2O, although the 600 cm^{-1} peak was no visible in the 10 Na_2O - 10 TiO_2 spectra until 800 °C. At 25 Na_2O, The 490 cm^{-1} peak shows a slight shift to lower frequencies with the increase in TiO_2, and the shift with temperature changes from slightly positive to almost zero at 10 TiO_2. The 600 cm^{-1} peak is still insensitive to temperature and TiO_2 content at 25 Na_2O. The intensity of the two breathing-mode peaks does change with TiO_2 content. At 10 Na_2O, the intensity of the 600 cm^{-1} increases from 0.02 to 0.06 between 50 °C and 800 °C for 4 TiO_2. At 10 TiO_2 the 600 cm^{-1} peak has an intensity of 0.04, so it likely also increased in intensity with temperature, but has a reduced intensity relative to 4 TiO_2. The 490 cm^{-1} peak decreases in intensity slightly with TiO_2, from 0.13 to 0.11 at 50 °C, and also develops a slight negative temperature response, decreasing by 0.03 from 50 C to 800 °C. At 25 Na_2O, the 490 cm^{-1} peak decreases steadily in intensity with increasing TiO_2, from 0.17 to 0.14 to 0.09 at 4, 7, and 10 TiO_2 respectively. The temperature response also becomes more negative, from ~0 to -0.02 to -0.03 over the same composition range. The 600 cm^{-1} peak behaves almost identically to the 490 cm^{-1} peak here, decreasing in intensity and slightly decreasing in slope with increasing TiO_2.

The 720 cm^{-1} peak occurs at 732 and 736 cm^{-1} at 50 °C for 4 TiO_2 with 10 and 25 Na_2O, respectively. The peak shifts to lower frequencies rapidly with temperature. Increasing TiO_2 to 10 mol% decreases the 50 °C peak frequency and changes the temperature response to roughly constant at 10 Na_2O and slightly positive at 25 Na_2O. The intensity of the 720 cm^{-1} peak increases with TiO_2 content, from 0.21 at 4, to 0.3 at 7, to 0.54 at 10 mol% for 10 Na_2O and from 0.04 to 0.08 to 0.27 at TiO_2 is increased for 25 Na_2O. The temperature response of the intensity changes slightly with increasing TiO_2, but not in a consistent way and generally stays around its 50 °C value.

The 800 cm^{-1} peak shifts to high frequencies with increasing TiO_2 at both 10 and 25 Na_2O, with a small shift between 4 and 7 TiO_2 and much larger shift between 7 and 10 TiO_2. At 10 Na_2O, the 800 cm^{-1} peak position is insensitive to temperature, while at 25 Na_2O it shifts to

lower frequencies with increasing temperature, and this shift is greater at higher TiO_2 contents. The intensity of the 800 cm^{-1} peak increasing with increasing TiO_2 in the same way the peak position shifts to higher frequencies, a small increasing from 4 to 7 and a larger increase from 7 to 10 TiO_2. The temperature response of the intensity is slightly positive at 10 Na_2O, although it is closer to being constant for the 10 TiO_2 glass. At 25 Na_2O the temperature response is almost constant for at TiO_2 contents.

The 840 cm^{-1} peak position shifts to higher frequencies slightly with increasing TiO_2 at 10 Na_2O and the temperature response is almost constant at 4 TiO_2 and becomes slightly negative at 10 TiO_2, with a shift of -6 cm^{-1} between 50 and 800 °C. At 25 Na_2O, the temperature response is much stronger, shifting almost -15 cm^{-1} between 50 and 800 °C, but increasing TiO_2 from 4 to 10 mol% does not change the peak position or sensitivity significantly. The intensity of the 840 cm^{-1} peak does not change significantly with increasing TiO_2 for 10 Na_2O glasses, but the temperature response changes from negative to zero to positive for 4, 7, and 10 TiO_2 glasses, respectively. So while the peak intensities are quite similar at 50 °C, at 0.34, 0.39, and 0.43, they differ far more at 800 °C, at 0.16, 0.31, and 0.49 for 4, 7, and 10 TiO_2, respectively. At 25 Na_2O, the trend is almost opposite, with a very slight positive temperature response at 4 TiO_2, which gradually changes to a negative temperature response at 10 TiO_2. Additionally, at 25 Na_2O increasing TiO_2 increases the 840 cm^{-1} peak intensity more significantly at 50 °C, from 0.14 at 4 TiO_2 to 0.48 at 10 TiO_2.

The 900 cm^{-1} peak does not change significantly in position with changing TiO_2 content, but does show a linear, negative temperature dependence, shifting -2 cm^{-1} every 200 °C for the 10 Na_2O glasses. This holds for the 25 Na_2O glasses was well, except that the temperature dependence becomes larger with increasing TiO_2. The intensity of the 900 cm^{-1} peak increases with increasing TiO_2, and the intensity gradually increases with increasing temperature uniformly for all TiO_2 and Na_2O contents.

The 980 cm^{-1} peak position generally shifts to lower frequencies with increasing TiO_2. At 10 Na_2O it appears to be insensitive to temperature for 4 and 7 TiO_2 and then to have a slight negative dependence at 10 TiO_2. At 25 Na_2O, all TiO_2 contents have a negative dependence to temperature, which does not appear to change significantly with varying TiO_2 content. The intensity of the 980 cm^{-1} peak increases with increasing TiO_2, and generally has a negative

temperature dependence. For 10 Na_2O glasses, this temperature dependence becomes larger with greater TiO_2 contents. For 25 Na_2O glasses, the temperature dependence remains fairly constant with changing TiO_2 content.

The 1080 cm^{-1} peak shifts to lower frequencies with increasing TiO_2 and increasing temperature. At 10 Na_2O, the temperature dependence appears to be larger for higher TiO_2 contents, but at 25 Na_2O the temperature dependence is approximately the same across all TiO_2 contents. For 10 Na_2O glasses, the intensity also decreases with increasing TiO_2 content, but increases with increasing temperature. This temperature dependence does not change significantly across TiO_2 contents. For 25 Na_2O glasses, the intensity is roughly constant for all TiO_2 contents and the temperature dependence is positive and roughly constant.

The 1100 cm^{-1} peak shifts significantly to lower frequencies with increasing TiO_2 content for 10 Na_2O glasses, but not for 25 Na_2O glasses. In 10 Na_2O glasses, the 50 °C peak position changes from 1088 to 1081 to 1077 cm^{-1} as TiO_2 is increased. In 25 Na_2O glasses, the peak position decreases from 1100 to 1098 cm^{-1} between 4 and 7 TiO_2, and then increases to 1101 cm^{-1} at 10 TiO_2. The temperature response in the 10 Na_2O glasses shifts from negative to zero with increasing TiO_2, while in the 25 Na_2O glasses it have a constant, negative response for all TiO_2 contents. The intensity of the 1100 cm^{-1} peak decreases with increasing TiO_2, while the change in temperature response is dependent on the Na_2O content. At 10 Na_2O, the intensity remains almost constant, decreasing only slightly between 600 and 800 °C, for all TiO_2 contents. At 25 Na_2O, the intensity increases with temperature for 4 and 7 TiO_2 glasses, but decreases initially between 50 and 600 °C before increasing again at 800 °C for the 10 TiO_2 glass.

To summarize the effects of changing TiO_2 content at 10 Na_2O, increasing the TiO_2 content causes the 460 and 800 cm^{-1} peaks to shift to higher frequencies and the 1080 and 1100 cm^{-1} peaks to shift to lower frequencies. It also makes the response to temperature more positive for the 460 cm^{-1} peak, less negative for the 1100 cm^{-1} peak, and more negative for the 1080 cm^{-1} peak. At 25 Na_2O, increasing the TiO_2 content causes the 460 and 540 cm^{-1} peaks to shift to higher frequencies and the 1080 cm^{-1} peak to shift to lower frequencies. The responses to temperature become more positive for the 460 cm^{-1} peak and change from positive to neutral for the 490 cm^{-1} peak.

For 10 Na_2O glasses, the intensity of the 460, 720, 800, 900, and 980 cm^{-1} peaks increase and the intensity of the 1080 and 1100 cm^{-1} peaks decrease with increasing TiO_2. The temperature response of intensities becomes less negative for the 460 cm^{-1} peak, changes from negative to positive for the 840 cm^{-1} peak, and becomes more negative for the 490, 540, and 980 cm^{-1} peaks. For the 25 Na_2O glasses, increasing the TiO_2 content causes the 460, 720, 800, 840, 900, and 980 cm^{-1} peaks to increase in intensity and the 490, 540, 600, and 1100 cm^{-1} peaks to decrease in intensity. This also causes the temperature response of the 490 cm^{-1} peak to become slightly negative, the 600 and 1100 cm^{-1} peaks to change from positive to neutral, and the 840 cm^{-1} peak to change from neutral to negative.

Table 4-1. Peak positions and intensities of high temperature Raman spectra for Na_2O-TiO_2-SiO_2 glasses.

10 Na_2O - 4 TiO_2 - 86 SiO_2 Peak Positions												
Position (cm^{-1})	460	460 small	490	540	600	720	800	840	900	980	1080	1100
50 °C	446	458	491	537	603	732	795	847	909	977	1077	1088
200 °C	449	458	491	534	599	730	796	844	907	976	1076	1087
400 °C	450	454	490	534	604	725	792	844	906	973	1074	1086
600 °C	453	459	490	531	605	717	796	844	904	974	1074	1084
800 °C	458	467	494	530	603	706	796	844	907	978	1079	1083
Peak Intensity												
Intensity (a.u.)	460	460 small	490	540	600	720	800	840	900	980	1080	1100
50 °C	0.88	0.09	0.12	0.05	0.02	0.21	0.37	0.34	1.50	0.64	0.83	0.30
200 °C	0.87	0.09	0.12	0.05	0.02	0.23	0.41	0.29	1.53	0.58	0.85	0.29
400 °C	0.86	0.09	0.13	0.06	0.03	0.23	0.43	0.36	1.58	0.56	0.88	0.30
600 °C	0.86	0.10	0.11	0.05	0.04	0.22	0.51	0.22	1.67	0.45	0.90	0.28
800 °C	0.83	0.10	0.13	0.05	0.06	0.18	0.54	0.16	1.70	0.40	0.98	0.23

10 Na_2O - 7 TiO_2 - 83 SiO_2 Peak Positions													
Position (cm^{-1})	340	460	460 small	490	540	600	720	800	840	900	980	1080	1100
50 °C		432	458	488	532		724	798	847	906	973	1072	1081
200 °C		468	461	488	545	602	726	796	844	908	976	1069	1078
400 °C	334	466	468	491	539		728	800	847	910	978	1066	1083
600 °C	340	467	470	491	541	602	726	797	841	907	978	1058	1083
800 °C	331	471	469	490	534	605	722	798	844	908	979	1069	1081
Peak Intensity													
Intensity (a.u.)	340	460	460 small	490	540	600	720	800	840	900	980	1080	1100
50 °C		0.89	0.08	0.14	0.10		0.30	0.56	0.39	2.22	1.26	0.74	0.18
200 °C		0.84	0.06	0.16	0.04	0.10	0.31	0.43	0.38	1.92	0.88	0.64	0.17
400 °C	0.10	0.92	0.04	0.08	0.05		0.40	0.52	0.41	2.28	0.86	0.82	0.16
600 °C	0.10	0.93	0.04	0.07	0.04	0.05	0.44	0.51	0.32	2.23	0.56	0.86	0.15
800 °C	0.07	0.92	0.04	0.08	0.03	0.06	0.41	0.58	0.31	2.42	0.56	0.88	0.18

10 Na_2O - 10 TiO_2 - 80 SiO_2 Peak Positions													
Position (cm^{-1})	340	460	460 small	490	540	600	720	800	840	900	980	1080	1100
50 °C	330	451	457	491	535		725	807	853	910	973	1062	1077
200 °C	330	458	455	490	536		723	807	855	909	971	1068	1075
400 °C	324	462	457	490	535		725	806	844	907	972	1054	1075
600 °C	320	465	460	490	532		724	806	845	905	969	1055	1070
800 °C	314	468	462	492	532	605	744	806	849	908	970	1051	1076
Peak Intensity													
Intensity (a.u.)	340	460	460 small	490	540	600	720	800	840	900	980	1080	1100
50 °C	0.05	0.92	0.05	0.11	0.08		0.54	0.85	0.43	2.36	1.40	0.67	0.11
200 °C	0.06	0.91	0.06	0.12	0.09		0.54	0.91	0.45	2.51	1.52	0.72	0.12
400 °C	0.07	0.91	0.05	0.10	0.06		0.53	0.86	0.29	2.32	1.07	0.72	0.14
600 °C	0.05	0.91	0.04	0.09	0.05		0.52	0.88	0.32	2.35	1.00	0.74	0.12
800 °C	0.04	0.90	0.06	0.09	0.03	0.04	0.58	0.68	0.49	2.5	0.71	0.93	0.07

15 Na_2O - 7 TiO_2 - 78 SiO_2 Peak Positions												
Position (cm^{-1})	460	460 small	490	540	600	720	800	840	900	980	1080	1100
50 °C	453	460	491	530	604	725	795	842	906	975	1068	1083
200 °C	457	456	489	530	601	726	800	846	905	973	1069	1079
400 °C	466	455	491	527	605	725	800	846	903	972	1066	1077
600 °C	467	451	489	523	605	724	800	842	901	968	1065	1074
800 °C	488		489	530	599	732	796	834	902	969	1066	1086
Peak Intensity												
Intensity (a.u.)	460	460 small	490	540	600	720	800	840	900	980	1080	1100
50 °C	0.80	0.10	0.19	0.06	0.04	0.26	0.48	0.37	1.78	0.81	0.70	0.15
200 °C	0.81	0.16	0.20	0.06	0.04	0.29	0.50	0.32	1.78	0.84	0.74	0.15
400 °C	0.82	0.11	0.18	0.06	0.04	0.31	0.55	0.28	1.89	0.75	0.81	0.18
600 °C	0.82	0.09	0.18	0.06	0.04	0.30	0.59	0.31	2.01	0.70	0.85	0.17
800 °C	0.86		0.12	0.07	0.03	0.33	0.66	0.40	3.28	0.75	1.45	0.22

20 Na_2O - 7 TiO_2 - 73 SiO_2 Peak Positions												
Position (cm^{-1})	340	460	460 small	490	540	600	720	800	840	900	980	1080	1100
50 °C	351	508	458	495	541	584	732	796	849	909	978	1082	1096
200 °C	344	514	458	496	541	582	728	798	850	908	977	1081	1094
400 °C	342	521	455	497	543	585	724	795	846	906	975	1076	1095
600 °C	336	526	456	495	541	585	731	797	846	905	974	1077	1092
800 °C	340	532	458	498	541	592	730	798	845	916	973	1077	1091
Peak Intensity													
Intensity (a.u.)	340	460	460 small	490	540	600	720	800	840	900	980	1080	1100
50 °C	0.04	0.70	0.05	0.16	0.30	0.08	0.24	0.44	0.47	2.71	1.27	1.32	0.24
200 °C	0.04	0.71	0.04	0.15	0.27	0.08	0.24	0.49	0.43	2.72	1.20	1.30	0.26
400 °C	0.04	0.72	0.04	0.16	0.27	0.07	0.20	0.51	0.38	2.82	1.10	1.33	0.31
600 °C	0.03	0.76	0.03	0.14	0.23	0.07	0.23	0.55	0.47	3.14	1.00	1.44	0.31
800 °C	0.03	0.77	0.04	0.15	0.21	0.12	0.18	0.63	0.72	2.92	0.97	1.74	0.28

25 Na_2O - 4 TiO_2 - 71 SiO_2 Peak Positions												
Position (cm^{-1})	340	460	490	540	600	720	800	840	900	980	1080	1100
50 °C	337	498	498	551	597	736	790	837	901	978	1086	1100
200 °C	346	480	497	550	598	736	789	846	900	978	1091	1097
400 °C	338	504	504	549	595	735	789	841	898	971	1083	1095
600 °C	351	501	504	547	595	728	789	837	898	972	1081	1093
800 °C	333	516	510	545	595	742	787	831	898	974	1077	1092
Peak Intensity												
Intensity (a.u.)	340	460	490	540	600	720	800	840	900	980	1080	1100
50 °C	0.04	0.63	0.14	0.36	0.16	0.06	0.26	0.14	1.55	0.57	1.22	0.68
200 °C	0.03	0.58	0.17	0.40	0.20	0.03	0.22	0.07	1.65	0.66	1.60	0.45
400 °C	0.03	0.65	0.15	0.30	0.17	0.06	0.28	0.20	1.70	0.58	1.40	0.75
600 °C	0.03	0.66	0.18	0.25	0.20	0.05	0.30	0.17	1.93	0.50	1.40	0.90
800 °C	0.02	0.62	0.17	0.25	0.28	0.07	0.23	0.16	2.11	0.36	1.60	0.98

25 Na_2O - 7 TiO_2 - 68 SiO_2 Peak Positions													
Position (cm^{-1})	340	460	460 small	490	540	600	720	800	840	900	980	1080	1100
50 °C	342	509	447	491	551	597	712	791	840	897	973	1083	1098
200 °C	340	502	452	491	550	597	728	789	841	897	973	1080	1096
400 °C	340	516	445	489	549	597	722	788	837	895	967	1074	1094
600 °C	330	528	448	491	546	594	732	787	836	895	967	1072	1092
800 °C	331	539	454	491	538	591	742	789	830	893	961	1067	1091
Peak Intensity													
Intensity (a.u.)	340	460	460 small	490	540	600	720	800	840	900	980	1080	1100
50 °C	0.04	0.66	0.03	0.14	0.36	0.13	0.06	0.36	0.16	2.34	0.84	1.45	0.52
200 °C	0.05	0.65	0.02	0.12	0.35	0.13	0.10	0.35	0.25	2.51	0.80	1.45	0.67
400 °C	0.05	0.68	0.03	0.12	0.33	0.11	0.06	0.35	0.24	2.46	0.72	1.38	0.76
600 °C	0.03	0.68	0.03	0.13	0.30	0.15	0.10	0.34	0.29	2.68	0.61	1.55	0.72
800 °C	0.02	0.63	0.04	0.12	0.33	0.26	0.08	0.30	0.28	2.99	0.55	1.70	0.88

25 Na_2O - 10 TiO_2 - 65 SiO_2 Peak Positions													
Position (cm^{-1})	340	460	460 small	490	540	600	720	800	840	900	980	1080	1100
50 °C	342	520	528	499	560	598	726	795	847	902	974	1072	1102
200 °C	346	522	528	497	559	597	734	794	841	900	975	1072	1102
400 °C	340	534	527	499	560	599	738	799	839	897	972	1071	1098
600 °C	345	538	527	497	557	597	727	791	834	896	971	1068	1095
800 °C	340	546	529	498	556	599	738	790	831	894	968	1062	1091
Peak Intensity													
Intensity (a.u.)	340	460	460 small	490	540	600	720	800	840	900	980	1080	1100
50 °C	0.08	0.78	0.09	0.09	0.02	0.09	0.27	0.54	0.48	3.72	1.00	1.24	0.55
200 °C	0.07	0.80	0.09	0.09	0.03	0.10	0.28	0.47	0.40	3.69	1.00	1.30	0.48
400 °C	0.08	0.81	0.07	0.07	0.03	0.07	0.33	0.50	0.37	3.74	0.96	1.45	0.43
600 °C	0.06	0.82	0.07	0.07	0.03	0.11	0.26	0.62	0.37	4.12	0.86	1.64	0.42
800 °C	0.06	0.81	0.06	0.06	0.04	0.13	0.30	0.56	0.53	4.21	0.66	1.70	0.56

4.5: Discussions:

A thorough discussion of changes in elastic moduli, Raman spectra, and coefficients of thermal expansion with composition has been done previously [22]. The discussion here will build off of the previous discussion. Since changes in the Raman spectra, both in position and intensity, will be the main focus in attempting to explain changes in the elastic moduli and thermal expansion coefficient, it is convenient to briefly summarize the Raman peak assignments.

The low frequency peaks at 460, 490, 540, and 600 cm^{-1} are generally agreed upon in their assignments. The main band at 460 cm^{-1} corresponds to Si-O-Si symmetric vibrations, and tends to broaden and shift to higher frequencies as the structure becomes less organized and more densely packed. The small peaks at 490 and 600 cm^{-1} correspond to 4- and 3- member Si-O ring breathing mode vibrations [3]. These rings tend to be stiff and resistant to changes, so their position tends not to change significantly with composition. The 540 cm^{-1} peak is assigned to Si-O delocalized vibrational modes caused by the presence of non-bridging oxygens in the silica network [25]. This peak appears with the addition of Na_2O, and its position and intensity is strongly tied to the glass composition.

The high frequency peaks at 900, 980, 1080, and 1100 cm^{-1} are slightly more difficult to assign, as they either do not appear exactly in the binary systems or they appear in both binary systems. The 900 cm^{-1} peak has been assigned to the Ti=O titanyl bond of $^{[5]}Ti$ in a square pyramidal coordination [17,19,20]. The 980 cm^{-1} peak intensity is strongly dependent on the TiO_2 content of the glass, and is assigned to the Ti-O bond of $^{[5]}Ti$. In the binary system the Ti-O peak appears at 950 cm^{-1} for $^{[4]}Ti$, so a shift to higher frequencies corresponds to the increased packing density in the ternary system. A peak appears at 1100 cm^{-1} appears in both binary silicate systems and has been generally assigned to anti-symmetric oxygen vibrations of Q^3 species. In our ternary system, there can be both Si Q^3 and Ti Q^3 species. We assign the 1080 cm^{-1} peak to the Ti Q^3 and the 1100 cm^{-1} peak to the Si Q^3 species for two reasons. The longer and weaker Ti-O bond should produce a lower frequency than the Si-O bond and the polarizability of Ti bonds is greater than that of the Si-O bond, which corresponds to the greater intensity of the 1080 cm^{-1} peak.

The 720, 800, and 840 cm^{-1} peaks are assigned to cation oxygen vibrations, primarily caused by cation motion. Peaks at 800 and 840 cm^{-1} are observed in pure silica glasses and are assigned to Si-O_4 silicon vibrations [4]. The 720 cm^{-1} peak appears with the addition of TiO_2, and thus can be assigned to Ti-O_4 titanium vibrations. The 720 cm^{-1} peak's shift to higher frequencies with increasing TiO_2 corresponds to the transition from a combination of $^{[4]}Ti$ and $^{[5]}Ti$ to almost completely $^{[5]}Ti$. This peak has been reported at ~750 cm^{-1} in 25 mol% TiO_2 glasses and is compared to the 767 cm^{-1} band in Ba_2TiO_4 [17].

Additional small peaks appears at 340 cm^{-1} and 460 cm^{-1}, the assignments of which are uncertain. The 340 cm^{-1} peak has been tentatively assigned to the presence $^{[6]}Ti$ [26]. The small peak at 460 cm^{-1} has not been reported in previous literature to the authors' knowledge and a specific assignment is not possible.

Assuming these assignments are valid, it should be possible to observe a correlation with the shift in peak positions and intensities with temperature to the changes in elastic moduli and thermal expansion. The temperature response of the elastic moduli, seen in Figs. 4-2 and 4-3a-d, show a general trend of decreasing slope with increasing Na_2O, and a greater change in slope at the glass transition for higher Na_2O contents. Thermal expansion likewise increases in slope

with increasing Na_2O. The temperature responses of both are largely unaffected by changes in the TiO_2 content.

Examining changes in the temperature responses of Raman peaks when Na_2O content is increased, we can see that there are changes in the 540, 720, 800, 840, 980, 1080, and 1100 cm^{-1} peaks. The responses of 460, 490, 600, and 900 cm^{-1} peaks to temperature is almost unchanged by varying the Na_2O content, even if their room temperature positions and intensities are. The 460, 490, and 600 cm^{-1} peaks are all associated with Si-O vibrations of bridging oxygens. Increasing the Na_2O content appears to decrease the population of structures with symmetric vibrations, but does not disrupt them otherwise; if that were the case, a change in their temperature response would be expected. The fact that the 900 cm^{-1} peak is also unaffected simply suggests that the behavior of the titanyl oxygen vibrations are not sensitive to changes in the Na_2O concentration.

The 540 cm^{-1} peak both decreases in intensity more and shifts further to lower frequencies at high Na_2O contents. The frequency change would suggest that the glass increases free volume with temperature more quickly at higher Na_2O contents. The intensity change possibly suggests that the delocalized vibrations caused by nBOs are weaker; that the difference between a BO and a nBO is less at increased temperatures. It is also possible that it signifies a decrease in the population of nBO, but this seems less likely.

The 720 cm^{-1} peak increases in intensity with temperature at 10 Na_2O, and this response decreases until it is slightly negative at 20 Na_2O. As this peak is assigned to cation vibrations of Ti with four bridging oxygens, this suggests that the population of Q^4 Ti decreases with temperature at an increased rate at higher Na_2O. The 800 cm^{-1} peak sees a similar change of a negative temperature response, but only at 25 Na_2O, where the population of the Ti Q^4 species is extremely low. This suggests that Q^4 Ti change bonding to form nBO more easily than the Q^4 Si, possibly explaining why there is little change in the Si-O symmetric vibrational peaks: 460, 490, and 600 cm^{-1}. Interestingly, the 840 cm^{-1} peak, while reduced in intensity overall with increasing Na_2O, actually has a more positive temperature response at higher Na_2O contents. The change in the 800 cm^{-1} peak matches an increased temperature response in the 1100 cm^{-1} peak, suggesting a decrease in the Q^4 Si population and an increase in the Q^3 Si population with temperature. It might be expected that similar changes would occur in the Q^4 and Q^3 Ti

populations. However, that appears not to be the case. Rather, the 980 and 1080 cm^{-1} peaks both show an increased shift to lower frequencies, but unchanged intensity temperature responses. A lower frequency could correspond to an increased local free volume, a change in the bond angle, or a reduced bond strength.

To seek an explanation for this, let's start from the percolation model proposed by Farges et al. [27]. In this model, clusters with relatively high concentrations of Ti and Na form. Titanyl oxygens would likely initially act to balance the Na^+ charge. As the Na^+ concentration increases, further charge balancing would require the formation of non-bridging oxygens. This is seen in the decrease in intensity of the 720 cm^{-1} peak and increase in intensities of the 1080 and 1100 cm^{-1} peaks with increasing Na_2O. As the temperature is increased, mobility and the amplitude of vibrations of Na^+ cations is going to increase significantly faster than that of Si or Ti cations, simply due to the lower mass and weaker bonding. Since the Na^+ concentration is higher in these clusters, there should be an effectively higher packing density in the clusters than in the surrounding glass. The 800 and 840 cm^{-1} Si cation vibrational peaks are dependent on symmetry of bonds surrounding the cation [4], and this would logically extend to the 720 cm^{-1} peak as well for Ti. The difference in Na^+ concentration in the outside and inside of the clusters could decrease this symmetry as the temperature is increased and Na^+ vibrations increase. The change in the temperature response of the 720 cm^{-1} peak from positive to negative with increasing Na_2O could then be caused by either a change in Na_2O concentrations in these clusters or a greater fraction of the Ti participating in the clusters at higher Na_2O contents. The fact that there appears to be a saturation limit, where between 20 and 25 Na_2O the intensity of the 720 cm^{-1} peak decreases drastically and the intensity of the 800 cm^{-1} peak also begins to decrease, suggesting that the increased participation of TiO_2 in these clusters at higher Na_2O concentrations is more likely.

The change in the temperature responses of the 720 and 800 cm^{-1} peaks closely matches that of the changes in the temperature responses of the elastic moduli. The 10 Na_2O glasses have a positive temperature response of elastic moduli, which matches the increase in intensity of the 720 cm^{-1} peak. From 10 to 20 Na_2O, the 720 cm^{-1} peak intensity change its temperature response, transitioning from positive to negative between 15 and 20 Na_2O. The elastic moduli's responses to temperature follow a similar decrease, passing through zero at 15 Na_2O for Young's

modulus and the shear modulus and between 15 and 20 Na_2O for the bulk modulus. At 25 Na_2O, the decrease in the 720 cm^{-1} peak intensity is no longer visible, probably because the peak intensity is very low. However, at 25 Na_2O the 800 cm^{-1} peak intensity changes from a positive temperature response to a negative response. This change accompanies a decrease in the slope of elastic moduli, but also a large increase in the fragility of the glass, seen in the much larger change in slope of the Poisson's ratio at T_g in the 25 Na_2O glasses (Fig. 4-2d). Farges et al. found that there was no significant change in the structure of the Ti-rich domains between the glass and melt [28]. This would suggest that the Na^+ mobility is greater within the silica network than inside of the Ti-rich domains. Once the Na_2O concentration exceeds that can be accommodated in the Ti-rich domains and it begins to occur in higher concentrations outside of the clusters, the susceptibility of the network to temperature increases significantly.

The temperature response of thermal expansion matches the increasing shift of the 540, 980, 1080, and 1100 cm^{-1} peaks to lower frequencies with increasing temperature. This corresponds to an increase in the Ti-O and Si-O bond lengths within the lower connectivity glass regions. As the Na_2O content is increased and these regions occupy a greater volume fraction of the glass, they are less constrained by the silica network and are able to expand more freely. Or equivalently, as the silica network is more disrupted, free volume is decreased and the increase in bond length is accommodated by volume expansion instead of bond rotation of tetrahedra. It is interesting that that CTE does not change as the TiO_2 content is increased, as it is expected that Ti^{4+} transitions from a mixture of $^{[4]}Ti$ and $^{[5]}Ti$ at 4 mol% TiO_2 to primarily $^{[5]}Ti$ at 10 mol% TiO_2 [17,27]. An increase in the TiO_2 content has a significant impact on the intensities and positions of peaks, but has only a slight influence on their thermal expansion responses to temperature. Farges et al. suggested that Ti-rich domains formed were quite rigid and resistant to thermal expansion [28]. So it is possible that the increase in stiffness and increase in density that accompany the increase in TiO_2 offset each other somewhat, resulting in only a small change in thermal expansion.

4.6: Conclusions:

Changes in structure, elastic moduli, and thermal expansion of Na_2O-TiO_2-SiO_2 glasses with temperature have been investigated through *in-situ* high temperature Raman spectroscopy,

Brillouin light scattering, and dilatometry. Increasing the Na_2O content decreases the Young's modulus and shear modulus, while it increases the bulk modulus and the Poisson's ratio, in agreement with changes observed at room temperature [22]. It also changes the elastic response to temperature, shifting from an anomalously increase in elastic moduli with temperature at 10 Na_2O to a normal decrease at 20 and 25 Na_2O, with 15 Na_2O having an intermediate response. Increasing the TiO_2 content increases the magnitude of elastic moduli, but does not change the temperature response appreciably. The coefficient of thermal expansion increases both magnitude and slope with increasing Na_2O content, but showing almost no change with variation in TiO_2 content.

Changes in the Raman spectra with temperature and Na_2O content have been discussed. Some correlations between changes in the temperature responses of peak positions and intensities and changes in the temperatures responses of CTE and elastic moduli have been observed. The change in the slope of elastic moduli with temperature matches an explanation based on the percolation model proposed by Farges et al. [27].

4.7: References:

[1] W.H. Wang, The Elastic Properties, Elastic Models and Elastic Perspectives of Metallic Glasses, Prog. Mater. Sci. 57 (2012) 487–656.

[2] R. Vukcevich, A new interpretation of the anomalous properties of vitreous silica, J. Non-Cryst. Solids. 11 (1972) 25–63.

[3] P. McMillan, B. Poe, P.H. Gillet, B. Reynard, A study of SiO_2 glass and supercooled liquid to 1950 K via high-temperature Raman spectroscopy, Geochim. Cosmochim. Acta. 58 (1994) 3653–3664.

[4] A. Kalampounias, S. Yannopoulos, G. Papatheodorou, Temperature-induced structural changes in glassy, supercooled molten silica from 77 to 2150 K, J. Chem. Phys. 124 (2006) 014504.

[5] T. Deschamps, C. Martinet, D. de Ligny, B. Champagnon, Elastic anomalous behavior of silica glass under high-pressure: In-situ Raman study, J. Non-Cryst. Solids. 355 (2009) 1095–1098.

[6] T. Rouxel, Elastic Properties and Short-to Medium-Range Order in Glasses, J. Am. Ceram. Soc. 90 (2007) 3019–3039.

[7] L. Wondraczek, J. Mauro, J. Eckert, U. Kuhn, J. Horbach, J. Deubener, et al., Towards Ultrastong Glasses, Adv. Mater. 23 (2011) 4578–4586.

[8] K. Kamiya, S. Sakka, Thermal Expansion of TiO_2-SiO_2 and TiO_2-GeO_2 glasses, J. Non-Cryst. Solids. 52 (1982) 357–363.

[9] V. Pukh, L. Baikova, M. Kireenko, L. Tikhonova, Properties of silica glass doped with titanium oxide, in: Glass - The Challenge for the 21st Century, Trans Tech Publications, 2008: pp. 153–158.
[10] S. Gulati, Mechanical Properties of SiO_2 vs. SiO_2-TiO_2 Bulk Glasses and Fibers, Mat. Res. Soc. Symp. Proc. 244 (1992) 67–83.
[11] K. Hirao, K. Tanaka, S. Furukawa, N. Soga, Anomalous temperature dependence of the sound velocities of SiO_2-TiO_2 glasses, J. Mater. Sci. Lett. 14 (1995) 697–699.
[12] S. Webb, D. Dingwell, Compressibility of titanosilicate melts, Contrib. Mineral. Petrol. 118 (1994) 157–168.
[13] Q. Liu, R. Lange, Y. Ai, Acoustic velocity measurements on Na_2O-TiO_2-SiO_2 liquids: Evidence for a highly compressible TiO_2 component related to five-coordinated Ti, Geochim. Cosmochim. Acta. 71 (2007) 4314–4326.
[14] D. Dingwell, Shear Viscosity of alkali and alkaline earth titanium silicate liquids, Am. Mineral. 77 (1992) 270–274.
[15] Q. Liu, R. Lange, The partial molar volume and thermal expansivity of TiO_2 in alkali silicate melts: systemicatic variation with Ti coordination, Geochim. Cosmochim. Acta. 65 (2001) 2379–2393.
[16] M. Bouhifd, A. Sipp, P. Richet, Heat Capacity, viscosity, and configurational entropy of alkali titanosilicate melts, Geochim. Cosmochim. Acta. 63 (1999) 2429–2437.
[17] G. Henderson, X. Liu, M. Fleet, A Ti L-edge X-ray absorption of Ti-silicate glasses, Phys. Chem. Miner. 29 (2002) 32–42.
[18] H. Hidaka, N. Iwamoto, N. Umesaki, T. Fukunaga, K. Suzuki, Structural analysis of sodium silicate glasses containing TiO_2 by pulsed neutron scattering, J. Mater. Sci. 20 (1985) 2497–2502.
[19] B. Reynard, S. Webb, High-temperature Raman spectroscopy of $Na_2TiSi_2O_7$ glass and melt: coordination of Ti^{4+} and nature of the configurational changes in the liquid, Eur. J. Mineral. 10 (1998) 49–58.
[20] B. Mysen, D. Neuville, Effect of temperature and TiO_2 content on the structure of $Na_2Si_2O_5$-$Na_2Ti_2O_5$ melts and glasses, Geochimica et Cosmochimica Acta. 59 (1995) 325–342.
[21] M. Manghnani, Pressure and Temperature dependence of the elastic moduli of Na_2O-TiO_2-SiO_2 glasses, J. Am. Ceram. Soc. 55 (1972) 360–365.
[22] G. Scannell, S. Barra, L. Huang, Structure and Properties of Na_2O-TiO_2-SiO_2 Glasses: Role of Na and Ti on Modifying the Silica Network, under review with J. Non-Cryst. Solids. (2016).
[23] G. Scannell, L. Huang, T. Rouxel, Elastic properties and indentation cracking behavior of Na_2O-TiO_2-SiO_2 glasses, J. Non-Cryst. Solids. 429 (2015) 129–142.
[24] M. Wojdyr, Fityk: a general-purpose peak fitting program, J. Appl. Crystallogr. 43 (2010) 1126–1128.
[25] P. McMillan, Structural studies of silicate glasses and melts--applications and limitations of Raman spectroscopy, Am. Mineral. 69 (1984) 622–644.
[26] K. Kusabiraki, Infrared and Raman spectra of vitreous silica and sodium silicates containing titanium, J. Non-Cryst. Solids. 95-96 (1987) 411–418.
[27] F. Farges, G.E.J. Brown, A. Navrotsky, H. Gan, J.J. Rehr, Coordination Chemistry of Ti(IV) in Silicate Glasses and Melts: II. Glasses at Ambient Temperature and Pressure, Geochim. Cosmochim. Acta. 60 (1996) 3039–3053.

[28] F. Farges, A Ti K-edge EXAFS Study of the Medium Range Environment Around Ti in Oxide Glasses, J. Non-Cryst. Solids. 244 (1999) 25–33.

Chapter 5 : Elastic properties and indentation cracking behavior of Na_2O-TiO_2-SiO_2 glasses

5.1: Abstract

The effects of composition on indentation deformation and cracking behavior of Na_2O-TiO_2-SiO_2 glasses were studied in the light of structural considerations and parameters such as the atomic packing density (C_g) and the network energy, using a combination of elastic measurements and micro-hardness indentation experiments. Na_2O-TiO_2-SiO_2 glasses with titania contents of 4-10 mol% and sodium oxide contents of 10-25 mol% were prepared through a traditional melt-quench process. Indentation experiments were conducted using a Vickers indenter with loads ranging from 10 mN to 49 N. Critical loads for crack initiation and cracking patterns were systematically investigated and correlated with the elastic properties of glass. In this ternary system concerning a relatively large range of Poisson's ratio (ν), a minimum in critical crack initiation load was observed at a ν of 0.21-0.22. This study brings to light the unusual role of titanium in the glass network that gives birth to peculiar trends in the structural and mechanical properties.

5.2: Introduction

An intriguing correlation was observed recently in oxide glasses and in metallic glasses: the fracture energy (G) increases with the Poisson's ratio (v), with a sharp brittle-to-ductile (BTD) transition at a critical v_{BTD}=0.31-0.32 [1]. A similar Poisson's ratio-ductility correlation has also been reported in crystalline metals [2]. Recently, Rouxel also showed that densified silica, when v increases from 0.15 to 0.25, is capable of shear flow under indentation resulting in pile-ups [3] and found that v is directly correlated with the atomic packing density (C_g) and the glass network dimensionality [4].

This chapter previously appeared as: G. Scannell, L. Huang, T. Rouxel, Elastic properties and indentation cracking behavior of Na_2O-TiO_2-SiO_2 glasses, J. Non-Cryst. Solids. 429 (2015) 129–142.

Such a far-from-equilibrium fracture property versus near-equilibrium elastic property relation is quite unexpected, yet highly beneficial by setting *v* as an optimization target to make stronger and tougher glasses. The precise measurement of fracture toughness and the associated fracture energy requires large samples and tedious sample preparation. However, elastic characteristics, especially Poisson's ratio can be measured relatively easily, using much smaller samples, such as mm sized samples for ultrasonic measurements and tens of μm sized samples for Brillouin light scattering experiments. In both methods, *v* can be easily calculated from the measured longitudinal (V_L) and transverse (V_T) sound velocities: $v = (V_L^2 - 2V_T^2) / [2(V_L^2 - V_T^2)]$. The *v*-*G* relation has already been proposed as a guide to obtain tough metallic glasses [5,6]. It is of great scientific and technological interest to investigate whether a similar relation holds in oxide glasses, as stronger and tougher glasses are increasingly demanded for applications such as personal electronics, windows for transportation systems, architectural materials, solar panels, and submarine communications cables, etc.

Indentation is a relatively simple way to observe the mechanical behavior of glass and the initiation of cracks under contact loading. Wada et al. described the susceptibility to cracking in a glass by its crack resistance, or the critical load to initiate two cracks from a Vickers indentation [7]. Sehgal and Ito [8] used a "brittleness" index, proposed by Lawn and Marshall as a ratio of hardness to fracture toughness [9], as a measure of glass resistance toward cracking. However, it is unclear whether this relationship is sufficiently refined to allow for the comparison of glasses with slight changes in composition. Additionally, Kato et al. showed that the crack resistance does not have a clear relationship with either Vickers hardness or the fracture toughness [10]. It seems that to predict the cracking behavior of glass under indentation, the effects of permanent deformation during indentation (densification and shear flow) on the stress field need to be better understood. At lower *v*, the primary mode of deformation under indentation is densification, as *v* increases, a shift from densification to shear flow is expected [3]. This shift is accompanied by a change in the cracking behavior [11].

In this work, we examine whether relationships between the mechanical properties measured through indentation and the *v* exist by focusing on soda-titania-silicate glasses covering a range of *v* from 0.18 to 0.24. The Na_2O-TiO_2-SiO_2 glass system was chosen because it covered a large range of Poisson's ratio, both Na_2O and TiO_2 are known to separately cause

unusual behavior in silicate glasses (anomalous elastic moduli behavior with respect to temperature and anomalous thermal expansion respectively).

To understand the elastic properties and the indentation behaviors of glass, it is important to consider the glasses from a structural standpoint. The basic bonding environment of Si and Na is fairly well known, with Si forming tetrahedrally coordinated with four oxygen atoms and Na breaking a Si-O-Si bond to form a non-bridging oxygen, Si-O-Na. The basic bonding environment of Ti is more complicated, being able to adopt four, five, or six-fold coordinations, depending on the concentration and species of the other cations present in the glass. Farges, et al. found that in Na_2O-TiO_2-SiO_2 glasses, Ti primarily adopts a fivefold coordination with a square pyramidal geometry, with four bridging oxygens and one double bonded non-bridging oxygen [12,13]. The effect of TiO_2 on the mechanical properties and the structure of glasses depends strongly on its coordination state, and is still poorly understood.

5.3: Experimental details

Soda-titania-silicate glasses were synthesized through a traditional melt-quench method from powders. Glasses with compositions of (x)Na_2O-(y)TiO_2-(1-x-y)SiO_2, where x=10, 15, 20, and 25 and y=4, 7, and 10 mol%, were chosen to cover a range of Poisson's ratios (ν=0.18-0.24). Powders used were of 99% purity or higher. Powders were mixed for approximately 30 minutes and then melted in a Pt or a 10%Rh-90%Pt crucible at 1400-1500 °C for three hours, with the powder added in three to four intervals during the first hour. The temperature was increased to 1600-1700 °C for ten minutes prior to quenching to make pouring the glass easier. After pouring, the glasses were quickly transferred into an annealing furnace set slightly above their glass transition temperatures (550-600 °C) for 1-2 hours and furnace cooled overnight. Glasses were visually checked for residual stresses using a polarizer and re-melted if excessive residual stresses were observed.

For indentation experiments, samples of approximately 10 mm x 10 mm x 4 mm were prepared. Samples were cut using a diamond saw and two parallel faces were polished with 240, 400, and 600 grit Al_2O_3 paper followed by a cerium oxide slurry.

Vickers indents were made using a Matsuzawa hardness indenter at 49 N, 9.8 N, 4.9 N, and 2.9 N and using a Fischer indenter at 1 N, 0.5 N, and 0.1 N. Ten indents were made at each load and images of each indent were taken using either an Olympus BX60 optical microscope or

a scanning electron microscope (SEM) for indents made with the Matsuzawa and the Fischer indention machine, respectively. Apparent surface roughness/scratches in some of the images is due to residual organics from temporary storage in soft plastic containers, which was removed with alcohol/acetone after the problem was observed in initial samples. All indentations were done in air, cracking patterns surrounding indents were studied after crack growth had stopped. To determine when crack growth had stopped, images of indents across four compositions (x=10, 15, 20, 25 and y=4) were taken at 5 images/sec for up to 24 hours. Crack growth stopped and no new cracks appeared after two hours for all compositions. Fig. 5-1 shows the crack growth around a 1 kg indent in a 15 Na_2O - 4 TiO_2 - 81 SiO_2 glass over a 20 hour period. In order to compare the behavior of glasses with different compositions regardless of environmental fatigue effects, it was decided to investigate the indentation patterns at least two hours after indentation.

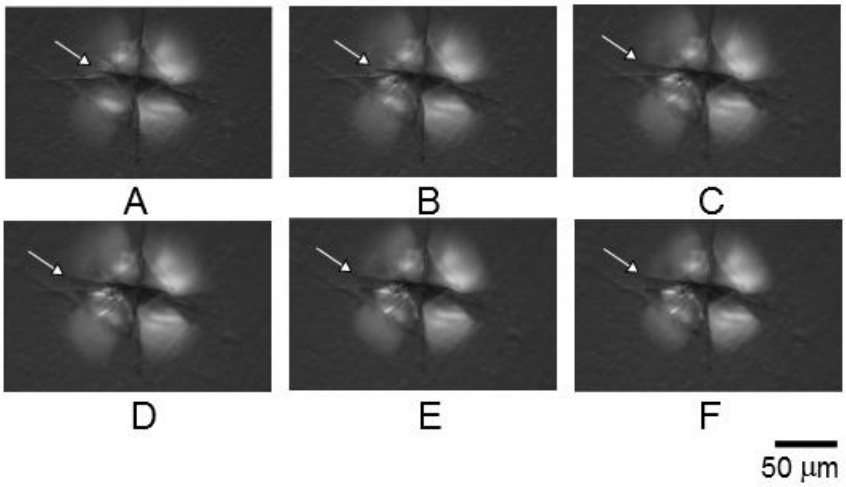

Fig. 5-1. Optical microscope images showing crack growth around a 1 kg Vickers indent in a $15Na_2O$-$4TiO_2$-$81SiO_2$ glass at 5 minutes (A), 30 minutes (B), 1 hour (C), 2 hours (D), 10 hours (E), and 20 hours (F). Crack growth is significant over the first hour, slight over the second, and non-existent over the next 18 hours. This can be most clearly seen by following the crack growth from the left-most corner of the indent (white arrows).

For each indent, the number of primary cracks, secondary cracks, and circular cracks around the indent were counted. Primary cracks are defined as cracks originating from the corners of the Vickers indent and secondary cracks are cracks originating from one of the sides of the indent. The crack lengths and indent diagonals were measured under an optical microscope. Vickers hardness, and the average primary crack length were calculated. For indents made with the Fischer indenter, the loading/unloading curve for each indent was collected. The

loading/unloading curves show the applied load (mN) versus indentation depth (μm) over the entire indentation cycle. From these curves the energies associated with the reversible and irreversible deformation components of the indentation process were calculated by integrating the areas underneath the curve. Reversible energy is the area under the unloading curve, while irreversible energy is the area under the loading curve minus the area under the unloading curve.

To study how the indentation behaviors change relative to the elastic properties of the glass, the transverse and longitudinal sound velocity were measured for each composition by ultrasonic pulse-echo technique using piezoelectric transducers (10 MHz range) and by Brillouin light scattering using a six-pass high contrast Fabry-Pérot interferometer. Density was measured by means of the Archimedes method using distilled water for the medium with an error of less than ±0.01 g/cm^3. Elastic moduli and Poisson's ratio were calculated from the sound velocity and the density of the glasses.

$$E = \rho V_T^2(3V_L^2-4V_T^2)/(V_L^2-V_T^2) \quad (5\text{-}1)$$

$$\mu = \rho V_T^2 \quad (5\text{-}2)$$

$$\nu = (V_L^2-2V_T^2)/2(V_L^2-V_T^2) \quad (5\text{-}3)$$

$$K = E/(3(1-2v)) \quad (5\text{-}4)$$

where V_L and V_T are longitudinal and transverse sound velocities, ρ is sample density, E is Young's modulus, K is bulk modulus, μ is shear modulus, v is Poisson's ratio. Brillouin values represent the average of five measurements taken across different points on a sample and have standard deviations of 0.7 GPa for Young's modulus, 0.7 GPa for bulk modulus, 0.4 GPa for shear modulus, and 0.006 for Poisson's ratio. Ultrasonic measurements are averages of two measurements made on a single sample, and varied by approximately 1.3 GPa for Young's modulus, 1.4 GPa for bulk modulus, 0.5 GPa for shear modulus, and 0.01 for Poisson's ratio. Thus, ultrasonic measurements for Young's modulus and shear modulus are precise enough to be used as a comparison to those from Brillouin light scattering, while Poisson's ratio values show too much variance.

The number of bridging oxygen per network former (Si or Ti) was calculated by assuming that the environment of Ti consists of four bridging oxygen atoms and one double-bonded oxygen that preferentially attracts a Na^+ ion [12,13] (see Fig. 5-2), so that

$$n_{BO} = (4([Si] + [Ti]) - ([Na] - [Ti]))/([Si] + [Ti]) \quad (5\text{-}5)$$

which, according to the stoichimetry of the glass compositions, gives

$$n_{BO} = (4(1-x)-(2x-y))/(1-x) \quad (5\text{-}6)$$

where x is the molar fraction of Na_2O and y is the molar fraction of TiO_2 in the glass.

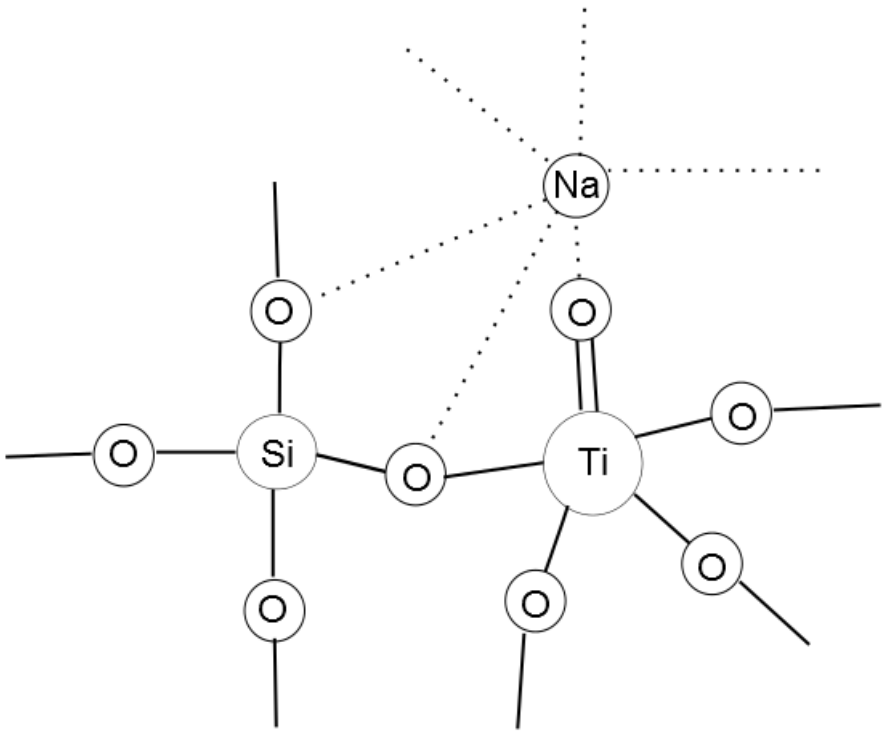

Fig. 5-2. Model structural units of Na_2O-TiO_2-SiO_2 glass at a titanium site, where Si forms four coordinated tetrahedra and Ti forms five-coordinated square pyramids.

Another important parameter is the glass atomic packing density (C_g), defined as the ratio between the minimum theoretical volume occupied by the ions and the corresponding effective volume of glass:

$$C_g = 1/\rho\ ((\Sigma f_i V_i)/(\Sigma f_i M_i)) \quad (5\text{-}7)$$

For the i^{th} constituent with A_xB_y chemical formula: $V_i=4/3\pi N\ (xr_A^3+yr_B^3)$, where N is Avogadro number, r_A and r_B are the ionic radii, ρ is the density, f_i is the molar fraction and M_i is the molar mass. The effective ionic radii in glass are usually not known with high accuracy. Shannon [14] tabulated the crystal radius and the effective ionic radius of halides and chalcogenides (including oxides). Whittaker [15] suggested using the mean of both values in the case of silicate glasses. An ab initio (i.e., when ρ is unknown) estimation of C_g can also be obtained by considering the density of the oxides used as constituents (as in Eq. 5-7) to estimate the effective volumes from the mass and the corresponding density.

Glass transition temperatures were measured using differential thermal analysis (DTA) using a DTG-60 detector and a TA-60WS thermal analyzer. Prepared glasses were ground into a fine powder, added to platinum pans using alumina as a reference material. 50 mg of glass powder was used at each composition. Powders were heated from room temperature to 400 °C at 20 °C per minute and then from 400 °C to 800 °C at 10 °C per minute under a nitrogen atmosphere (25 ml/min). The onset, midpoint, and end of the glass transition range were found using the built-in function in the TA-60WS software.

Error in measured results is the standard deviation across the series of measurements taken whenever possible. Error in results calculated from measured results is the calculated variance assuming a covariance of zero. For theoretically calculated values, no error bars are shown. Error for the glass transition temperature is shown as the onset and end of the glass transition range, as this is larger than error between measurements. Error in the critical load to initiate cracks was estimated using a fitting method and is described in the results in more detail.

5.4: Results

Indentation micrographs for the twelve Na_2O-TiO_2-SiO_2 glasses are shown in Figs. 5-(3-6). At 49 N (Fig. 5-3), all samples exhibit radial-median cracks. Samples with 10 mol% Na_2O also appear to have cone/ring cracks, while 15, 20, 25 mol% Na_2O samples have lateral cracks, as exhibited by the lack and presence of chipping and birefringence patterns, respectively. As the load is decreased, cone/ring cracking disappears almost immediately, with slight signs of it in the

10 Na_2O - 4 TiO_2 - 86 SiO_2 sample at 9.8 N. Radial-median and lateral cracks appear to shrink relative to indent diameter as load decreases. Samples with 10% Na_2O and 25% Na_2O appear most resistant to crack initiation, with some samples beginning to show less than four cracks at 4.9 N. Crack length appeared to increase with increasing Na_2O content, particularly visible at 2.9 N in Fig. 5-6.

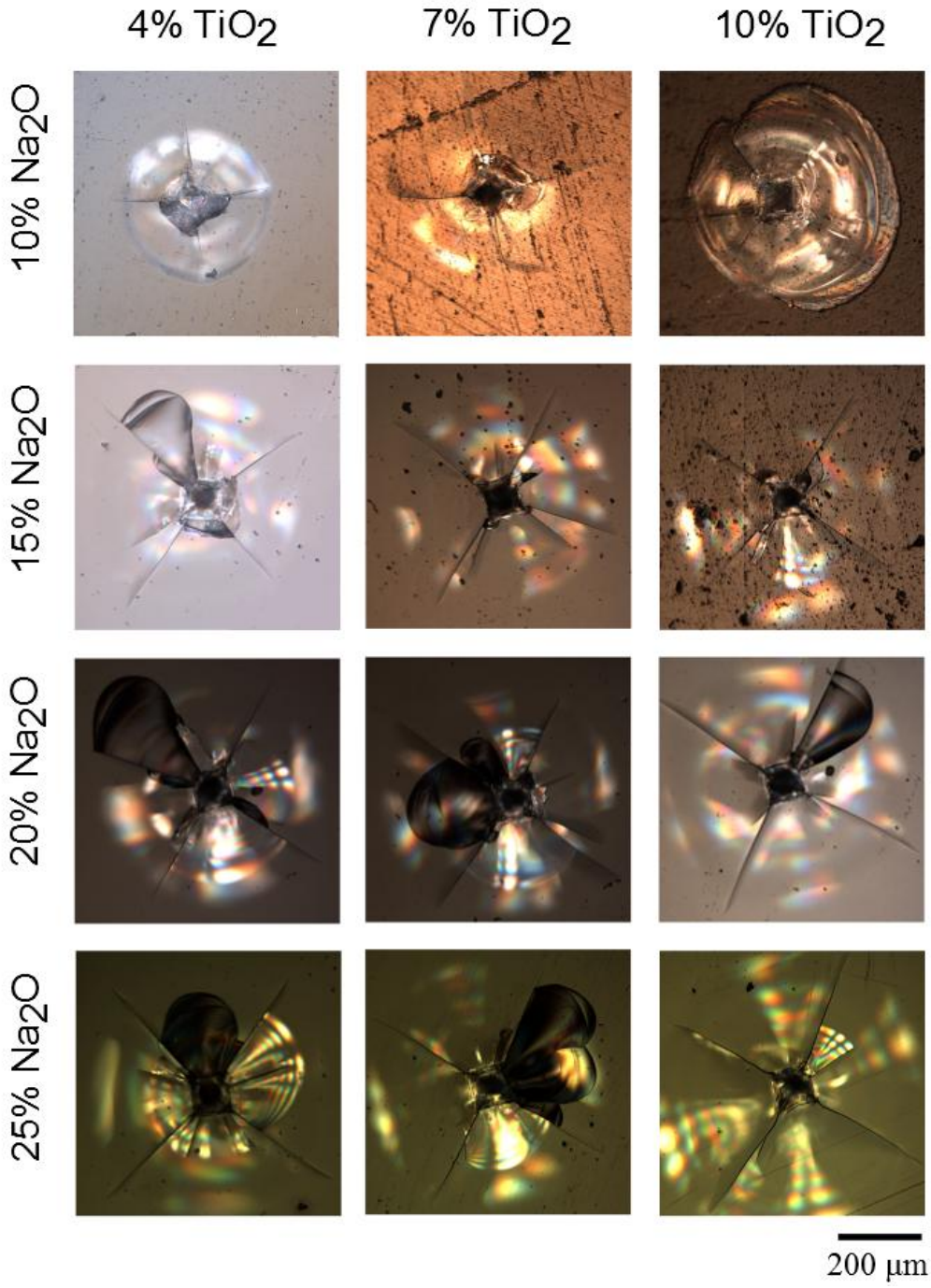

Fig. 5-3. Vickers indentations performed at 49 N on Na_2O-TiO_2-SiO_2 glasses.

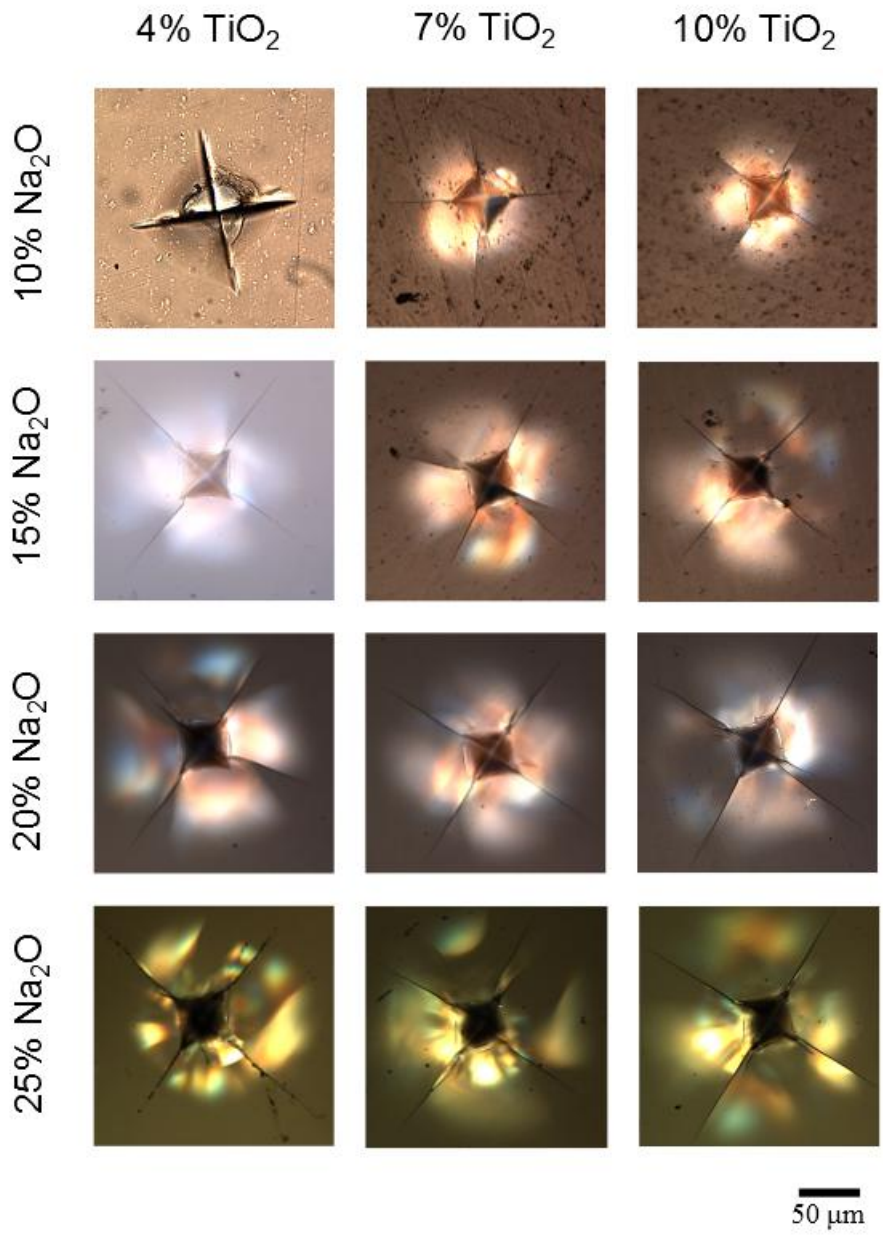

Fig. 5-4. Vickers indentations performed at 9.8 N on Na_2O-TiO_2-SiO_2 glasses.

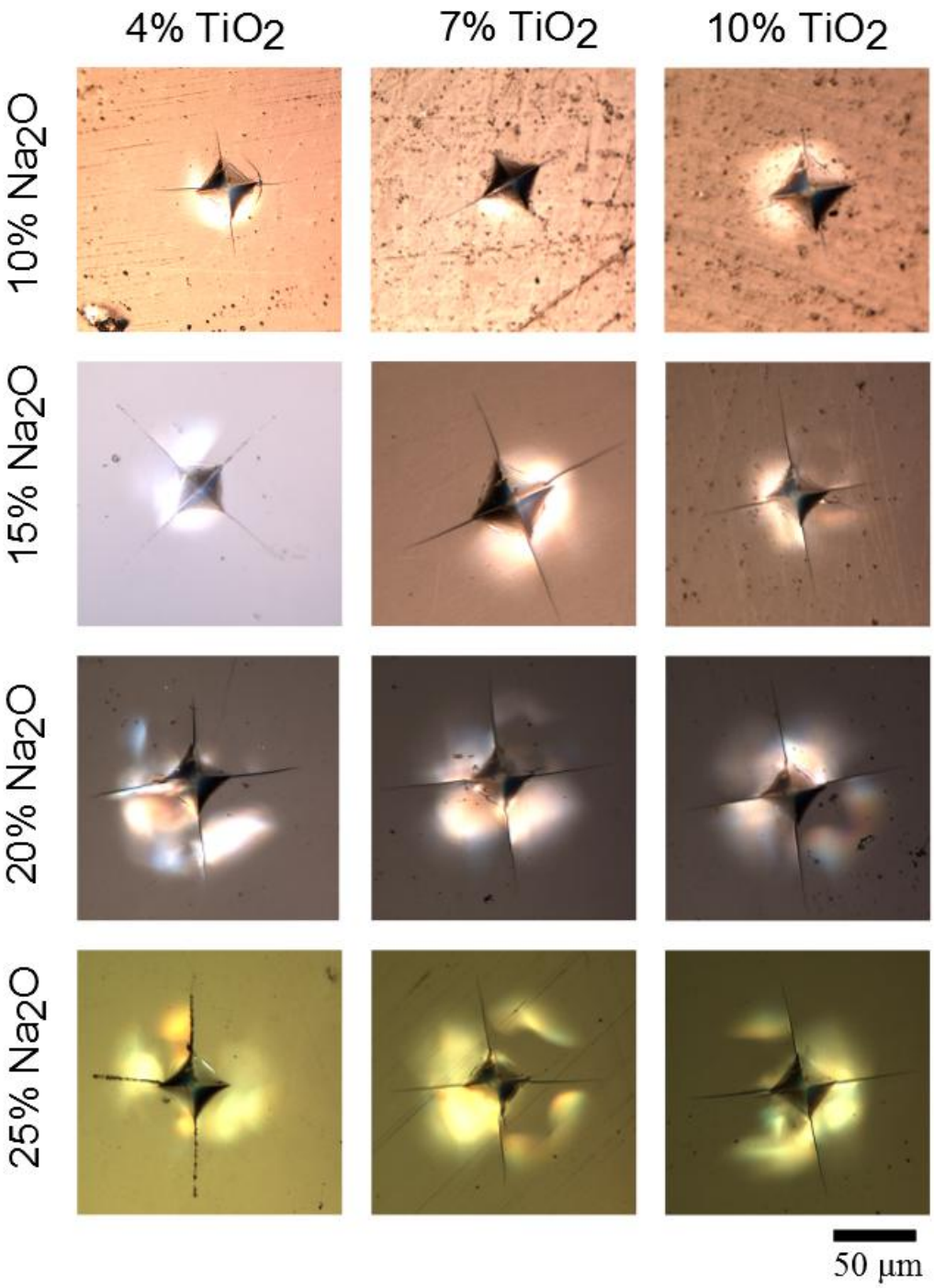

Fig. 5-5. Vickers indentations performed at 4.9 N on Na_2O-TiO_2-SiO_2 glasses.

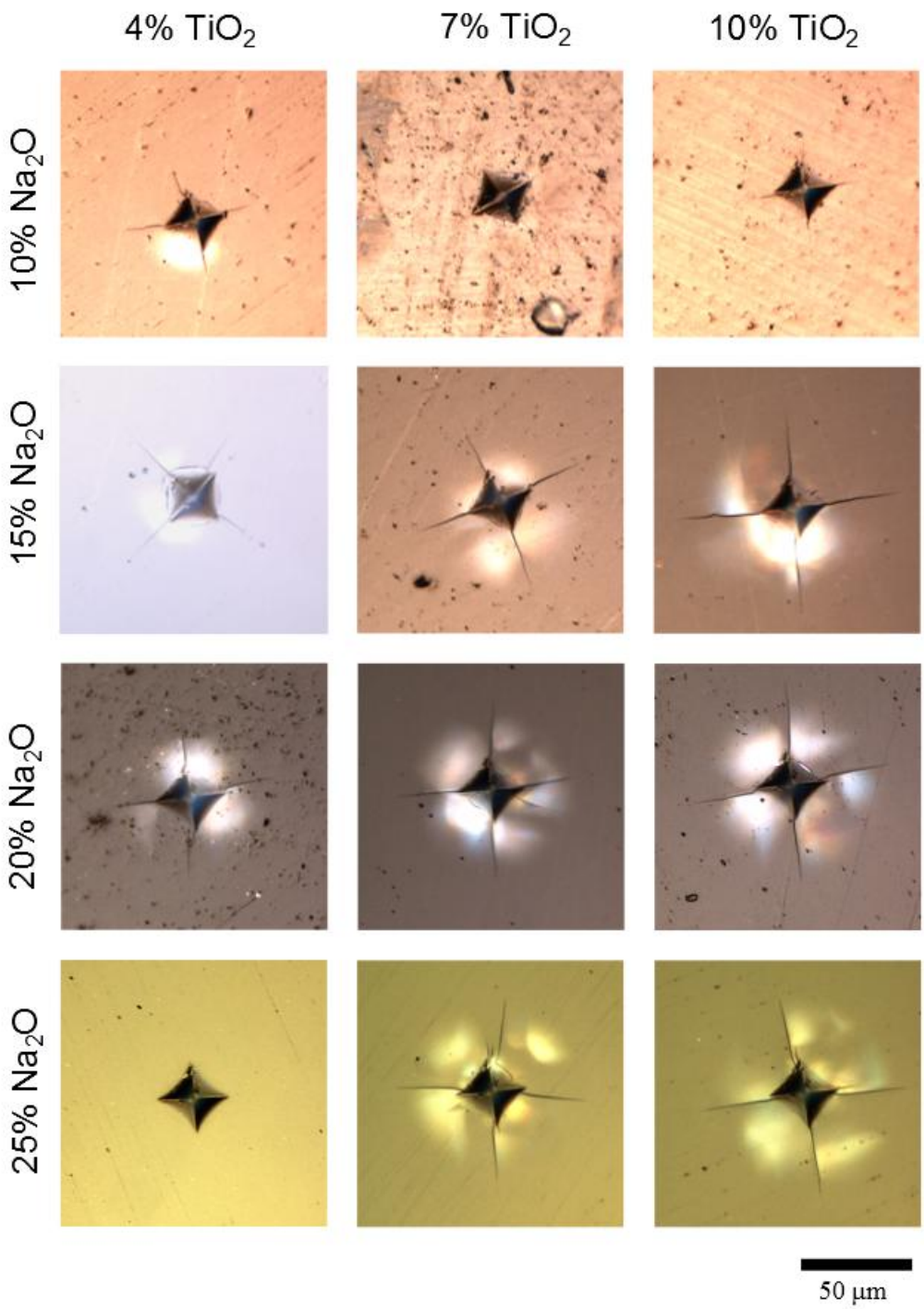

Fig. 5-6. Vickers indentations performed at 2.9 N on Na_2O-TiO_2-SiO_2 glasses.

Fig. 5-7 shows representative cracking patterns for all samples across loads tested. The number of cracks originating from each indent was averaged across the ten indents examined for each load and composition according to the following categories: radial-median cracks starting at

the four corners of the indent; radial-median cracks starting from anywhere other than the four corners; and ring/cone cracking or chipping around the indent. All samples showed a good resistance to cracking relative to the wide range of compositions previously studied by Sellapan et al. [16]. In the 10% Na_2O samples ring/cone cracking is present, while chipping occurs for all the other compositions. Fig. 5-7 is only intended to show average crack initiation, and does not represent indent size or crack length. Glasses initially become more susceptible to cracking with increasing Na_2O content from 10% to 20%, before quickly become less susceptible at 25% Na_2O. TiO_2 appears to have an effect of making glass more susceptible to cracking that is dependent on the Na_2O concentration. At 10% Na_2O increasing the TiO_2 content does not appear to have a noticeable effect on crack initiation. Some increase in susceptibility to cracking is observed at 15% and 20% Na_2O, but at 25% Na_2O increasing TiO_2 concentration significantly decreases the load required for cracking.

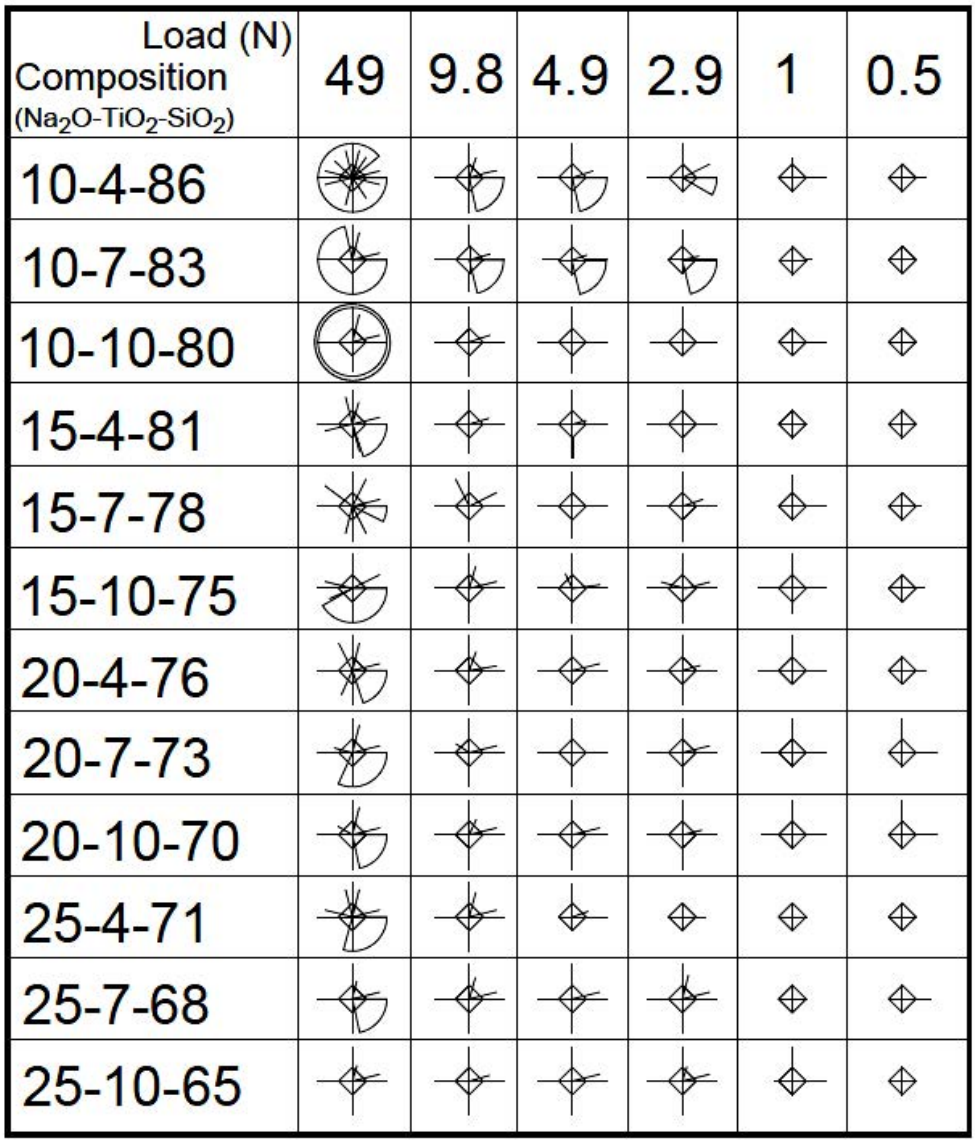

Fig. 5-7. Cracking patterns around Vickers indentations in Na_2O-TiO_2-SiO_2 glasses over a range of loads. Compositions are in mol percent. Cracking patterns shown represent an average of ten indents and show the average number of primary, secondary, and circular cracks. Indents made at 49, 9.8, 4.9, and 2.9 N were studied under an optical microscope, at 1 and 0.5 N were studied under SEM.

Hardness values and the contribution of reversible (elasticity based) and irreversible deformation to the energy from indentation tests are shown in Table 5-1. Hardness values were calculated using the indentation load and the surface area of the indentation, averaged across ten indents. The standard deviation of hardness values is approximately 0.5 GPa. The hardness measurements show a slight load dependence, increasing as the load is decreased (as is typically

the case and referred to as the Indentation Size Effect). Hardness appears to decrease with increasing Na_2O content and increase with increasing TiO_2 content. The elastic and permanent components of the deformation energy were calculated using the indentation loading and unloading curves and are expressed as fractions of the total work required to create the indent. The permanent and elastic components of the indentation deformation energy do not show load dependence. Values presented in Table 5-1 are averages of measurements taken at 1 N, 0.5 N, and 0.1 N and have a standard deviation of 0.7%. There appears to be a slight increase in the permanent energy component as the fraction of SiO_2 in the glass decreases until around 70%, where it starts to decrease again.

Table 5-1. Hardness and indentation energy of Na_2O-TiO_2-SiO_2 glasses for indentations made at six different loads. Error is given as the standard deviations.

Composition	Hardness (GPa)						Deformation Energy	
Na_2O-TiO_2-SiO_2	49 N	9.8 N	4.9 N	2.9 N	1 N	0.5 N	Reversible (%)	Permanent (%)
10-4-86	3.8±0.6	5.7±0.8	6.3±0.8	5.5±0.2	5.0±0.4	6.0±0.5	58.8±0.1	41.2±0.1
10-7-83	4.8±0.4	4.7±0.4	4.8±0.1	6.6±0.2	5.9±0.4	5.1±0.4	56.6±0.6	43.4±0.6
10-10-80	5.4±1.0	5.9±0.4	5.3±0.2	5.8±0.2	6.7±0.3	6.2±0.2	58.2±0.5	41.8±0.5
15-4-81	5.5±0.7	5.9±0.2	6.2±0.2	6.6±0.2	5.7±0.9	5.1±0.3	58.6±1.0	41.4±1.0
15-7-78	4.7±0.3	4.9±0.2	4.9±0.1	5.1±0.2	5.7±0.1	6.2±0.2	56.5±0.9	43.5±0.9
15-10-75	4.4±0.9	5.4±0.3	5.2±0.3	5.7±0.2	5.8±0.1	6.3±0.2	55.5±0.7	44.5±0.7
20-4-76	4.5±0.5	4.5±0.2	4.4±0.2	4.9±0.1	5.0±0.1	5.1±0.1	54.9±0.9	45.1±0.9
20-7-73	4.7±0.3	4.9±0.1	5.0±0.2	5.3±0.2	5.5±0.3	5.8±0.5	54.9±1.0	45.1±1.0
20-10-70	4.5±0.2	4.8±0.2	5.0±0.2	5.2±0.3	5.1±0.5	5.7±0.3	53.9±0.5	46.1±0.5
25-4-71	4.2±0.3	4.2±0.3	4.2±0.2	4.2±0.3	4.9±1.3	4.7±0.1	55.4±1.4	44.6±1.4
25-7-68	4.5±0.1	4.4±0.2	4.6±0.2	4.7±0.2	4.1±0.1	5.3±0.4	55.0±0.9	45.0±0.9
25-10-65	4.4±0.3	4.6±0.2	4.7±0.3	4.9±0.1	5.5±0.7	5.3±0.2	56.2±0.3	43.8±0.3

The crack resistance of a glass can be found by plotting the average number of cracks as a function of load [10]. A linear relationship was observed between the log of the indentation load and the number of cracks up to the maximum of four primary cracks. Crack resistances were calculated using logarithmic fits using the points between the maximum load at which zero cracks were observed and the minimum load where four cracks were observed. Error in the crack resistances were approximated using the same fitting method except using a number of cracks one standard deviation above average and one standard deviation below average. When adding or subtracting standard deviations, the number of cracks was still limited to a maximum

of 4 and a minimum of 0. These restrictions create non-symmetrical error bars. Table 5-2 shows the crack resistance of the glasses examined as the loads required to generate up to four cracks around a Vickers indent. Due to the relatively large increase in load between 2.9 N, 9.8 N, and 49 N, predictions for the minimum load when four cracks will be generated can be expected to be less accurate for samples for which four cracks were only observed above 2.9 N. The load to generate cracks appears to decrease with decreasing SiO_2 content up to 70-76% SiO_2 before increasing again.

Table 5-2. The minimum load required to generate a given number of cracks around a Vickers indent for Na_2O-TiO_2-SiO_2 glasses. The zero cracks column represents the maximum load at which no cracks could be detected (SEM and Optical microscope) at the corners of a Vickers indent.

Composition	Minimum load to generate cracks (N)				Maximum Load (N)
Na_2O-TiO_2-SiO_2	4 Cracks	3 Cracks	2 Cracks	1 Crack	0 Cracks
10-4-86	4.6	2.8	1.6	0.8	0.54
10-7-83	10.5	6.3	3.2	1.4	0.76
10-10-80	5.7	3.4	1.8	0.84	0.51
15-4-81	14.7	4.3	2.9	1.0	0.50
15-7-78	2.9	1.8	1.1	0.65	0.50
15-10-75	1.1	0.9	0.75	0.60	0.44
20-4-76	1.2	1.0	0.81	0.61	0.42
20-7-73	2.9	1.2	0.50	0.20	0.08
20-10-70	2.9	2.1	1.4	0.74	0.15
25-4-71	9.8	7.2	5.1	3.5	2.6
25-7-68	2.9	2.5	2.0	1.5	1.0
25-10-65	9.8	6.7	4.5	3.3	2.9

Values for Young's modulus, bulk modulus, shear modulus, and Poisson's ratio measured using Brillouin light scattering [17] and ultrasonic pulse techniques [4] are shown in Table 5-3. Values for elastic moduli measured through Brillouin light scattering tend to be slightly higher than those measured through the ultrasonic pulse technique, with the exception of the 25 Na_2O glasses. This can be tentatively associated with the volume of glass being measured and the acoustic wavelength used to measure that volume. Brillouin light scattering has a spot size on the order of tens of microns while the ultrasonic method measures across a sample approximately 1 cm x 1 cm x 0.4 cm. Additionally, Brillouin light scattering has an acoustic wavelength of ~0.5 μm while ultrasonic resonance has an acoustic wavelength of 0.05-10 mm. Thus the

ultrasonic measurements are more likely to include any defect in the volume measured, such as small bubbles or microcracks, and for these defects to alter the measured acoustic velocities.

Table 5-3. Elastic properties of Na_2O-TiO_2-SiO_2 glasses as measured by Brillouin light scattering and by ultrasonic pulse techniques. Error for Brillouin measurements is the standard deviation across ten measurements. E is Young's modulus, K is bulk modulus, μ is shear modulus, and ν is Poisson's ratio.

Composition	E (GPa)		K (GPa)		μ (GPa)		ν	
Na_2O-TiO_2-SiO_2	Brillouin ±0.7	Ultrasonic ±1.3	Brillouin ±0.7	Ultrasonic ±1.4	Brillouin ±0.4	Ultrasonic ±0.5	Brillouin ±0.006	Ultrasonic ±0.01
10-4-86	68.2	65.3	35.7	38.2	28.9	26.9	0.182	0.215
10-7-83	71.0	70.4	37.3	38.8	30.0	29.4	0.183	0.198
10-10-80	71.8	71.8	39.4	39.0	30.0	30.1	0.196	0.194
15-4-81	68.2	66.1	38.3	36.9	28.4	27.5	0.203	0.201
15-7-78	69.3	68.3	39.8	41.1	28.6	27.9	0.210	0.224
15-10-75	71.2	69.3	41.9	40.4	29.3	28.6	0.217	0.214
20-4-76	64.6	63.9	40.2	39.8	26.2	25.9	0.232	0.232
20-7-73	67.7	65.8	41.8	41.5	27.5	26.6	0.230	0.236
20-10-70	69.8	67.3	43.9	47.7	28.3	27.6	0.235	0.222
25-4-71	64.2	66.3	40.4	34.2	26.0	28.0	0.235	0.184
25-7-68	69.1	70.9	43.6	37.4	28.0	29.7	0.236	0.192
25-10-65	69.2	73.4	43.9	40.7	27.9	30.3	0.237	0.212

Young's modulus consistently increases with increasing TiO_2 concentration and generally decreases with increasing Na_2O content. Shear modulus also increases with increasing TiO_2 concentration, but shows less of a decrease with increasing Na_2O concentration. Bulk modulus increases with both TiO_2 and Na_2O concentration. Poisson's ratio increases slightly with increasing TiO_2 concentration and strongly with increasing Na_2O content. The change in Poisson's ratio is less noticeable between the 20% Na_2O series and the 25% Na_2O series.

5.5: Discussion

5.5.1: Network connectivity and elasticity

The calculated n_{BO} ranges from 3.3 to 4 and brings to light some interesting correlations between the atomic structure and the mechanical properties. Increases in the n_{BO} result from either an increase of the TiO_2/SiO_2 ratio or a decrease of the sodium content at a given TiO_2/SiO_2 ratio, but while a decrease of the sodium content results in a decrease of ν (as expected in regard of the decrease of the atomic packing efficiency), an increase of the titanium content induces an opposite effect, i.e. ν increases, suggesting a better atomic packing even though Ti is playing the role of a glass network former. The overall decrease of ν with increasing n_{BO} (Fig. 5-8), especially for $n_{BO}>3.6$, would corroborate the increase in the cross-linkage of the atomic network, making shear more difficult with respect to volume change (ν scales with K/μ, where K and μ are bulk and shear modulus, respectively).

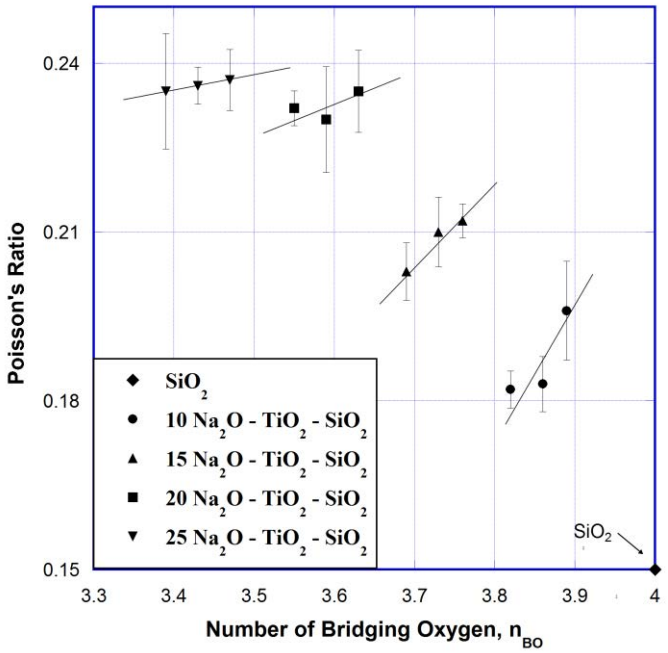

Fig. 5-8. Number of bridging oxygen per (Si,Ti)-centered tetrahedron versus Poisson's ratio measured through Brillouin light scattering. Error bars represent standard deviation across ten measurements. TiO_2 content increases from 4 to 10 percent moving from left to right for at each Na_2O content. Lines are provided as guides for the eyes.

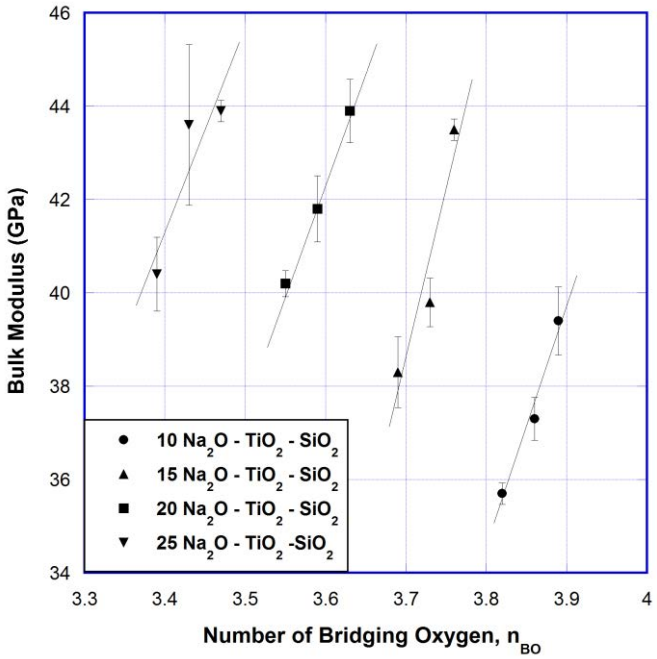

Fig. 5-9. Bulk modulus as obtained by Brillouin light scattering as a function of the number of bridging oxygen atoms per (Si,Ti)-centered tetrahedron. Lines are provided as guides for the eyes. TiO_2 content increases from 4 to 10 percent moving from left to right for at each Na_2O content.

The bulk modulus (as obtained by Brillouin light scattering) is given as a function of the TiO_2/SiO_2 ratio (number of bridging oxygen) for series at fixed sodium content in Fig. 5-9. Interestingly, in this ternary system, sodium has little influence on K, especially at large Ti content (for instance glasses with 10% TiO_2 have almost identical K values, between 43 and 44 GPa regardless of the sodium content), whereas at a given sodium content K markedly increases with TiO_2/SiO_2. Following Grüneisen [18] and previous reports focusing on glasses of a wide range of compositions [4,19,20], K, being expressed in Pa (i.e., J/m^3) can be viewed as a volume density of energy. For a multi-constituent glass, the volume density of energy (dissociation enthalpy per unit volume) can be roughly estimated from the properties of the constituents (Fig. 5-10) according to

$$<U_o/V_o>=\Sigma f_i \Delta H_{ai}/(\Sigma f_i M_i/\rho_i) \quad (5\text{-}8)$$

where ρ_i is the density, and f_i and M_i are the molar fraction and the molar mass, respectively. For the i^{th} constituent written as A_xB_y, according to an ordinary Born-Haber cycle:

$$\Delta H_{ai} = x\,\Delta H^o_f(A,g)+y\Delta H^o_f(B,g)-\Delta H^o_f(A_xB_y) \quad (5\text{-}9)$$

where ΔH_{ai} is the formation enthalpy of the glass component A_xB_y, $\Delta H^o_f(A,g)$ is the standard formation enthalpy of the cation (A_x), $\Delta H^o_f(B,g)$ is the standard formation enthalpy of the anion (B_y), and x and y are the amounts of elements A and B in the glass components, respectively.

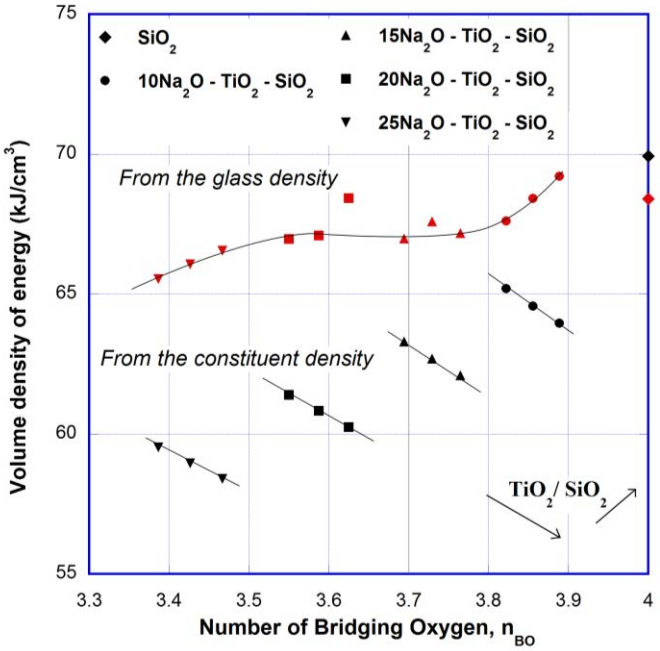

Fig. 5-10. Volume density of energy as estimated from thermochemistry data using the actual molar volume for the glass (from the experimental density; red symbols) or the molar volume calculated from the density of the constituents as a function of the number of bridging oxygen atoms per (Si,Ti)-centered tetrahedron (black symbols). Lines provided as guides for the eyes. Arrows indicate the direction of increasing TiO_2 or SiO_2 respectively.

The standard formation enthalpy of a cation is equal to its sublimation enthalpy; whereas, for an anion, gaseous in its standard state, the molar dissociation energy of the gas molecules must be considered. The denominator in the right hand side of Eq. (5-7) represents the whole volume occupied by the atoms of an "equivalent" mole of glass, provided the volume occupied by each atom is the same as in the crystal of the raw material of each component of the glass. The presence of free volume in the glass and the fact that inter-atomic distances, angles and coordination numbers in the glass network differ from those in the crystalline compounds, is thus not taken into account in this *ab initio* approach. The actual trends might thus differ from the predicted ones and this provides interesting information relevant to the glass network structure. For instance, the actual increase of K with the titania content (Fig. 5-9), which contrasts with the

prediction from the constituent, is thus consistent with the fact that TiO_2 is efficient to increase ν (Fig. 5-8), as well as the network energy as illustrated by the steep rise of T_g as a function of the TiO_2/SiO_2 ratio (number of bridging oxygen) for given Na_2O series (Fig. 5-12). Note that i) T_g is less sensitive to changes in the sodium content than it is to the titanium content (Fig. 5-12); and ii) titanium tends to tighten the atomic network, so that $<U_o>/<V_o>$ increases whereas a decrease of the volume density of energy was expected from the density and thermochemistry of the starting oxides. The role of titanium is quite unusual. The atomic packing density is generally found to decrease as a glass becomes richer in glass-forming elements (because a highly cross-linked network follows with less room for the flexibility required for good packing). The present analysis suggests that the environment and bonding strength of titanium in the glass significantly differs from the one in the crystalline titanium oxide.

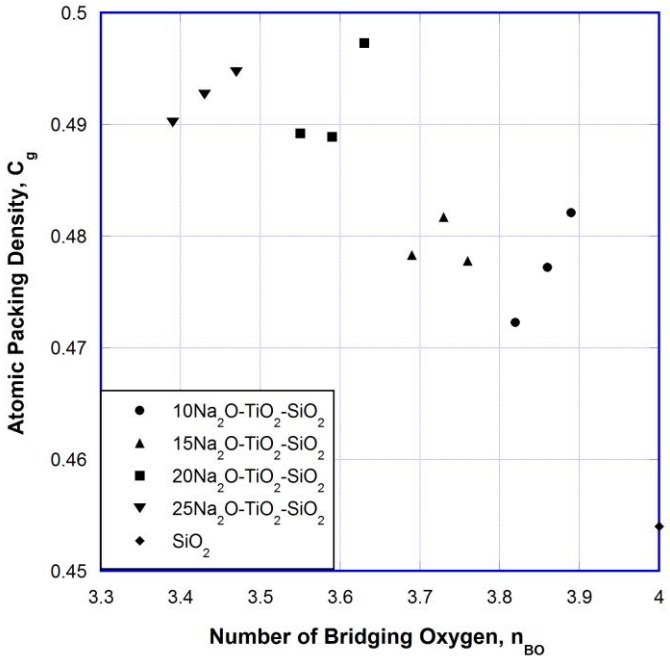

Fig. 5-11. Atomic packing density (defined in Eq. 5-7) as a function of the number of bridging oxygen atoms per (Si,Ti)-centered tetrahedron. TiO_2 content increases from 4 to 10 percent moving from left to right for at each Na_2O content.

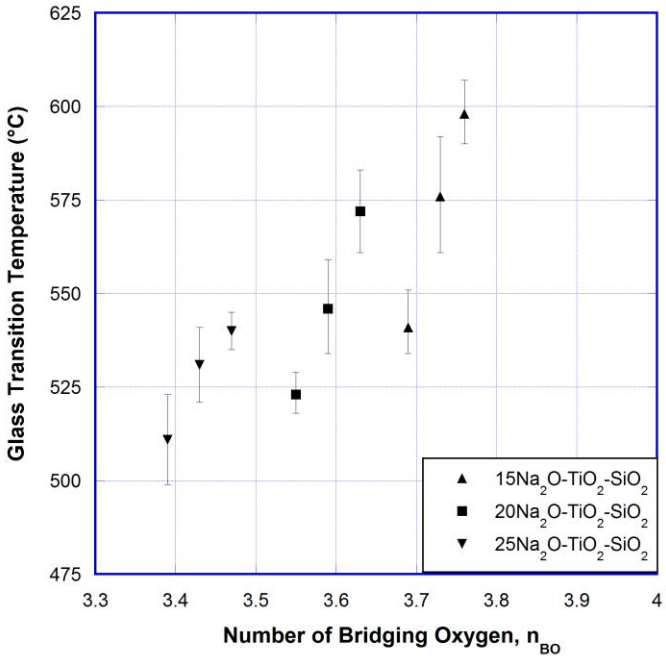

Fig. 5-12. Glass transition temperature (from DTA) as a function of the number of bridging oxygen atoms per (Si,Ti)-centered tetrahedron. TiO_2 content increases from 4 to 10 percent moving from left to right for at each Na_2O content. Temperatures plotted are the midpoint of the glass transition, and error bars represent the onset and end of the glass transition.

The bonding environment in soda-titania-silica glasses has been studied previously through X-ray absorption near edge structure (XANES) and extended X-ray absorption fine structure (EXAFS). Henderson and Fleet observed a mixture of $^{[4]}$Ti and $^{[5]}$Ti in Na_2SiO_3-TiO_2 glasses [21]. Farges et al. has published numerous studies on the role of Ti in the structure of a variety of glasses [12,13,22,23] and found that in Na_2O-TiO_2-SiO_2 glasses $^{[5]}$Ti made up more than 80% of the Ti in the glasses. $^{[5]}$Ti takes a square pyramidal geometry with four Ti-O bonds and one T=O bond. These bonds were found to have lengths of approximately 1.91 Å and 1.7 Å and valences of approximately 0.7 v.u. and 1.7 v.u., respectively. Bond valences are given in valence units and were calculated using the relationship of Brown and Altermatt [13].

Because of the large differences in bonding energies (Ti-O versus Ti=O) and bond distances suggested by neutron scattering, a percolation model where Ti occupied positions between regions relatively rich in Na and those relatively poor in Na has been suggested [13]. $^{[5]}$Ti was proposed to act as both a network modifier and a network former. Simply considered as a network former, such as how it behaves in pure titanium oxide, we would expect it to open the structure, reduce the packing density, and lower the volume density of energy. As the observed

result is entirely opposite (Figs. 5-10 and 5-11), the role of Ti as a network modifier must have a significant impact on the medium range structure in the glass.

5.5.2: Indentation cracking

As the titania content decreases or the sodium oxide content increases, the number of bridging oxygen decreases and the atomic packing density increases in the glass, and it is expected that the primary inelastic indentation deformation mechanism will shift from densification to shear flow. This shift is expected to be accompanied by a change in the cracking behavior. In pure silica we expect median-radial cracks and some ring cracking depending on the indentation load. Na has a strong effect of decreasing the number of bridging oxygen and increasing the atomic packing density. This should decrease the driving force for ring/cone cracking and increase the driving force for lateral cracking [11]. It may decrease the driving force for radial-median cracks as well.

Ti as a network former with a weaker bond strength than Si would be expected to increase the glass's susceptibility to cracking. However, in the presence of Na, titania strengthens the glass (Table 5-3). A possible explanation, using the model proposed by Farges et al. [13], would be that the Ti promotes some local ordering in the glass and preferentially attracts Na, reducing the effective number of non-bridging oxygen in the silica tetrahedral network. Ti increases both the atomic packing density and stiffens the network. It is unclear which of these properties will have the stronger effect on the cracking behavior of the glass; however, it is reasonable to expect a shift from densification to shear flow for the deformation mechanism.

Driving forces for different cracking modes are shown in Fig. 5-13. The lines for each cracking mode show where the driving force for the mode is zero, and pluses and minuses indicate that the driving force is either tensile or compressive, respectively. Error bars in E/H values is the variance calculated from standard deviations in Young's modulus and hardness assuming covariance is zero. Details for the calculation of the driving forces for cracking (accounting for the elastic recovery) is given in [11].

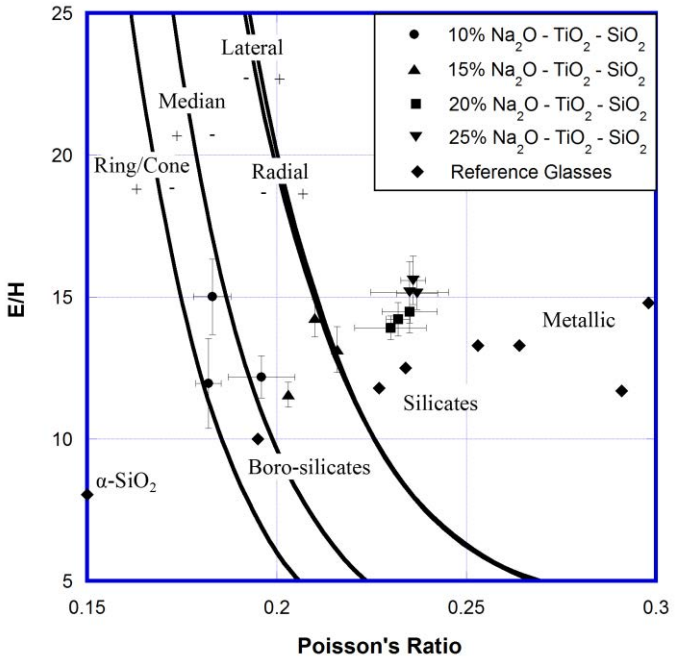

Fig. 5-13. Plot of Young's modulus (GPa) over hardness (GPa) versus Poisson's ratio. E/H provides a unitless measure of a material's resistance to deformation that combines elastic and plastic stiffnesses. Lines represent the transition from tensile (+) to compressive (-) driving forces for different cracking modes. Calculation of these stresses and data for the reference glasses can be found in [11].

The ratio of elastic modulus over hardness and Poisson's ratio is necessary information to predict the driving force for cracking using the Boussinesq stress field [24]. As seen in Figs. 5-(3-6), changes in the soda concentration strongly promote radial and lateral cracking over median and ring/cone. Ring/cone cracking was only seen in the 10% Na_2O samples and only at high loads, which matches the driving force predictions reasonably well. As TiO_2 and Na_2O concentrations are increased and Poisson's ratio shifts to higher values, it would be expected that radial and lateral cracks would become more prominent and cone/ring cracking would disappear.

5.5.3: Indentation deformation and hardness

Plot of the critical loads to generate two and four cracks around an indent versus Poisson's ratio reveals an unexpected trend (Fig. 5-14). As Poisson's ratio is increased, the load required to create cracks in the glass initially decreases quickly until it reaches a minimum at approximately $\nu = 0.22$ (worse case in terms of visible crack initiation resistance). Further increasing Poisson's ratio above $\nu = 0.23$ results in a sharp increase in the critical crack initiation

load. This behavior is not predicted by the driving force calculations shown in Fig. 5-13, which suggest that the driving force for radial cracks should continue increasing as Poisson's ratio is increased. The observed behavior could be explained by a change in the deformation behavior in the glass. At low Poisson's ratio, the primary mode of deformation is densification, while as Poisson's ratio increases, a shift from densification to shear flow is expected, as is observed for instance as one moves from oxide glasses to metallic ones. At intermediate Poisson's ratio neither densification nor shear flow dissipate the stresses sufficiently to prevent cracking. The deformation mechanism and the fracture toughness are both likely to depend on the composition of the system, and a significant increase of K_{IC} might compensate for the rise of the driving force for indentation cracking.

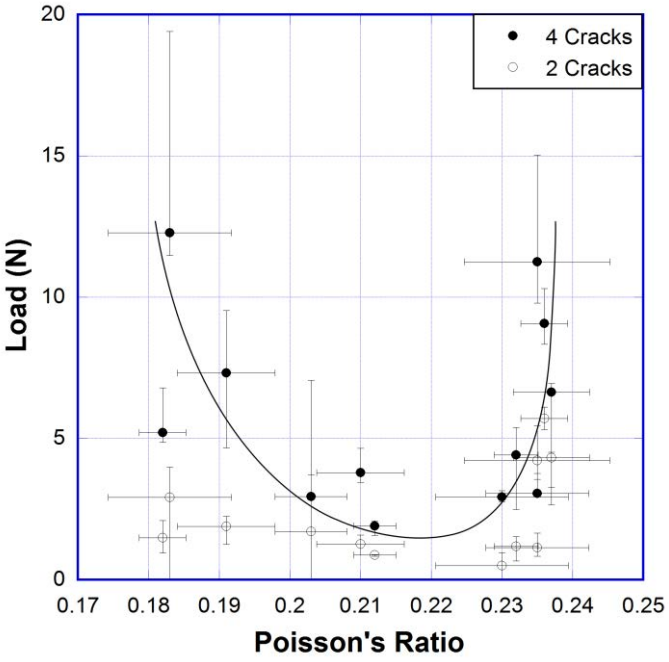

Fig. 5-14. Critical load to create cracks around a Vickers indent versus Poisson's ratio measured by Brillouin light scattering. Poisson's ratio values are averages of ten measurements. Line provided as a guide for the eyes through data points for 4 cracks.

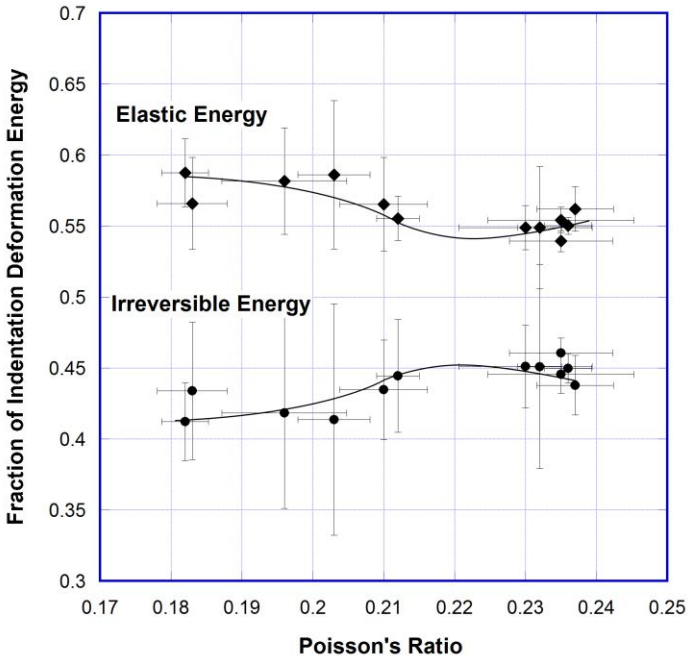

Fig. 5-15. Reversible and permanent fractions of the energy required to create an indent versus the number of bridging oxygen for Na_2O-TiO_2-SiO_2 glasses. Energies were determined using the loading and unloading curves of indentations at 1 N, 0.5 N, and 0.1 N, with 10 indents at each load. No dependence on load was observed for the relative fractions of plastic and elastic energy. Lines are provided as guides to the eyes.

This result is peculiar, because the indentation energy loss associated with the irreversible deformation process exhibits a bell-shape curve as a function of Poisson's ratio, with a maximum at $\nu \approx 0.21$-0.23 corresponding to the range where the critical load for cracking is minimum (Fig. 5-15). One would expect that the resistance to cracking should increase with the amount of dissipated energy by means of irreversible processes ("plastic" deformation). However, it seems from a comparison between the bell-shape energy and the U-shape critical load curves that the increase of the dissipated energy coincides to the building-up of residual stresses, possibly because shear flow combined with densification in this range results in the displacement of matter downward, to produce an elastically constrained axisymmetric region. Further investigations are required to get more insight into this phenomenon. Two hypothesis can be invoked, namely

i) Fracture toughness comes into play in the initiation of cracking and might change with composition in such a way that K_{IC} is larger as ν increases to 0.23. Crack initiation might be further retarded thanks to the ease for irreversible flow in this ν range (as per the irreversible indentation energy plot)

ii) As ν increases, the indentation cracking pattern evolves toward more lateral and radial cracking, and Palmqvist cracking prevail, so that the available mechanical energy might dissipate through the formation of more and longer radial cracks (for a given fracture area, the depth being smaller, cracks must be longer).

It has been shown that the crack resistance of glasses is strongly affected by the humidity present during the indentation process [25]. In this study humidity was not controlled during indentation experiments. Its effect on the critical crack initiation load will be investigated in our future study. Humidity seems unlikely to affect the fractions of permanent and elastic deformation energy at loads, which were measured at loads where cracking did not occur.

5.6: Conclusion

Our study shows that TiO_2 has a striking tightening effect on the glass network, increasing both the packing density and the network energy. This is expressed in the measured elastic properties by an increase in Young's modulus and Poisson's ratio. In regard to a previously reported indentation-damage map, Na_2O-TiO_2-SiO_2 glasses turn out to fall in the property range (E/H, *v*) where the driving force for indentation cracking, whatever the cracking pattern of concern (radial, median, lateral), is relatively limited and exhibit a good indentation damage resistance, especially for the 15 Na_2O - 4 TiO_2 - 81 SiO_2 and 25 Na_2O - 4 TiO_2 - 71 SiO_2 compositions. A minimum in the critical crack initiation load was observed in the range of v = 0.21-0.22.

5.7: References

[1] J. Lewandowski, W. Wang, A. Greer, Intrinsic Plasticity or Brittleness of Metallic Glasses, Philos. Mag. Lett. 85 (2005) 77–87.
[2] S.F. Pugh, Relations between the Elastic Moduli and the Plastic Properties of Polycrystalline Pure Metals, Philos. Mag., 45 (1954) 823-843.
[3] T. Rouxel, H. Ji, J. Guin, F. Augereau, B. Ruffle, Indentation Deformation Mechanism in Glass: Densification versus Shear Flow, J. Appl. Phys. 107 (2010) 094903.
[4] T. Rouxel, Elastic Properties and Short-to Medium-Range Order in Glasses, J. Am. Ceram. Soc. 90 (2007) 3019–3039.
[5] Y.H. Liu, G. Wang, R.J. Wang, D.Q. Zhao, M.X. Pan, and W.H. Wang, Super plastic bulk metallic glasses at room temperature, Science, 315 (2007) 1385-1388.

[6] M.D. Demetriou, M.E. Launey, G. Garrett, J.P. Schramm, D.C. Hofmann, W.L. Johnson, and R.O. Ritchie, A damage-tolerant glass. Nature Materials, 10 (2011) 123-128.
[7] M. Wada, H. Furukawa, K. Fujita, Crack Resistance of Glass on Vickers Indentation, Proc. Xth I.C.G. 11 (1974) 39-46.
[8] J. Sehgal, S. Ito, A New Low-Brittleness Glass in the Soda-Lime-Silica Glass Family, J. Am. Ceram. Soc. 81 (1998) 2485-2488.
[9] B. Lawn, D. Marshall, Hardness, Toughness, and Brittleness: An Indentation Analysis, J. Am. Ceram. Soc. 62 (1979) 347–350.
[10] Y. Kato, H. Yamazaki, S. Yoshida, J. Matsuoka, Effect of densification on crack initiation under Vickers Indentation test, J. Non-Cryst. Solids. 356 (2010) 1768–1773.
[11] T. Rouxel, Driving Force for Indentation Cracking in Glass: Composition, pressure and temperature dependence, Phil. Trans. R. Soc. A. 373 (2015) 20140140.
[12] F. Farges, A Ti K-edge EXAFS Study of the Medium Range Environment around Ti in Oxide Glasses, J. Non-Cryst. Solids. 244 (1999) 25–33.
[13] F. Farges, G.E.J. Brown, A. Navrotsky, H. Gan, J.J. Rehr, Coordination Chemistry of Ti(IV) in Silicate Glasses and Melts: II. Glasses at Ambient Temperature and Pressure, Geochim. Cosmochim. Acta. 60 (1996) 3039–3053.
[14] R. Shannon, Revised Effective Ionic-Radii and Systematic Studies of Interatomic Distances in Halides and Chalcogenides, Acta Crystallogr. Sect. A. 32 (1976) 751–767.
[15] E. Whittake, R. Muntus, Ionic Radii for use in Geochemistry, Geochim. Cosmochim. Acta. 34 (1970) 945-956.
[16] P. Sellappan, T. Rouxel, F. Celarie, E. Becker, P. Houizot, R. Conradt, Composition Dependence of Indentation Deformation and Indentation Cracking in Glass, Acta Mater. 61 (2013) 5949–5965.
[17] M. Guerette, L. Huang, A simple and convenient set-up for high-temperature Brillouin light scattering, J. Phys. D: Appl. Phys. 45 (2012) 275302.
[18] C. Zwikker, Physical Properties of Solids Materials, 2nd ed., Interscience Publishers, New York, 1954.
[19] A. Makishima, J. Mackenzie, Calculation of Bulk Modulus, Shear Modulus and Poisson's Ratio of Glass, J. Non-Cryst. Solids. 17 (1975) 147–157.
[20] S. Inaba, S. Fujino, K. Morinage, Young's Modulus and Compositional Parameters of Oxide Glasses, J. Am. Ceram. Soc. 82 (1999) 3501–507.
[21] G.S. Henderson, M.E. Fleet, The Structure of Titanium Silicate Glasses Investigated by Si K-edge X-ray Absorption Spectroscopy., J. Non-Cryst. Solids. 211 (1997) 214–221.
[22] F. Farges, G.E.J. Brown, J.J. Rehr, Coordination Chemistry of Ti(IV) in Silicate Glasses and Melts: I. XAFS Study of Titanium Coordination in Oxide Model Compounds, Geochim. Cosmochim. Acta. 60 (1996) 3023–3038.
[23] F. Farges, Coordination of Ti in Crystalline Fresnoites: A High-resolution XANES Spectroscopy Study at the Ti K-edge, J. Non-Cryst. Solids. 204 (1996) 53–64.
[24] Boussinesq J. 1885 *Applications des potentiels aÌ l'étude de l'équilibre et du mouvement des solides élastiques*. Paris, France: Gauthier-Villars.
[25] S. Striepe, J. Deubener, M. Smedskjaer, M. Potuzak, Environmental effects on fatigue of alkaline earth aluminosilicate glass with varying fictive temperature, J. Non-Cryst. Solids. 379 (2013) 161–168.

Chapter 6 : Deformation and Crack Initiation in Na_2O-TiO_2-SiO_2 glasses

6.1: Abstract

An observed minimum in the critical crack initiation load at Poisson's ratio of 0.21-0.22 in Na_2O-TiO_2-SiO_2 glasses was investigated. Vickers indentation was used to examine hardness and average cracking length, fracture toughness was measured through the single-edge precracked beam method (SEPB), and volumes of densification and shear flow around indentations were measured using atomic force microscopy (AFM). Relations between the critical crack initiation load and hardness, average crack length, fracture toughness, and the volume and mechanisms of permanent deformation were studied. No correlations were observed between hardness, average crack length, or fracture toughness with the critical crack initiation load. Correlation between the minimum in crack initiation load and the change in deformation mechanisms over the same Poisson's ratio range was observed.

6.2: Introduction

Understanding structure-property relationships in glasses remains a distinct challenge in designing new glasses for specific applications [1]. In the pursuit of developing ultrastrong glasses, an improved understanding of what structural characteristics and properties contribute to either hindering or promoting crack initiation and propagation in glasses is of great importance [2]. Lewandowski et al. observed an interesting correlation between fracture energy and Poisson's ratio (ν) in oxide and metallic glasses, where a brittle-to-ductile transition occurs between ν = 0.31-0.32 [3]. Rouxel et al. developed indentation cracking maps to predict driving forces for cracking in glasses [4]. They found a critical value at $\nu \approx 0.22$ where the indentation stress field was greatly reduced as well as transition from easily damaged to highly resilient glasses at $\nu = 0.33$.

In a recent study by the authors, an unexpected trend was observed (Fig. 5-14), where the critical load for initiating cracks at the corners of Vickers indentations went through a minimum as the Poisson's ratio was increased from 0.18 to 0.24 in Na_2O-TiO_2-SiO_2 glasses [5], with the minimum occurring between ν = 0.21 - 0.22. This behavior was not predicted by the driving

forces maps developed by Rouxel et al. [4], which predict that the driving forces for radial cracking should increase with the Poisson's ratio across the examined range (0.18-0.24). It is likely that as the glass transitions from primarily deforming through densification to shear flow, an intermediate region could exist where the competing deformation mechanisms result in an increase in residual stresses around the indent.

The purpose of this study is to investigate this behavior further. Since both the deformation mechanism and fracture toughness are dependent on the composition, it is possible that a change in fracture toughness could compensate for changes in the driving forces for cracking. It is also possible that as the driving forces for radial and lateral cracks increase and those for median and conical cracks decrease with increasing ν, more energy could be dissipated through the formation of more and longer radial cracks. To investigate these possibilities, Na_2O-TiO_2-SiO_2 glasses of the same compositions in Scannell et al. [5] were examined. The hardness and average crack length were investigated through Vickers indentation, the fracture toughness was measured through the single-edge precracked beam method (SEPB), and the fractions of shear flow and densification around Vickers indentations were measured using atomic force microscopy (AFM).

6.3: Experimental

Detailed discussion of glass synthesis, sample preparation, and indentation experiments are presented in the previous chapter.

Densification and shear flow under the Vickers indents were examined by making 0.5 N Vickers indents on samples with dimensions of approximately 5 mm x 5 mm x 1 mm with parallel, optically polished surfaces. A 0.5 N load was chosen to still have a relatively large indent while mostly avoiding cracking in all samples. Ten indents were made on a sample of each composition and the indentation profiles were mapped using an AFM. The samples were then annealed at 0.9 Tg for 1 hour and the indentation profiles were mapped again. Volume of the pile up above the glass surface and volume of the indentation below the surface were calculated from the indentation profiles using Gwyddion [6] for both pre- and post-annealing measurements. The volumes of permanent deformation that occurred through densification and through shear flow were calculated by Eqs. 6-1 and 6-2, respectively,

$$V_d = (V_i^- - V_a^-) + (V_a^+ - V_i^+) \quad (6\text{-}1)$$

$$V_s = V_i^- - V_d = V_i^- + V_i^+ - V_a^+ \quad (6\text{-}2)$$

where V_d is the densified volume, V_s is the volume deformed through shear flow, V^- is the volume of the indent before (i) and after (a) annealing, and V^+ is the pile-up volume. Further discussion on this type of analysis can be found in Yoshida et al. [7]. A profile of an AFM image of an indent before and after annealing are shown in Fig. 6-1. As all AFM measurements are done post unloading and elastic recovery, only the permanent deformation volumes at the indent are examined.

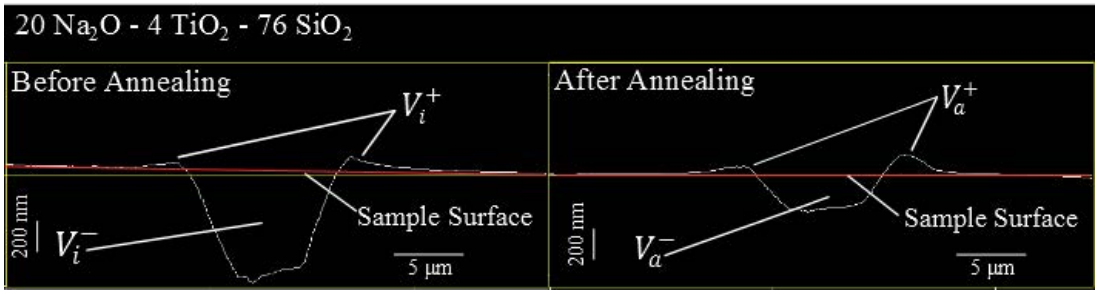

Fig. 6-1. AFM indentation profiles on 20 Na_2O - 4 TiO_2 - 76 SiO_2 glass before (left) and after (right) annealing.

Fracture toughness of glasses was measured through the SEPB [8] for four glasses with 4 mol% TiO_2 and 10, 15, 20, and 25 mol% Na_2O. For SEPB experiments, samples were prepared as 30 mm x 4 mm x 3 mm bars. All four sides of the bars were polished to an optical finish, with the opposite sides polished to be parallel to within ≤ 50 µm. The ends were also polished to an optical finish so that it was possible to see through the bar to observe the pre-crack growth. To make the initiation of the pre-cracks more reliable, a series of 9.8 N Vickers indentations in a line along the middle of the bottom face perpendicular to the length direction. Indentations were at a load where radial-median cracks regularly occurred with a minimum of other forms of cracking (lateral/conical/chipping). Indents were spaced approximately 30-40 µm apart.

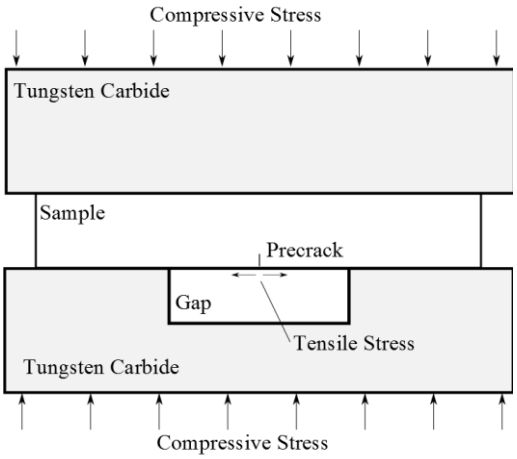

Fig. 6-2. Schematic of the experimental setup used to generate precracks in glass bars for SEPB tests.

The sample was placed between two tungsten carbide bars, the bottom of which had a gap in the middle (Fig. 6-2). This gap was aligned with the line of indents so that when a compressive stress was applied a crack would grow stably at the indentations. A Lloyd tester was used to load the sample, moving at 0.2 mm/min until 10 N was reached, then at 0.1 mm/min up to 200 N, and finally at 0.05 mm/min until the loading was manually stopped. By looking through the polished end of the bar using a camera, it was possible to observe the pre-crack growth. Loading was halted when the pre-crack had grown horizontally across the entire bottom surface of the sample and vertically was 20-40 percent of the height of the bar (~1-1.5 mm).

The fracture toughness of the pre-cracked bar was measured through a three-point bend test. Deflection and load were recorded every 0.05 s. Fracture toughness was calculated using Eq. 6-3,

$$K_{Ic} = Y a^{\frac{1}{2}} \frac{(3PL)}{(2BW^2)} \tag{6-3}$$

where Y is a geometric factor dependent on the a/W ratio for $4 \leq L/W \leq 8$ [8], P is the maximum load, B is the width, W is the height, L is the loaded span (20 mm), a is the pre-crack length, and K_{Ic} is the fracture toughness.

Experimental error for all measurements is given as the standard deviation of measured values. Vickers hardness was measured 10 times at each load for each composition, average

crack lengths are of all measured cracks for that load/composition, with a maximum of 40 cracks being averaged, densification and shear flow volumes were measured at 10 indents for each composition, and fracture toughness was measured 4-8 times at each composition. Some fracture toughness measurements were excluded based on a variety of criteria, which will be discussed in more detail in the following section.

6.4: Results

The hardness of Na_2O-TiO_2-SiO_2 glasses versus Poisson's ratio is shown in Fig. 6-3. This data was presented previously in a tabular form with hardness versus composition [5]. The 9.8 and 4.9 N loads are of particular interest because that is where four radial/median cracks are initiated at the corners of the Vickers indents consistently, for all compositions, without the generation of significant lateral or conical cracking. Scatter in hardness measurements was quite large, but trend of decreasing hardness with Poisson's ratio is observed.

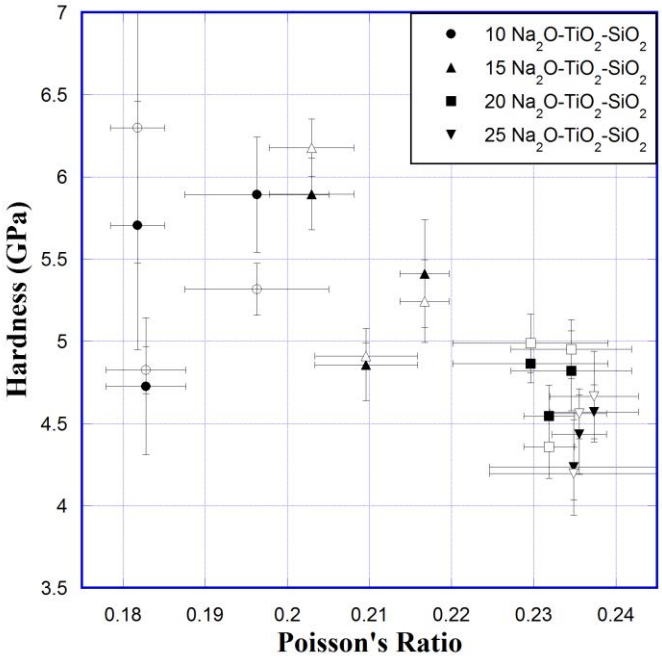

Fig. 6-3. Hardness versus Poisson's ratio for Na_2O-TiO_2-SiO_2 glasses. Hardness at 9.8 N (closed) and 4.9 N (open) is shown. Error bars represent standard deviation across ten measurements at each load for hardness and five measurements of each composition for Poisson's ratio.

Fig. 6-4 shows the log of average crack length of radial/median cracks originating from the corners of Vickers indents at 2.9, 4.9, 9.8, and 49 N. Log of crack length increases linearly

with increasing Poisson's ratio. A few glasses, at ν = 0.183, ν = 0.196, and ν = 0.235, have much lower observed crack lengths at 2.9 and 4.9 N. It is difficult to tell if these extremely small average crack lengths are representative. These glasses are the most resistant to crack initiation, and particularly at 2.9 N many of the indents had no visible cracking. It is possible for these glasses that cracks that formed did not exit the surface completely. It should be noted that the error bars were not calculated on a log scale, so the error bar above each point is shorter than that below the point.

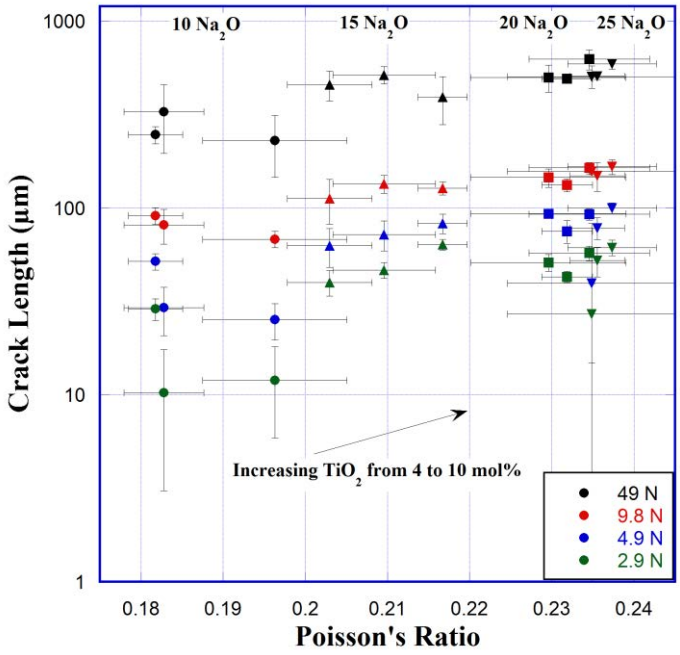

Fig. 6-4. Average crack length at the corners of Vickers indents versus Poisson's ratio. Error bars represent the standard deviation across all cracks measured at each load. Na_2O content is denoted by the marker shape: 10 Na_2O (closed circle), 15 Na_2O (triangle), 20 Na_2O (square), and 25 Na_2O (upside down triangle). TiO_2 content increases from 4 to 10 mol% from left to right for each Na_2O content.

Fracture toughness of Na_2O-TiO_2-SiO_2 bars is plotted versus Poisson's ratio in Fig. 6-5. Samples with 4 mol% TiO_2 and 10, 15, 20, and 25 Na_2O were measured. The fracture toughness appears to decrease slightly with increasing Poisson's ratio; however, the decrease is significantly lower than the experimental error. Error bars represent the standard deviation across three to six measurements made at each composition. The measured values of fracture toughness were found to deviate significantly if the precrack was smaller than ~20% or greater than 80% of the sample bar height, if the precrack did not form perpendicular to the bar length, or if the length to

height ratio, L/W, was not between 4 and 8. Samples that fell into these categories were not included in the values presented in Fig. 6-5.

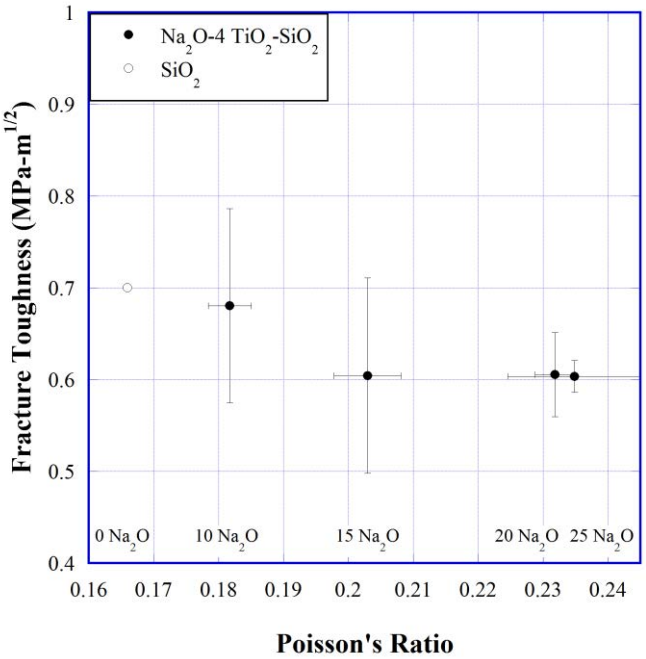

Fig. 6-5. Fracture toughness versus Poisson's ratio. Fracture toughness was measured using the SEPB method on Na_2O-TiO_2-SiO_2 glasses with 4 mol% TiO_2. Error bars represent the standard deviation across two to four measurements. SiO_2 fracture toughness was taken from literature [10,11].

The results of the AFM indentation recovery experiments are shown in Fig. 6-6. The volume assigned to shear flow increases slowly with Poisson's ratio between 0.18 and 0.23, from 4.5 μm^3 to 6.4 μm^3. At $\nu = 0.237$ there is a large jump in sheared volume to 12.9 μm^3. Two samples with $\nu = 0.182$ and 0.203 are have sheared volumes of ~7.5 μm^3, which is larger than would be expected from the linear trend of sheared volume increasing with the Poisson's ratio. The densification volume also increases slowly between 0.18 and 0.23, from 13.2 μm^3 to 16.5 μm^3. The large densification volume at $\nu = 0.21$ and 0.23 can be seen in Fig. 6-7. Then the densification volume decreases rapidly between 0.23 and 0.24. This sharp change is quite peculiar and bears some addition investigating.

With regards to compositional changes, the densification volume increases significantly between 10 and 15 Na_2O and then remains almost constant between 15 and 25 Na_2O. Increasing TiO_2 decreases the densification volume linearly, with an exception for 20 Na_2O - 10 TiO_2 - 70 SiO_2 glass, which can be attributed to the low Na_2O and TiO_2 content of the glass, and for the 10

Na_2O - 10 TiO_2 - 80 SiO_2 sample, which is possibly caused by the low Na_2O content of the glass. The shear flow volume increases slowly with increasing Na_2O and decreases with increasing TiO_2. At 25 Na_2O, however, increasing TiO_2 increases the shear flow volume rather than decreasing it. The rather sharp increase between 25 Na_2O - 7 TiO_2 - 68 SiO_2 and 25 Na_2O - 10 TiO_2 - 65 SiO_2 is exaggerated by the low TiO_2 content of the 25 Na_2O - 7 TiO_2 - 68 SiO_2 sample.

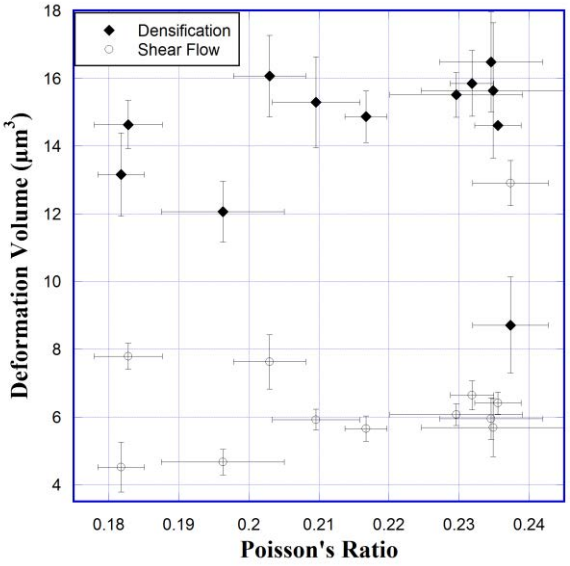

Fig. 6-6. Deformation volume for 0.5 N Vickers indents versus Poisson's ratio.

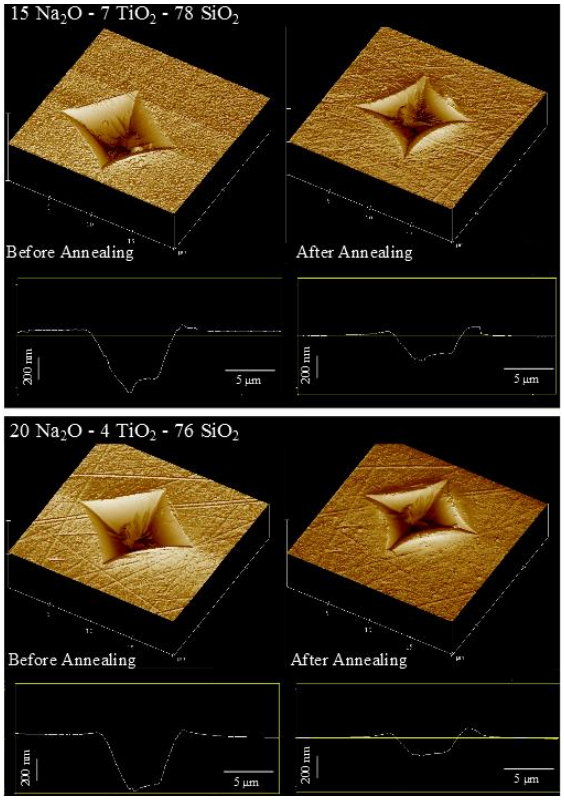

Fig. 6-7. AFM images of 15 Na_2O - 7 TiO_2 - 78 SiO_2 ($\nu = 0.210$) and 20 Na_2O - 4 TiO_2 - 76 SiO_2 ($\nu = 0.232$) glass before and after annealing. AFM image dimensions are 20 µm x 20 µm x 0.5 µm at a 45° angle. Depth profiles are perpendicular to the indent edge.

6.5: Discussion

From our previous study [5], it was observed that the ratio of Young's modulus to hardness (E/H) increased with increasing Poisson's ratio, suggesting that driving forces for radial and lateral cracks should be larger at higher ν [7]. Additionally, the fraction of energy that was irreversible in the indentation process was found to increase at $\nu = 0.21$-0.22 then appears to decrease at $\nu \approx 0.235$ [5]. The increasing driving forces should promote crack formation. A greater irreversible fraction of energy used to generate the indent could indicate several things: that there is an increase in the ability of the glass to deform (either through densification or shear flow), an increase in the amount of energy used for the generation of cracks around the indent, and/or an increase in the residual stresses around the indent. The changes would not lead us to expect the minimum in the crack initiation load seen in Fig. 5-14. To further explore and possibly find an explanation for this minimum let's go over the data present and trends observed in literature.

The decrease in hardness (Fig. 6-3) with increasing Poisson's ratio indicates that the size of the indentation is increasing. This hardness change corresponds more to the increase in the Na_2O content in the glass, with no consistent change observed between different TiO_2 contents. While an increased hardness generally corresponds to a greater fracture toughness, this is complicated when multiple deformation mechanisms are present [12]. Reports on glasses with high crack resistances show that hardness does not directly correlate with fracture toughness or crack resistance [10,13,14]. Sehgal and Ito did observe a correlation between the crack initiation load and a brittleness factor [10]. Calculating the brittleness from the indentation in Na_2O-TiO_2-SiO_2 glasses, a trend of increasing brittleness with increasing Poisson's ratio is observed for 9.8 and 49 N loads (Fig. 6-8a). At 4.9 and 2.9 N loads (Fig. 6-8b), the brittleness increases with Poisson's ratio up to $\nu = 0.22$-0.23 and then it decreases. However, the analysis of brittleness in these glasses at 4.9 and 2.9 N loads is somewhat questionable. At these loads, the crack length is approximately equal to or shorter than the indentation diagonal. Lawn and Marshall pointed out that this is where the mechanical response transitions from being hardness-controlled to toughness-controlled [12].

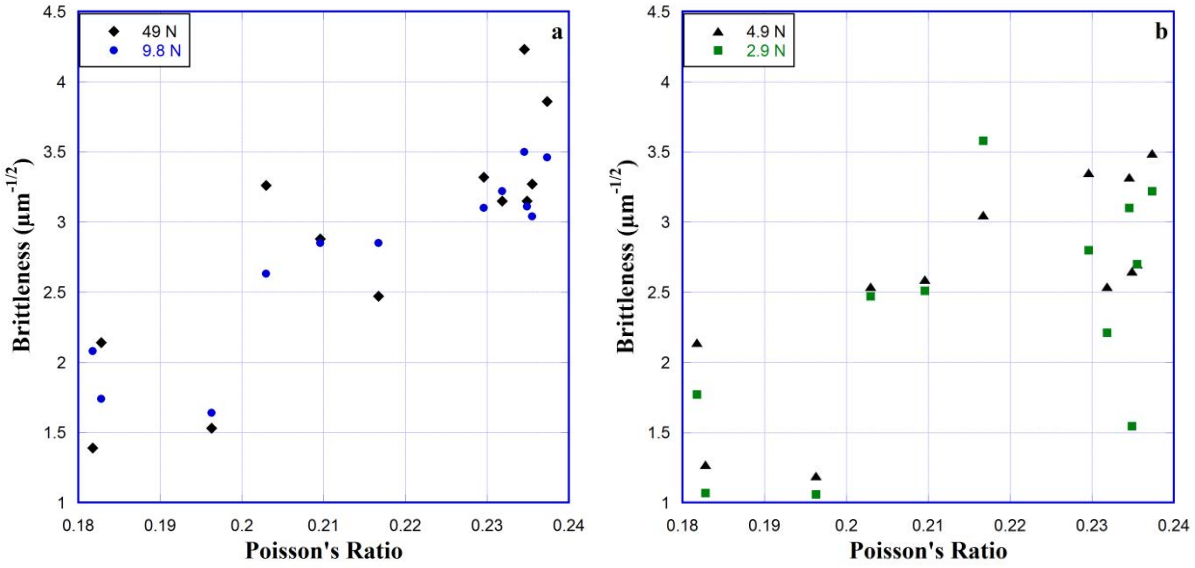

Fig. 6-8. Brittleness of glasses versus Poisson's ratio for a) 49 and 9.8 N loads and b) 4.9 and 2.9 N loads. Brittleness was calculated using the method described by Sehgal and Ito [12].

The indentation diagonals (a) are roughly 30, 45, 65, and 150 μm in length at 2.9, 4.9, 9.8, and 49 N loads. Looking at the average crack lengths (c) over a range of loads versus Poisson's ratio (Fig. 6-4), we see that c quickly grows to be larger than a, but they are quite

comparable at low loads. The average crack length appears to increase logarithmically with increasing Poisson's ratio, with a few exception at 2.9 and 4.9 N loads, where the crack length is significantly shorter. But this decrease in crack length does not occur for all glasses that have crack lengths approximately equal to the indentation diagonal. So it is likely that the relative lengths of *a* and *c* are not the explanation for this behavior.

The fracture toughness, K_{Ic}, remains approximately constant, possibly decreasing slightly, with increasing Poisson's ratio. This change directly follows an increase in the Na_2O content, which corresponds to an increase in the number of weaker inter-atomic bonds in the network. This would be expected to promote an easier path to fracture, so a slight decrease in the fracture toughness would be expected. These values approximately match literature values of glasses with similar compositions [10,13,14]. The fracture toughness does not appear to have any correlation with the minimum observed in the critical crack initiation load. This is in agreement with the findings of Kato et al [13].

Kato et al. did observe a correlation between the crack resistance and the recovery of indentation depth (RID) [13]. RID is a measure of the change in depth of the Vickers indent, which effectively estimates the fraction of deformation volume that was deformed through densification. In their study, glasses with a greater amount of densification were found to have higher crack resistance. Volume recovery of indentations has been observed to have a dependency on the indentation load, but becomes almost constant at loads above 0.50 N [7]. Indentations examined in this study were performed at 50 gf, so it is unlikely that indentation size effect has a significant influence on the densification volumes observed. Seen in Fig. 6-6, the densification volume increases from 13.1 to 16.5 μm^3 as Poisson's ratio increases from 0.18 to 0.23. As the densification volume increases the load to initiate cracks decreases. At the same time the volume of materials deformed through shear flow increases from 4.5 to 6.4 μm^3. At $\nu >$ 0.235, the observed densified volume starts to decrease rapidly, while the sheared volume continues to increase gradually. At $\nu = 0.237$, the densification volume and sheared volume switch roles, with the densification volume becoming smaller than the sheared volume.

The transition between densification and shear flow at $\nu = 0.237$ matches the decrease in volume recovery at indents observed by Sellappan et al. [11]. However, the increase in crack initiation load between $\nu = 0.23$ and 0.24 does not. Sellappan et al. [11] and Kato et al. [13] both observed a decrease in the load to initiate cracks with a decrease in the volume recovery ratio.

Aakermann et al. observed a decrease in the crack resistance of mixed alkali aluminosilicate glasses when compressed, which they attributed to a change in the volume ratio of the two permanent deformation mechanisms [16]. The minimum in the crack initiation load in our glasses occurs as the densification volume goes through a slight maximum at 15 and 20 Na_2O, with lower densification volumes at 10 and 25 Na_2O. This corresponds to the much lower crack initiation load for the 15 and 20 Na_2O glasses, relative to the 10 or 25 Na_2O glasses, suggesting that there is likely a correlation between these two phenomena.

A significant change in the structure of the glass would be expected between 20 and 25 Na_2O, where the main deformation mechanism changes. Raman spectra of Na_2O-TiO_2-SiO_2 glasses showed a gradual shift in peaks between 10 and 20 Na_2O, with a greater shift for some peaks between 20 and 25 [15]. The densification volume for silica glass has been reported around 7.5 μm^3 for 0.5 N Vickers indentations [17]. The difference between the densification volume of pure silica and of the 10 Na_2O glasses studied is quite large. Assuming both measurements are comparable, the difference may be caused by a change in how the resistance to deformation changes with increasing Na_2O. There is a large increase in densification volume between glasses with 10 and 15 Na_2O, compared to between 15 and 20 or 25 Na_2O. Initial additions of Na_2O may have a much larger effect on the resistance to deformation than later additions when a significant concentration of Na_2O is already present.

A possible explanation for the observed behavior is that as the sodium content in the glass is increased, and the number of weaker bonds increases and the inter-connectivity of the network decreases, shear flow becomes easier. At some critical level of Na_2O shear flow becomes much easier. This could be due to the formation of 2D regions with localized high concentrations of weaker bonds, as per the percolation model suggested by Farges et al. [18] (Fig. 6-9). This would be seen in the large jump in shear flow volume at $\nu = 0.237$. It has also been observed that shear flow can promote densification in silica glass [19]. If this is also the case in our glasses, when the shear flow is large but not quite at the critical level, it is possible that the increased shear flow facilitates the densification of glass underneath the indent.

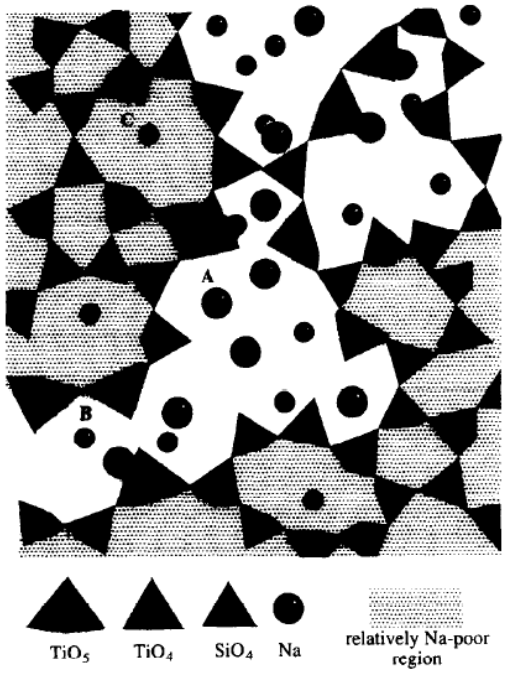

Fig. 6-9. Percolation model proposed by Farges et al. [18], with clusters of Na-rich regions surrounded by Na-poor regions and a high Ti content along the boundary of the clusters.

In this study humidity was not controlled during indentation experiments. The resistance of glasses to both crack initiation [20,21] and deformation [22] has been shown to be affected by the humidity present during the indentation process. These effects should be minimized by performing all indentation tests under similar environmental conditions, but it is possible that greater diffusion of water into the glass at high silica contents or a greater susceptibility to water corrosion at high Na_2O contents could affect the deformation and/or cracking behavior. The effects of water on the cracking of glasses in the Na_2O-TiO_2-SiO_2 system will be investigated to see if there is any significant change in the susceptibility to water with changes in composition.

6.6: Conclusions

A minimum in the critical crack initiation load at ν = 0.21-0.22 was investigated. Hardness decreased slightly with increasing Poisson's ratio, from ~5.5 GPa to ~4.5 GPa. Crack length increased with increasing Poisson's ratio, approximately doubling between 0.18 and 0.24. The fracture toughness did not change appreciably with changing Poisson's ratio, remaining at 0.6 ± 0.1 MPa-$m^{1/2}$. No correlations between the minimum in crack initiation load and hardness, crack length, or fracture toughness were observed.

The volume of glass deformed through shear flow was found to gradually increase with Poisson's ratio, from 4 μm^3 to 7 μm^3 between 0.18 and 0.23, before increasing to 15 μm^3 at ν = 0.237. Densification volume increases from 13.1 μm^3 to 16.5 μm^3 between ν = 0.18 and ν = 0.23 and then decreases to 8.7 μm^3 between ν = 0.235 and 0.237. The maximum in densification volume occurs over the same range of Poisson's ratio as the minimum in crack initiation load.

6.7: References

[1] J. Mauro, C. Philip, D. Vaughn, M. Pambianchi, Glass Science in the United States: Current Status and Future Directions, Int. J. Appl. Glass Sci. (2014) 1–14.
[2] L. Wondraczek, J. Mauro, J. Eckert, U. Kuhn, J. Horbach, J. Deubener, et al., Towards Ultrastrong Glasses, Adv. Mater. 23 (2011) 4578–4586.
[3] J. Lewandowski, W. Wang, A. Greer, Intrinsic Plasticity or Brittleness of Metallic Glasses, Philos. Mag. Lett. 85 (2005) 77–87.
[4] T. Rouxel, P. Sellappan, F. Celarie, P. Houizot, J.C. Sangleboeuf, Towards Glasses with Better Indentation Cracking Resistance, C. R. Mec. 342 (2014) 46–51.
[5] G. Scannell, L. Huang, T. Rouxel, Elastic properties and indentation cracking behavior of Na_2O-TiO_2-SiO_2 glasses, J. Non-Cryst. Solids. 429 (2015) 129–142.
[6] D. Necas, P. Klapetek, Gwyddion: an open-source software for SPM data analysis, Cent. Eur. J. Phys. 10 (2012) 181–188.
[7] S. Yoshida, J.-C. Sangleboeuf, T. Rouxel, Indentation-induced densification of soda-lime silicate glass, Int. J. Mat. Res. 98 (2007) 360–364.
[8] J.E. Srawley, Wide-range stress intensity factor expressions for ASTM E 399 standard fracture toughness specimens, Int. J. Fract. 12 (1976) 475–480.
[9] T. Nose, T. Fujii, Evaluation of Fracture Toughness for Ceramic Materials by a Single-Edge-Precracked-Beam Method, J. Am. Ceram. Soc. 71 (1988) 328–333.
[10] J. Sehgal, S. Ito, Brittleness of glass, J. Non-Cryst. Solids. 253 (1999) 126–132.
[11] P. Sellappan, T. Rouxel, F. Celarie, E. Becker, P. Houizot, R. Conradt, Composition Dependence of Indentation Deformation and Indentation Cracking in Glass, Acta Mater. 61 (2013) 5949–5965.
[12] B. Lawn, D. Marshall, Hardness, Toughness, and Brittleness: An Indentation Analysis, J. Am. Ceram. Soc. 62 (1979) 347–350.
[13] Y. Kato, H. Yamazaki, S. Yoshida, J. Matsuoka, Effect of densification on crack initiation under Vickers indentation test, J. Non-Cryst. Solids. 356 (2010) 1768–1773.
[14] J. Sehgal, S. Ito, A New Low-Brittleness Glass in the Soda-Lime-Silica Glass Family, J. Am. Ceram. Soc. 81 (1998) 2485–2488.
[15] G. Scannell, S. Barra, L. Huang, Structure and Properties of Na_2O-TiO_2-SiO_2 Glasses: Role of Na and Ti on Modifying the Silica Network, To be submitted to J. Non-Cryst. Solids. (2016).
[16] K. Aakermann, K. Januchta, J. Pedersen, M. Svenson, S. Rzoska, M. Bockowiski, et al., Indentation deformation mechanism of isostatically compressed mixed alkali aluminosilicate glasses, J. Non-Cryst. Solids. 426 (2015) 175–183.
[17] H. Ji, V. Keryvin, T. Rouxel, T. Hammouda, Densification of window glass under very high pressure and its relevance to Vickers indentation, Scr. Mater. 55 (2006) 1159–1162.

[18] F. Farges, G.E.J. Brown, A. Navrotsky, H. Gan, J.J. Rehr, Coordination Chemistry of Ti(IV) in Silicate Glasses and Melts: II. Glasses at Ambient Temperature and Pressure, Geochim. Cosmochim. Acta. 60 (1996) 3039–3053.
[19] J.D. Mackenzie, High-Pressure Effects on oxide Glasses: I, Densification in a Rigid State, J. Am. Ceram. Soc. 46 (1963) 461–470.
[20] S. Striepe, J. Deubener, M. Smedskjaer, M. Potuzak, Environmental effects on fatigue of alkaline earth aluminosilicate glass with varying fictive temperature, J. Non-Cryst. Solids. 379 (2013) 161–168.
[21] T.M. Gross, M. Tomozawa, Crack-free high load Vickers indentation of silica glass, J. Non-Cryst. Solids. 354 (2008) 5567–5569.
[22] K. Hirao, M. Tomozawa, Microhardness of SiO_2 Glass in Various Environments, J. Am. Ceram. Soc. 70 (1987) 497–502.

Chapter 7 : Conclusions and Future Work

Conclusions

Titanium dioxide in glasses is of particular interest due to its ability to adopt four-, five-, and six-fold coordination states, effectively allowing it to act as a network former, a network modifier, or a combination of both. The purpose of this study has been to investigate the role of TiO_2 in silicate glasses, namely TiO_2-SiO_2 and Na_2O-TiO_2-SiO_2 systems, by examining how their elastic moduli and structure change as a function of composition and temperature. Additionally, the response of the Na_2O-TiO_2-SiO_2 system to stress and plastic deformation was examined.

In the TiO_2-SiO_2 system, Ti atoms are four-fold coordinated in silica network. The addition of TiO_2 reduces the elastic moduli and shifts Raman peaks at room temperature to lower frequencies due to the heavier mass of Ti atoms and from the creation of a more open and flexible network given by the longer and weaker Ti-O bonds. The balance between increased mass and free volume from the addition of TiO_2 results in an almost constant density of TiO_2-SiO_2 glasses, independent of TiO_2 content. Our *in-situ* high temperature studies showed that the anomalies in TiO_2-SiO_2 glasses are similar to those in pure SiO_2 glass, which can be explained by the conformational and angular changes with temperature. The incorporation of TiO_2 into silica increases the network flexibility and the free volume of the glass while preserving the tetrahedral network structure, and thus facilitates the ring conformational transitions given enough thermal energy to overcome the energy barrier. The increased conformational transitions between softer α-like and stiffer β-like rings compensate the sensitivity of weaker bonds to temperature, so the amount of stiffening of the network with increasing temperature does not change obviously with TiO_2 content. The resulting opening up and increased flexibility of the glass structure promotes the cooperative rotation of adjacent tetrahedra, resulting in a net decrease in the average inter-tetrahedral angles. The larger change (reduction) of the average inter-tetrahedral angles with temperature is the underlying mechanism for the Raman band at 450 cm^{-1} to shift further to higher frequencies with increasing TiO_2. The normal thermal expansion due to bond elongation with temperature is counter-balanced by the free volume reduction facilitated by the cooperative rotation of adjacent tetrahedra assisted by thermal energy. As the network flexibility increases with the amount of TiO_2 addition to silica, the coefficient of thermal

expansion decreases with TiO_2 content, as long as the silica tetrahedral network is preserved, i.e., in the composition range where $^{[4]}$Ti atoms adopt four-fold coordinated sites.

In Na_2O-TiO_2-SiO_2 glasses, Ti atoms adopt a mixture of four- and five-fold coordinated states, with the proportion of five-fold coordinated titanium greater at higher TiO_2 contents. The addition of TiO_2 increases density, refractive index, Young's modulus, shear modulus, bulk modulus, and Poisson's ratio. TiO_2 was observed to provide a stiffening effect by increasing the intensity and shifting to higher frequencies of peaks associated with network formers, namely the 720, 800, and 840 cm^{-1} peaks, while decreasing the intensity of the Si-O nBO peak at 1100 cm^{-1}. TiO_2 appears to reduce the effect of Na_2O on the silica network through the formation of clusters with localized high Ti and Na contents, which has both a shielding effect on the silica network and increases the overall volume bond density, both of which increase the stiffness of the network. These clusters form a double percolation structure, with localized regions of high Na content surrounded by a boundary of high Ti content, outside of which the silica network persists with relatively lower contents of Na and Ti. Increasing the TiO_2 content in the glass increases the volume fraction of these clusters without increasing their size, increasing both the density and stiffness of the glass. At 25 Na_2O, the concentration of Na is too large to be accommodated by the Ti and a more significant disruption of the silica network is observed.

TiO_2 has a striking tightening effect on the glass network, increasing both the packing density and the network energy. In regard to a previously reported indentation-damage map, Na_2O-TiO_2-SiO_2 glasses turn out to fall in the property range (E/H, ν) where the driving force for indentation cracking, whatever the cracking pattern of concern (radial, median, lateral), is relatively limited and exhibit a good indentation damage resistance, especially for the 15 Na_2O-4 TiO_2-81 SiO_2 and 25 Na_2O-4 TiO_2-71 SiO_2 compositions. A minimum in the critical crack initiation load was observed in the range of ν = 0.21-0.22. The minimum was found not to be correlated to hardness, crack length, or fracture toughness. Hardness decreases slightly with increasing Poisson's ratio, from ~5.5 GPa to ~4.5 GPa. Crack length increases with increasing Poisson's ratio, approximately doubling between 0.18 and 0.24. The fracture toughness does not change appreciably with changing Poisson's ratio, remaining at 0.6 ± 0.1 MPa-$m^{1/2}$.

The deformation behavior of glass changes as Poisson's ratio increases. Volume deformed through shear flow was found to gradually increase with Poisson's ratio, from 4.5 μm^3 to 6.4 μm^3 between 0.18 and 0.23, before increasing to 12.9 μm^3 at ν = 0.237. Densification

volume increases from 13.1 μm^3 to 16.5 μm^3 between $\nu = 0.18$ and $\nu = 0.235$ and the decreases to 8.7 μm^3 at $\nu = 0.235$-0.237. The maximum in densification volume occurs over the same range of Poisson's ratio as the minimum in crack initiation load.

Future Work

The minimum in the crack initiation load is very interesting and has not been fully investigated. That an increase in the densification volume is observed over the same range of Poisson's ratio as this minimum suggests that as the glass transitions from primarily densification at low Poisson's ratios to primarily shear flow at high Poisson's ratios the structure becomes significantly more susceptible to densification. This indicates that either shear deformation assists densification, or that the stress to cause the glass to densify becomes significantly lower, such that the volume of glass densified under the same loading conditions is greater [1].

This could be investigated by studying the structure, elastic moduli, and equation of state under *in-situ* high pressure conditions using a diamond anvil cell [2,3]. If there is a substantial change in the stress required for densification in the glass from $\nu = 0.18$ and 0.23, this would significantly strength the argument as to what is the underlying structural cause of the minimum in crack initiation load. *In-situ* high pressure Raman studies would provide both qualitative information as to how the structure is changing during densification, as well as a way to quantitatively estimate residual stresses in this system.

Having a way to get quantitative stress/strain information from Raman spectra would enable mapping of residual stresses around indentations by 3D Raman mapping [4,5]. Prof. Rouxel has indicated that large internal stresses were observed in the less brittle glasses tested by Sehgal and Ito [6]. If the residual stresses around the indent went through either a maximum or a minimum in the same range of Poisson's ratio as the minimum in crack initiation load, this would provide valuable insight into the structural mechanisms that promote or suppress cracking in glasses.

Studying the response of deformation and cracking behaviors to temperature through *in-situ* high temperature indentation experiments would also be of interest. By observing how the susceptibility of the glasses to deformation and crack initiation changes with temperature and comparing it to the high temperature elasticity and structural data, a more robust model of how

the glass responds to elastic and plastic deformations and where those responses overlap and interact can be developed [7,8].

Furthermore, it is important to determine the effect of water, if any, on the cracking and deformation behavior of these glasses as a function of composition. Water diffusion into the glass during indentation has been shown to promote crack growth [9] and reduce hardness [10]. It is possible that a greater diffusion of water into the glass could occur at high silica contents or that glasses with high Na_2O contents would be more susceptible to water corrosion. This can be investigated by performing indentation experiments in a dry nitrogen atmosphere. If the susceptibility to water changes with composition, either TiO_2 or Na_2O content, it should be apparent in a difference in trend of hardness or crack initiation load.

Finally, it has been suggested that $^{[5]}Ti$ is susceptible to conformation changes, particularly in the melt [11]. It would be interesting to pressure quench these glasses above and below T_g to see if there is a significant difference in their structure and elastic moduli.

References

[1] J.D. Mackenzie, High-Pressure Effects on oxide Glasses: I, Densification in a Rigid State, J. Am. Ceram. Soc. 46 (1963) 461–470.
[2] T. Deschamps, C. Martinet, D. de Ligny, B. Champagnon, Elastic anomalous behavior of silica glass under high-pressure: In-situ Raman study, J. Non-Cryst. Solids. 355 (2009) 1095–1098.
[3] T. Rouxel, H. Ji, T. Hammouda, A. Moreac, Poisson's ratio and the Densification of Glass under High Pressure, Phys. Rev. Lett. PRL 100 (2008) 225501.
[4] A. Kassir-Bodon, T. Deschamps, C. Martinet, B. Champagnon, J. Teisseire, G. Kermouche, Raman Mapping of the Indentation-Induced Densification of a Soda-Lime-Silicate Glass, Int. J. Appl. Glass Sci. 3 (2012) 29–35.
[5] A. Perriot, D. Vandembroucq, E. Barthel, V. Martinez, L. Grosvalet, C. Martinet, B. Champagnon, Raman Microspectroscopic Characterization of Amorphous Silica, J. Am. Ceram. Soc. 89 (2006) 596–601.
[6] J. Sehgal, S. Ito, A New Low-Brittleness Glass in the Soda-Lime-Silica Glass Family, J. Am. Ceram. Soc. 81 (1998) 2485.
[7] K. Kese, J.-C. Sangleboeuf, T. Rouxel, Effect of high-temperature ambience during sharp indentation on the residual contact site properties, J. Phys. D: Appl. Phys. 41 (2008) 074025.
[8] J.-C. Sangleboeuf, T. Rouxel, Indentation and Scratching of Glass: Load, Composition and Temperature Effects, Fract. Mech. Ceram. 14 (2005) 121–133.
[9] T.M. Gross, M. Tomozawa, Crack-free high load Vickers indentation of silica glass, J. Non-Cryst. Solids. 354 (2008) 5567–5569.

[10] K. Hirao, M. Tomozawa, Microhardness of SiO_2 Glass in Various Environments, J. Am. Ceram. Soc. 70 (1987) 497–502.
[11] Q. Liu, R. Lange, Y. Ai, Acoustic velocity measurements on Na_2O-TiO_2-SiO_2 liquids: Evidence for a highly compressible TiO_2 component related to five-coordinated Ti, Geochim. Cosmochim. Acta. 71 (2007) 4314–4326.